e - ISSN 2586-9396

Current Applied Science and Technology

Vol. 18 No. 2

May - August 2018

KING MONGKUT'S INSTITUTE OF TECHNOLOGY LADKRABANG

Current Applied Science and Technology or CAST, formerly KMITL Science and Technology Journal, has been established since its inception as KMITL Science Journal in 2001. The journal has been dedicated to publishing advanced and applied knowledge in the form of high quality research and review articles covering the main areas of Biotechnology, Environmental Science, Agricultural Technology, and other fields related to Applied Science and Technology. Special issues devoted to important topics in advanced science and technology will occasionally be published.

The highlight of this journal is to give an opportunity for those researchers with high quality research articles presented at International Conferences such as the International Symposium on Biocontrol and Biotechnology, the International Conference of Biotechnology and Environment, and the International Symposium on Mathematical, Statistical and Computer Sciences organized by various countries, mainly in ASIA, to be published in Current Applied Science and Technology.

The journal is an open access peer-reviewed and double blinded journal using Online Journal System (OJS). Previously, articles were published in print on a regular basis (two issues per year) since 2001 and since 2010 onward the articles have been published both in print and electronic forms starting from volume 10. In 2017, the journal title has been changed from *KMITL Science and Technology Journal* to *Current Applied Science and Technology* (CAST) (e-ISSN 2586-9396) to be more identifiable to the international scientific community according to the suggestion of Thai-Journal Citation Index Centre. The journal has been published online only since volume 2 (July-December, 2017). In addition, the journal has attracted researchers from other countries more than 22% according to the data. The examples of countries where researchers have chosen to publish the articles in CAST are as follows: UK., U.S.A., Australia, Japan, Nigeria, Malaysia, Iraq, Egypt, etc. As of 2017, the number of citation is 203 from 49 countries. Because of more demands on publication in CAST, the editorial board has decided to publish online original academic research and review articles three issues per year (April, August and December) from 2018 onward.

Furthermore, the advisory board and editorial board comprises honorable and wellknown members from around the world in which 50% of editorial board members are from various countries like U.K., Norway, Japan, India, China, Singapore and Egypt. Only 25% of Thai editorial board members are from the publisher organization and 25% from other publisher organizations. Most of advisory and editorial board members have high H-index according to SCOPUS.

The journal is also committed to maintaining the high level of integrity in the content published and has a Conflict of Interest policy in place. The journal uses plagiarism detection software to screen the submissions. The journal has been working closely with Thai-Journal Citation Index Centre to ensure that the journal complies with international standard of SCOPUS.

Current Applied Science and Technology (CAST)

(formerly KMITL Science and Technology Journal)

Editor

Dusanee Thanaboripat
King Mongkut's Institute of Technology Ladkrabang, Thailand

Editorial Board

CONTENTS

Current Applied Science and Technology Vol. 18 No. 2 May-August 2018
DOI: 10.14456/cast.2018.1

Dengue Forecasting Model using SARIMA model to predict the Incidence of Dengue in Thailand

Sadiporn Phuthomdee, Pichitpong Soontornpipit, Chukiat Viwatwongkasem and Jutatip Sillabutra*

Department of Biostatistics, Faculty of Public Health, Mahidol University, Bangkok, Thailand

Received: 15 September 2017, Revised: 25 December 2017, Accepted: 4 July 2018

Abstract

Dengue is one of the major public health problems in the tropical countries of the world. SARIMA model is a popular method used for forecasting dengue incidence. The aim of this study was to determine optimal model for forecasting the dengue incidence. SARIMA model with Box-Jenkins approach was conducted to forecast dengue incidence using the previous data from 2006 to 2015. Akaike's Information Criteria (AIC), Bayesian Information Criteria (BIC) and Root Mean Square Error (RMSE) were used to determine their accuracy. The results showed that SARIMA (6, 0, 3) $(0, 1, 1)_{52}$ were the best model that fitted with the actual data. It had the smallest AIC and BIC (3827.60 and 3873.30, respectively) and RMSE (0.8420).

Keywords: dengue incidence, SARIMA, forecasting model

1. Introduction

Dengue fever is a serious public health problem in the word. Billion people are now at risk with this disease. WHO estimated that 500,000 people requiring hospitalization each year and about 2.5 % of those died [1]. Moreover, there is now no available licensed dengue vaccine. Dengue vaccine candidates are now under phases of development [2]. To control the spread of disease, disease surveillance and mosquito vector eradication are implemented [1]. However, the dengue incidences have dramatically increased around the world in recent decades [1]. In the South-East Asia region, dengue is increasing with an exponential form every three to five years [3]. In 2015, the morbidity and mortality rates of Thailand are higher than those of five previous year. The incidence rate of Thailand was 219.46 per 100,000 populations (142,925 cases). There were 328.28 per 100,000 population in central, 201.10 per 100,000 population in the Northern, 166.21 per 100,000 population in the North-eastern and 127.52 per 100,000 population in the Southern, respectively. The death rate was 0.22 per 100,000 populations (141 cases). Female and male were equally incidence (1.01:1). The groups of aged 15 - 24 years old were the high incidence rate of dengue infection [4, 5].

*Corresponding author: Tel.: +66-2354-8530 Fax: +66-2354-8534
E-mail: jutatip.sil@mahidol.ac.th

The mathematical or statistical models were famously used to forecast and describe the phenomena of diseases. Forecasting is important as it is benefit for management, health risk assessment, and planning the equipment for control and prevention. [6, 7]. Moreover, the forecasting is taken into accounted as the Early Warning system [8]. The results of forecasting were not only for understanding size of problem, susceptibility host, period of disease, area, and pattern of disease, but also disease control [6].

Time Series Analysis was basically used to predict the incidence case in many diseases such as influenza [9, 10], malaria [11-13], and dengue [14-19]. The model has different degrees of complexity based upon many factors: previous data of dengue cases, climatic variables such as rainfall, evaporation, temperature, humidity, water budget, breeding sites, population density, virus serotypes and microclimates [19-22], Many studies revealed that Seasonal Autoregressive Integrated Moving Average (SARIMA) was used as the model for predicting dengue incidence [23].

SARIMA is reported as the great model for dengue forecasting due to dengue is none stationary problem. The seasonal was taken into account in model. In 2014, Monika S Sitepu *et al.* showed that SARIMA $(1,0,1)(0,1,1)_{12}$ was the best model for predicting dengue in Jakarta [16]. Bhatnagar *et al*. [6] revealed that forecasting model for dengue incidence in Rajasthan was SARIMA $(0,0,1)(0,1,1)_{12}$. The previous studies in Thailand revealed that the forecasting models of dengue incidence in Thailand were SARIMA $(2,0,1)(0,2,0)_{12}$ [24] and SARIMA $(2,0,1)(0,1,1)_{12}$ [25]. According to the previous studies, the most of forecasting models were proposed based on 12 months period of time interval. However, some studies were proposed 52 weeks as time interval in the models [15, 26]. In Thailand, only SARIMA models based on 12 months period of time interval were conducted. There is no study using 52 weeks of time interval in SARIMA model. Therefore, this study aims to determine optimal model for forecasting the dengue incidence in Thailand using SARIMA model with 52 weeks of time interval period. AIC and BIC were used to select the best model, and performance of model was measured by RMSE.

2. Materials and Methods

The SARIMA with Box-Jenkins approach was used to predict dengue incidence. The historical data from 2006 to 2015 were used in analysis. The performance of model was measured by RMSE. The presence of these two components determine the choice of SARIMA $(p,d,q)(P,D,Q)_s$ model equation:

$$Y_{t+k} = \frac{\psi_q(\alpha)\Psi_Q(\alpha)^s \varepsilon_t \Gamma_P(\alpha)^s}{\Gamma_P(\alpha)^s \gamma_p(\alpha)(1-\alpha)^d (1-\alpha^{sD})} \quad (1)$$

where Y_{t+k} is evidence weekly dengue incidence, $\psi_q(\alpha)$ is coefficient of moving average (MA) at q order, $\Psi_Q(\alpha)$ is coefficient of seasonal moving average (SMA) at Q order and S seasonal period, $\gamma_p(\alpha)$ is coefficient of autoregressive (AR) at p order, $\Gamma_P(\alpha)^s$ is coefficient of seasonal autoregressive (SAR) at P order and S seasonal period, d is order of different week period, D is order of seasonal different period, ε_t is white noise time or residual of time**,** t is weekly period time and k is weekly ledge time

According to previous studies, SARIMA $(p,d,q)(P,D,Q)_s$ were set as SARIMA $(p,d,q)(0,1,1)_s$ [12, 13]. In this study, the 52-week (s=52) was used in model. Therefore, SARIMA $(p,d,q)(0,1,1)_{52}$ was selected as the basic structure of candidate model. Logarithmic transformation was used to adjust data to meet the criteria of equally mean and variance in each period. Based on mean-rang plot analysis, Autoregressive function and Partial Autocorrelation function were used to

identify the order of Autoregressive part, order of Moving Average part and difference. The order of *d* was randomly from 0, 1, and 2. The order of *p* was randomly from 0 to 6 and the order of *q* was randomly from 0 to 3 (Figure 2). The first criteria for selection model was smallest AIC, BIC and RMSE and highest of Likelihood Ratio Test (LRT).

Finally, the evidence data in 2016 was used to compare with the estimation of model. The performance of model was determined by RMSE. The statistical software R [27] was used for all analysis.

3. Results and Discussion

The evidence dengue incidence in Thailand from 2006 - 2015 showed in Figure 1. It showed that there were two outbreaks in early 2010 to mid-2010, and early 2013 to late 2013. Large of Autocorrelation Function (ACF) and Partial Autocorrelation Function (PACF) were showed in Figure 2A and 2B, respectively. The sharp decrease in ACF value from lag 1 to lag 50 and the sharp increase in PACF value from after lag 50 indicated that there was evidence of long-term trend. Therefore, the first different term was taken into account. When considering the first different term as shown in Figure 2B, it showed that sharp of ACF of first difference of weekly dengue incidence were decreased after lag 1.

SARIMA $(6,0,3)(0,1,1)_{52}$ was selected as the best model with the smallest AIC (3827.60). BIC and RMSE were 3873.30 and 0.8420, respectively. The estimated variation of dengue incidence ($\hat{\sigma}^2$) from this models was 171.30. The model parameters were significance (*p*-value <0.0001) with 1st AR (-1.1042, S.E.=0.4364), 2nd AR (-0.2041, S.E.=0.3523), 3rd AR (-0.4611, S.E.=0.3804), 4th AR (-0.2251, S.E.=0.2725), 5th AR (-0.2474, S.E.=0.1115), 6th AR (-0.1029, S.E.=0.0723), 1st MA (1.1185, S.E.=0.4410), 2nd MA (0.4741, S.E.=0.1228), 3rd MA (0.1891, S.E.=0.4432) and seasonal MA (-0.8699, S.E.=0.0 4 6 4). The best fit model was model SARIMA $(6,0,3)(0,1,1)_{52}$. The comparison between actual dengue fever data in 2016 and forecast data form SARIMA $(6,0,3)(0,1,1)_{52}$ was presented in Figure 3.

In this study, SARIMA $(6,0,3)(0,1,1)_{52}$ was the most optimal predictive model which showed that the smallest AIC, BIC and RMSE. Our results were difference on AR, MA and SMA, when comparing with previous studies. SARIMA $(0,0,1)(0,1,1)_{12}$ was offered with no seasonal differences presented in Rajasthan [6]. Moreover, SARIMA $(1,0,1)(0,1,1)_{12}$ was the best model for predicting DHF cases in Jakarta [16]. According to time series plots analysis, AR and MA were determined and depended on timely interval of lags. AR and MA of this study were designed based on the dengue incidence of epidemiological weeks in one year (*s*= 52 weeks), but the previous studies were designed based on the dengue incidence of epidemiological months in one year (*s*=12). Moreover, the model may depend on geographical area. SARIMA$(0,1,1)(0,1,1)_{52}$, SARIMA $(0,0,1)(0,1,1)_{12}$, SARIMA $(1,0,1)(0,1,1)_{12}$ were the models conducted in island [6, 15, 16]. The different SARIMA models in different areas of Thailand were also found. The SARIMA models conducted in northern part and north-eastern part were SARIMA$(2,0,1)(0,2,0)_{12}$ and SARIMA$(2,0,1)(0,1,1)_{12}$, respectively [24, 25].

Current Applied Science and Technology Vol. 18 No. 2 May-August 2018
DOI: 10.14456/cast.2018.1

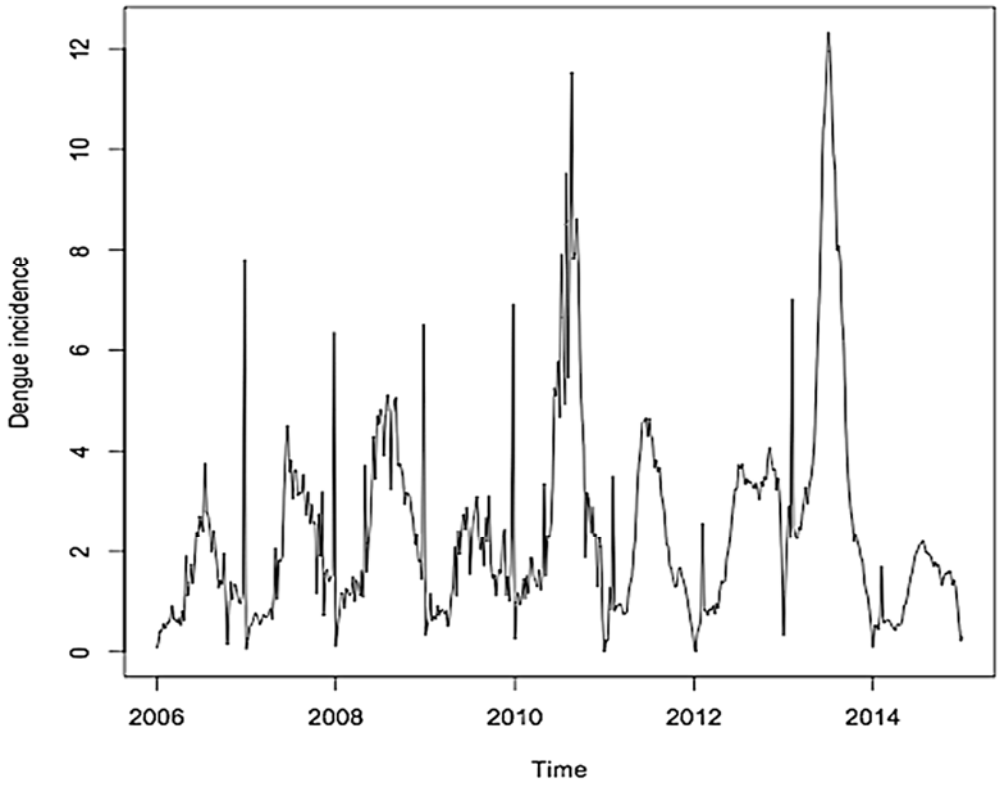

Figure 1. Weekly dengue incidence (per 100,000 populations) in Thailand from January 2006 to December 2015

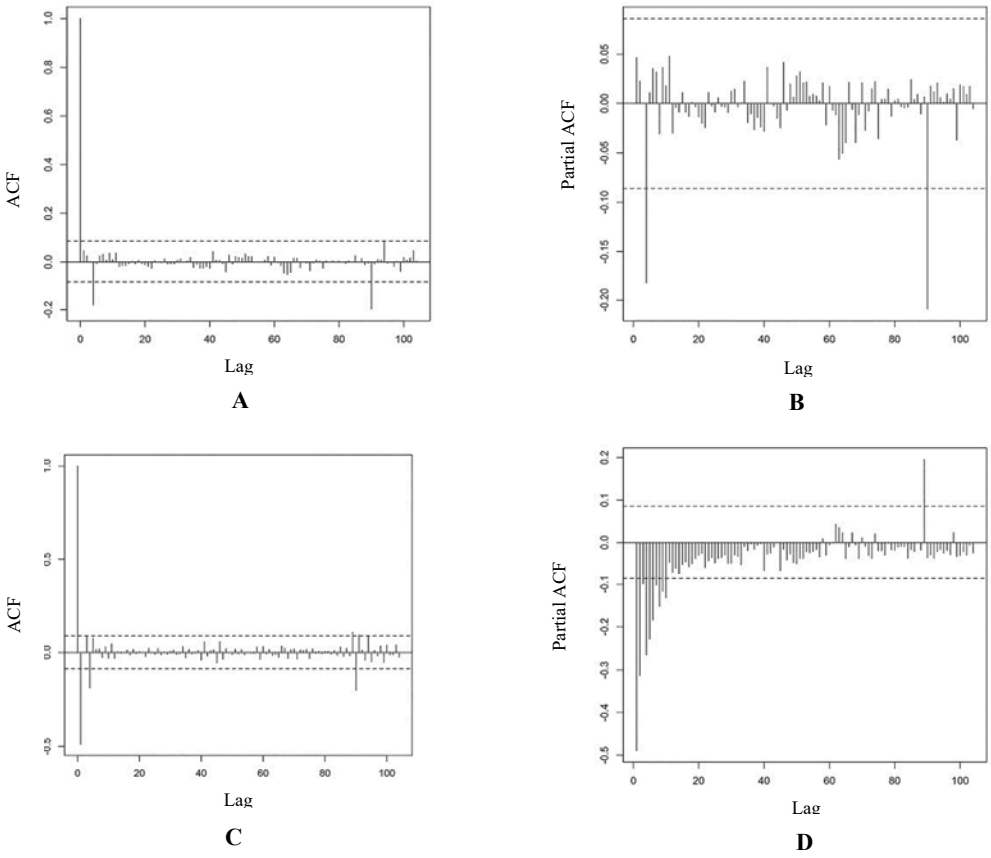

Figure 2. A and B) ACF and PACF of logarithm dengue incidence (per 100,000 populations) in Thailand from January 2006 to December 2015 C and D) ACF and PACF after differencing of logarithm dengue incidence (per 100,000 populations) in Thailand from January 2006 to December 2015

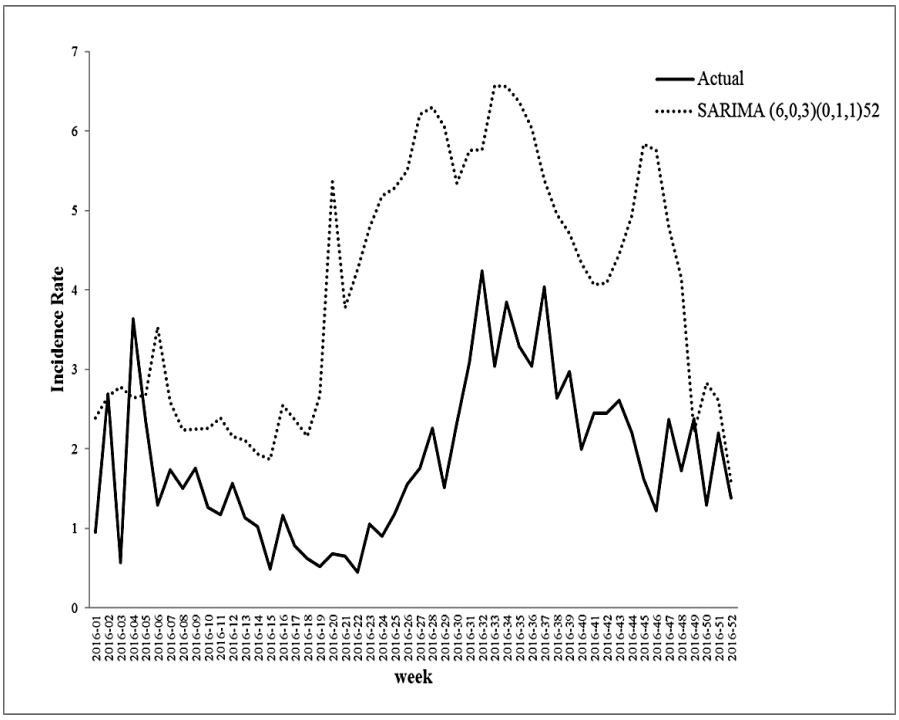

Figure 3. Comparative of dengue incidence rate in 2016 between actual data and forecast data from SARIMA $(6,0,3)(0,1,1)_{52}$.

4. Conclusions

Seasonal Autoregressive Moving Average (SARIMA) model was used to forecast dengue incidence. This model was the most popular model used for prediction in many communicable diseases including influenza, malaria, and dengue. Moreover, it was benefit to epidemiological surveillance and policy makers to manage and prevent the outbreak.

In this study, the forecasting model of dengue incidence was developed based on the secondary data of historical data from 2006 to 2015. The seasonal period with 52 weeks in a year was taken into accounted. SARIMA $(6,0,3)(0,1,1)_{52}$ was presented as the best fitted model with the actual data. However, dengue is also associated with the multiple risk factors such as climate, migration, the characteristic of virus and etc. Therefore, the further study should have taken the risk factors in the model to describe the pattern of dengue.

5. Acknowledgements

We are greatly thankful to Bureau of Epidemiology, Department of Disease Control, Ministry of Public Health, Bureau of Vector - Borne Disease, Department of Disease Control, Ministry of Public Health, Department of Provincial Administration, Ministry of Interior, and the Thai Meteorological Department, Ministry of Digital Economy and Society for their support the secondary data to developed model in this study.

References

[1] World Health Organization, 2009. *Dengue: Guidelines for Diagnosis, Treatment, Prevention and Control.* [online] Available at: www.who.int/tdr/publications/documents/dengue-diagnosis.pdf
[2] Ghosh, A. and Dar, L., 2015. Dengue vaccines: Challenges, development, current status and prospects. *Indian Journal of Medical Microbiology,* 33, 3-15.
[3] WHO Regional Office for South-East Asia., 2011. *Comprehensive Guidelines for Prevention and Control of Dengue and Dengue Hemorrhagic Fever*.
[4] Bureau of Epidemiology, Ministry of Public Health, 2016. *Surveillance Report (R 506) DHF Total.* [online] Available at: http://www.boe.moph.go.th/boedb/surdata/506wk/ y60/d262766_4860.pdf
[5] Bureau of epidemiology, Ministry of Public Health, 2015. *Surveillance Report (R 506) DHF Total*. [online] Available at: http://www.boe.moph.go.th/boedb/surdata/506wk/y59/d262766_5259.pdf
[6] Bhatnagar, S., Lal, V., Gupta, S.D. and Gupta, O.P., 2012. Forecasting incidence in Rajasthan, using time Series analysis. *Indian Journal Public Health*, 56(4), 281-285.
[7] Suthachana, S., Kaewnokkao, W., Suangtho, P., Sayumpurujinun, S. and Kongyu, S., 2012. Forecasting the situation of influenza in Thailand in 2012. In: Bureau of Epidemiology, Department of Diseases Control, Ministry of Public Health, *Workshop Conference in Analyzed and Forecasting.* Bangkok, Thailand, 12-14 September 2012. Bangkok: Ministry of Public Health.
[8] Drake, J.M., 2005. Fundamental limits to the precision of early warning systems for epidemic of infectious disease. *PLoS Medicine*, 2(5), e144. http://doi.org/10.1371/journal.pmed.0020144.
[9] Soebiyanyo, R.P., Adimi, F. and Kaing, R.K., 2010. Modeling and predicting seasonal influenza transmission in warm region using climatological parameters, *PLoS ONE*, 5(3), e9450. http://doi.org/10.1371/journal.pone.
[10] Parmsan, C., 2007. Influence of species, latitudes and methodologies on estimates of phonological response to global warming. *Global Chang Biology*, 13, 1860-1872.
[11] Loha, E. and Lindijorn, B., 2010. Model variation in prediction incidence of *Plasmodium falciparum* malaria using 1998-2007 morbidity and meteorological data from South Ethiopia. *Malaria Journal* 9, 166-173.
[12] Wangdi, K., Singhasivanon, P., Silawan, T., Lawpoolsri, S., White, N.J. and Kaewkungwal, J., 2010. Development of temporal modeling for forecasting and prediction of malaria infections using time series and ARIMAX analysis: A case study in endemic district of Bhutan. *Malaria Journal,* 9, 251-265.
[13] Tian, L., Bi, Y., Ho, S.C., Liu, W., Liang, S. and Goggins, W.B., 2008. One-year delayed effect of fog on malaria transmission: A time series analysis in the rain forest area of Mengla County, south-west China. *Malaria Journal*, 7, 110-123.
[14] Dom, N.C., Hassan, A.A., Ltif, Z.A. and Ismail R., 2012. Generating temporal model using climate variable for prediction of dengue case in subbing jaya, Malaysia. *Asian Pacific Journal of Tropical Disease*, 2, 352-361.
[15] Gharbi, M., Quenel, P., Gustave, J., Cassadou, S., Ruche, G.L., Girdary, L. and Marrama L., 2010. Time series analysis of dengue incidence in Guadeloupe, French West Indies: Forecasting model using climate variables as predictors, *BMC Infectious Diseases* 11, 166. http://doi.org/10.1186/1471-2334-11-166.
[16] Sitepu, M.S., Kaewkungwal, J., Lupleriop, N., Soonthornworasiri, N., Silawan, T., Poungsombat, S. and Lawpoolsri, S., 2013. Temporal patterns and a disease forecasting model for dengue hemorrhagic fever in Jakarta based on 10 years of surveillance data. *Southeast Asian Journal Tropical Medicine and Public Health*, 44(2), 206-217.
[17] Promprou, S., Jaroensutasinee, M. and Jaroensutasinee, K., 2006. Forecasting dengue hemorrhagic fever cases in Southern Thailand using ARIMA models. *Dengue Bulletin*, 30, 99-106.

[18] Institute of Research, Knowledge Management and Standards for Disease Control, Ministry of Public Health, 2017. A Predictive Model for Dengue Hemorrhagic Fever Epidemics in 8 Provinces, Northern Thailand. [online] Available at: http://irem2.ddc.moph.go.th/research/4803.

[19] Schmidt, W.P., Suzuki, M., Dinh Thiem, V., White, R.G., Tsuzuki, A., Yoshida, L.M., Yanai, H., Haque, U., Tho, L. H., Duc Anh, D. and Ariyoshi, K., 2011. Population density, water supply, and the risk of dengue fever in Vietnam: Cohort study and spatial analysis. *PLoS Medicine*, 8(8), e1001082. http://doi.org/10.1371/ journal.pmed.1001082.

[20] Thammapalo, S., Nagao, Y., Sakamoto, W., Saengtharatip, S., Tsujitani, M., Nakamura, Y., Coleman, P.G. and Davies, C., 2008. Relationship between transmission intensity and incidence of dengue hemorrhagic fever in Thailand. *PLoS Neglected Tropical Diseases,* 2(7), e263. http://doi.org/10.1371/journal.pntd.0000263.

[21] Mammen, M.P., Pimgate, C., Koenraadt, C.J.M., Rothman, A.L., Aldstadt, J., Nisalak, A., Jarman, R.G., Jones, J.W., Srikiatkhachorn, A., Ypil-Butac, C.A., Getis, A., Thammapalo, S., Morrison, A.C., Libraty, D.H., Green, S. and Scott, T.W., 2008. Spatial and temporal clustering of dengue virus transmission in Thai villages. *PLoS Medicine,* 5(11), e205. http://doi.org/10.1371/journal.pmed.0050205.

[22] Schreiber, K.V., 2001. An investigation of relationships between climate and dengue using a water budgeting technique. *International Journal of Biometeorology*, 45(2), 81-89.

[23] Halide, H. and Ridd, P., 2008. A Predictive model hemorrhagic fever epidemics. *International Journal of Environmental Health Research*, 18(4), 253-265.

[24] Wongkoon, S., Pollar, M., Jaroensutasinee, M. and Jaroensutasinee, K., 2007. Predicting DHF incidence in Northern Thailand using time series analysis technique. *International Journal of Medical, Health, Biomedical, Bioengineering and Pharmaceutical Engineering,* 1(8), 484-488.

[25] Silawan, T., Singhasivanon, P., Kaewkungwal, J., Nimmanitya, S. and Suwonkerd, W., 2008. Temporal patterns and forecast of dengue infection in Northeastern Thailand. *Southeast Asian Journal of Tropical Medicine and Public Health,* 39(1), 90-98.

[26] Dom, N.C., Hassan, A.A., Latif, Z.A. and Ismail, R., 2012. Generating temporal model using climate variables for the prediction of dengue case in Sunbang Jaya, Malaysia. *Asian Pacific Journal of Tropical Disease,* 3(5), 352-361.

[27] The R Foundation, 2017. *The R Project for Statistical Computing*. [online] Available at: http:// www.R-project.org/.

Current Applied Science and Technology Vol. 18 No. 2 May-August 2018
DOI: 10.14456/cast.2018.2

Lower Bound for *p*-Adic Exponential Polynomials Evaluated at Some Integer Points

Vichian Laohakosol and Angkana Sripayap*

Department of Mathematics, Faculty of Science, Kasetsart University, Bangkok, Thailand

Received: 29 March 2018, Revised: 1 July 2018, Accepted: 4 July 2018

Abstract

In 1981, a *p*-adic interpolation method based on divided differences was derived and was applied to derive, among other things, results on the number of zeros and the bound of certain *p*-adic exponential polynomials. Here, lower bounds for a *p*-adic exponential polynomial evaluated over some rational integers are derived using a method of van der Poorten.

Keywords: *p*-adic exponential polynomial, Turán's theorem

1. Introduction

In the paper , a *p*-adic interpolation method using divided differences [1] was developed, and was then applied to obtain results on the number of zeros and the bounds of the coefficients of *p*-adic exponential polynomials, as well as to obtain a *p*-adic analogue of Turán's first main theorem on sums of powers. In this paper, we continue their investigation on *p*-adic exponential polynomials in the spirit of Turán's main theorems. We shall establish lower bounds for a *p*-adic exponential polynomial, evaluated over some rational integers, in terms of its derivatives at the origin, its functional values at some other rational integral points, and its coefficients. Since the technique employed in Laohakosol and Pitman [1] to derive *p*-adic Turán's first main theorem does not generalize to exponential polynomials, we thus have to use different methods. The approach we adopt here is van der Poorten's method of evaluating determinants as appeared in van der Poorten [2,3].

Notation. The following will be standard throughout the entire paper:

1. *p* a fixed rational prime,
2. $|\cdot|_p$ the *p*-adic valuation so normalized that $|p|_p = 1/p$,
3. $\mathbb{Q}_p$ the field of *p*-adic numbers, that is the completion of $\mathbb{Q}$ (the field of rational numbers) with respect to the *p*-adic valuation $|\cdot|_p$,
4. $\mathbb{C}_p$ the completion of the algebraic closure of $\mathbb{Q}_p$

*Corresponding author: Tel.:662-5625555 ext 647086
E-mail: fscianr@ku.ac.th

We shall always be working in $\mathbb{C}_p$. In a few places, we find it useful to derive certain estimates via Schnirelman integrals. We use the symbol $\int_{a,R}$ to denote the Schnirelman integral over the circle in $\mathbb{C}_p$ with center *a* and radius *R*. For the definition and basis properties of Schnirelman integral, we refer to the appendix of Adams [4].

2. Preliminaries

The following lemma, due essentially to van der Poorten [2], is simple but quite fundamental for our investigation.

Lemma 1. *Let E be a function of the form*

$$E(z) = \sum_{k=1}^{M} b_k g_k(z)$$

where $b_1, b_2, \ldots, b_M$ *are constants in* $\mathbb{C}_p$ *and* $g_1, g_2, \ldots, g_M$ *are functions analytic on some domain G of* $\mathbb{C}_p$. *Further let* $z_1, z_2, \ldots, z_M$ *be points of G; let* $s_1, s_2, \ldots, s_M$ *be non-negative integers; and let* $H(Y_1, Y_2, \ldots, Y_L)$ *be a form linear in* $Y_1, Y_2, \ldots, Y_L$ $(1 \le L \le M)$. *Finally denote by* Δ_{ij} $(1 \le i, j \le M)$ *the cofactor of* $g_j^{(s_i)}(z_i)$ *in the determinant*

$$\Delta = \left| g_j^{(s_i)}(z_i) \right|_{1 \le j, i \le M}.$$

Then there is an integer v such that $1 \le v \le M$ *and*

$$\left| E^{(s_v)}(z_v) \right|_p \ge \frac{\left| H\left(b_{j(1)}, b_{j(2)}, \ldots, b_{j(L)}\right) \right|_p}{\max_{1 \le i \le M} \left| H\left(\Delta_{ij(1)}, \Delta_{ij(2)}, \ldots, \Delta_{ij(L)}\right) / \Delta \right|_p}$$

where $1 \le j(1) \le \ldots \le j(L) \le M$.

Proof By differentiating at $z_1, z_2, \ldots, z_M$, we obtain a system of *M* linear equations in $b_1, b_2, \ldots, b_M$ of the forms

$$\sum_{k=1}^{M} b_k g_k^{(s_i)}(z_i) = E^{(s_i)}(z_i) \quad (i = 1, 2, \ldots, M),$$

which we may solve by Cramer's rule to obtain

$$b_k \Delta = \sum_{i=1}^{M} \Delta_{ik} E^{(s_i)}(z_i) \quad (k = 1, 2, \ldots, M).$$

Thus

$$H(b_{j(1)}, b_{j(2)}, \ldots, b_{j(L)})\Delta = \sum_{i=1}^{M} H(\Delta_{ij(1)}, \Delta_{ij(2)}, \ldots, \Delta_{ij(L)}) E^{(s_i)}(z_i),$$

and so

$$\left| H(b_{j(1)}, b_{j(2)}, \ldots, b_{j(L)})\Delta \right|_p \le \max_{1 \le v \le M} \left| H(\Delta_{ij(1)}, \Delta_{ij(2)}, \ldots, \Delta_{ij(L)}) \right|_p \max_{1 \le v \le M} \left| E^{(s_v)}(z_v) \right|_p.$$

Note that the result remains meaningful though trivial even if the denominator on the right-hand side of the result should vanish, provided we then interpret the lower bound to be zero. Since we shall only be working with *p*-adic exponential polynomials, we shall first standardize our symbols. Let $\rho(1), \rho(2), \ldots, \rho(m)$ be non-negative integers with sum

$$\sum_{k=1}^{m} \rho(k) = M$$

and let $a_{ks}, 1 \le k \le m, 1 \le s \le \rho(k)$ be M elements of $\mathbb{C}_p$ not all 0. Let α_k $(k = 1,\ldots,m)$ be distinct elements of $\mathbb{C}_p$ satisfying

$$|\alpha_k - 1|_p < p^{-1/(p-1)} \qquad (k = 1,\ldots,m).$$

Therefore, each α_k^z is an analytic function of z in the domain $\{z \in \mathbb{C}_p; |z|_p \le 1\}$. We shall consider exponential polynomials of the form

$$E(z) = \sum_{k=1}^{m} \sum_{s=1}^{\rho(k)} a_{ks} z^{s-1} \alpha_k^z \qquad (|z|_p \le 1)$$

so that we shall be applying Lemma 1 to the M functions

$$z^{s-1}\alpha_k^z \qquad (k = 1,\ldots,m;\ s = 1,\ldots,\rho(k)).$$

To avoid any ambiguity, with regard to the terminology in Lemma 1 for $g_j(z)$ and the M functions $z^{s-1}\alpha_k^z$ $(k = 1,\ldots,m;\ s = 1,\ldots,\rho(k))$, we define

$$\begin{aligned}
&g_1(z) = \alpha_1^z, g_2(z) = z\alpha_1^z, \ldots, g_{\rho(1)}(z) = z^{\rho(1)-1}\alpha_1^z,\\
&g_{\rho(1)+1}(z) = \alpha_2^z, g_{\rho(1)+2}(z) = z\alpha_2^z, \ldots, g_{\rho(1)+\rho(2)}(z) = z^{\rho(2)-1}\alpha_2^z,\\
&\qquad\vdots\\
&g_{\rho(1)+\ldots+\rho(m-1)+1}(z) = \alpha_m^z, g_{\rho(1)+\ldots+\rho(m-1)+2}(z) = z\alpha_m^z,\\
&\qquad\vdots\\
&g_{\rho(1)+\ldots+\rho(m)}(z) = z^{\rho(m)-1}\alpha_m^z.
\end{aligned}$$

We also find it more convenient to specify the notation in Lemma 1, keeping in mind that the method is also applicable to much more general cases. Thus from Lemma 1, we set as follows:

1. n a fixed non-negative rational integer,
2. $z_j = n + j$ $(j = 1,2,\ldots,M)$,
3. $s_j = 0$ $(j = 1,2,\ldots,M)$,
4. r = a fixed positive rational integer

Let

$$H(Y_1, Y_2, \ldots, Y_M) := \sum_{h=1}^{m} \sum_{t=1}^{\rho(h)} \frac{(r-1)!}{(r-t)!} (\log \alpha_h)^{r-t} y_{ht},$$

where

$$\begin{aligned}
&Y_1 = y_{11}, Y_2 = y_{12}, \ldots, Y_{\rho(1)} = y_{1,\rho(1)},\\
&Y_{\rho(1)+1} = y_{21}, Y_{\rho(1)+2} = y_{22}, \ldots, Y_{\rho(1)+\rho(2)} = y_{2,\rho(2)},\\
&\qquad\vdots\\
&Y_{\rho(1)+\ldots+\rho(m-1)+1} = y_{m,1}, Y_{\rho(1)+\ldots+\rho(m-1)+2} = y_{m,2}, \ldots, Y_{\rho(1)+\ldots+\rho(m)} = y_{m,\rho(m)}.
\end{aligned}$$

We consider such linear form H because of the following identity

$$H(a_{11}, \ldots, a_{m,\rho(m)}) = \sum_{h=1}^{m} \sum_{t=1}^{\rho(h)} \frac{(r-1)!}{(r-t)!} (\log \alpha_h)^{r-t} a_{ht} = E^{(r-1)}(0).$$

Current Applied Science and Technology Vol. 18 No. 2 May-August 2018
DOI: 10.14456/cast.2018.2

3. Main Results

By Lemma 1, we must then consider the determinant

$$\Delta = \left| (n+j)^{t-1} \alpha_h^{n+j} \right|_{ht,j} \quad (1 \le h \le m, 1 \le t \le \rho(h), 1 \le j \le M)$$

(the numbering of row and column indexes is clear from the display of functions $g_j(z)$'s, and the linear form *H* in its cofactors).

The crux of van der Poorten's method, and indeed the most difficult part, is to handle these determinants effectively. Consequently, we first compute these determinants. Since the arguments used in van der Poorten's sledge-hammer approach to evaluate these determinants are algebraic in nature, then they are also applicable in the *p*-adic case. We shall be brief here and refer to a more detailed discussion in van der Poorten [3]. We first let

$$\alpha_{ht} \ (1 \le h \le m; 1 \le t \le \rho(h))$$

be formal quantities. The next lemma, again due to van der Poorten [2], enables us to obtain nice identities later. Its proof is elementary, and can be found in van der Poorten [2].

Lemma 2. *Denote by P the product*

$$P = \prod_{k=1}^{m} \prod_{s=1}^{\rho(k)} \prod_{l=1}^{s-1} (\alpha_{ks} - \alpha_{kl}),$$

and let R_1 *and* R_2 *be functions in the* α_{ht} $(i \le h \le m, 1 \le t \le \rho(h))$, *which are divisible by P. Then*

$$\lim_{\substack{\alpha_{ks} \to \alpha_k \\ \text{all } ks}} \left(\prod_{k=1}^{m} \prod_{s=1}^{\rho(k)} \frac{\left((\alpha_{ks} \frac{\partial}{\partial \alpha_{ks}})^{s-1} \right) R_1}{\left((\alpha_{ks} \frac{\partial}{\partial \alpha_{ks}})^{s-1} \right) R_2} \right) = \lim_{\substack{\alpha_{ks} \to \alpha_k \\ \text{all } ks}} \left(\frac{R_1 / P}{R_2 / P} \right).$$

(*The limiting processes in Lemma 2 and in what follows can be thought of as those with respect to the p-adic topology.*)

Next, let *D*be the Vandermonde determinant

$$D = \left| \alpha_{ht}^{n+i} \right|_{ht,i} = \prod_{k=1}^{m} \sum_{s=1}^{\rho(k)} \left(\alpha_{ks}^{n+1} \prod_{jr<ks} (\alpha_{ks} - \alpha_{jr}) \right),$$

where $jr < ks$ means either $j < k$ or if $j = k$, then $r < s$ .A more explicit form is

$$D = \prod_{k=1}^{m} \prod_{s=1}^{\rho(k)} \left(\alpha_{ks}^{n+1} \prod_{l=1}^{s-1} (\alpha_{ks} - \alpha_{kl}) \prod_{j=1}^{k-1} \prod_{r=1}^{\rho(k)} (\alpha_{ks} - \alpha_{jr}) \right),$$

By direct differentiation (see also [6] or [7]), we get

$$\begin{aligned} \Delta &:= \left| (n+i)^{t-1} \alpha_h^{n+i} \right|_{ht,i} \quad (1 \le h \le m, 1 \le t \le \rho(h), 1 \le i \le M) \\ &= \lim_{\substack{\alpha_{ks} \to \alpha_k \\ 1 \le k \le m; 1 \le s \le \rho(k)}} \left(\prod_{k=1}^{m} \prod_{s=1}^{\rho(k)} \left(\alpha_{ks} \frac{\partial}{\partial \alpha_{ks}} \right)^{s-1} \right) D \\ &= \prod_{k=1}^{m} \prod_{j=1}^{\rho(k)} \left(\alpha_k^{n+s} (s-1)! \prod_{j=1}^{k-1} (\alpha_k - \alpha_j)^{\rho(j)} \right). \end{aligned} \tag{3.1}$$

Denote by $D_{i,ht}$ and, respectively, $\Delta_{i,ht}$ the cofactor of α_{ht}^{n+i} and, respectively, of $(n+i)^{t-1} \alpha_h^{n+i}$ in *D* and respectively in Δ. In a similar manner as we derived Δ from *D*, we also have

$$\Delta_{i,ht} = \lim_{\substack{\alpha_{ks}\to\alpha_k \\ \text{all } ks}} \left(\prod_{k=1}^{m} \prod_{\substack{s=1 \\ ks\neq ht}}^{\rho(k)} \left(\alpha_{ks} \frac{\partial}{\partial \alpha_{ks}}\right)^{s-1} \right) D_{i,ht}.$$

By expanding the determinant *D* through its cofactors, we see that

$$\frac{D}{\alpha_{ht}^{n+1}} \delta_{ks,ht} = \sum_{i=1}^{M} \alpha_{ks}^{i-1} D_{i,ht} \qquad (1 \le k \le m, 1 \le s \le \rho(k)),$$

(where $\delta_{ks,ht}$ is the usual Kronecker δ), which asserts that $D_{i,ht}$ is exactly the coefficient of z^{i-1} in the polynomial

$$\frac{D}{\alpha_{ht}^{n+1}} \prod_{k=1}^{m} \prod_{\substack{s=1 \\ ks\neq ht}}^{\rho(k)} \left(\frac{z-\alpha_{ks}}{\alpha_{ht}-\alpha_{ks}}\right).$$

Thus for any *u* we have by the above expressions

$$\alpha_h^u \sum_{t=1}^{\rho(h)} u^{t-1} \Delta_{i,ht} = \lim_{\substack{\alpha_{ks}\to\alpha_k \\ \text{all } ks}} \left(\prod_{k=1}^{m} \prod_{s=1}^{\rho(k)} \left(\alpha_{ks} \frac{\partial}{\partial \alpha_{ks}}\right)^{s-1} \right) \sum_{t=1}^{\rho(h)} \alpha_{ht}^u D_{i,ht},$$

and by Lemma 2, we see that it is the coefficient of z^{i-1} in the polynomial

$$\lim_{\substack{\alpha_{ks}\to\alpha_k \\ \text{all } ks}} \Delta \sum_{t=1}^{\rho(h)} \frac{1}{\alpha_{ht}^{n+1-u}} \prod_{k=1}^{m} \prod_{\substack{s=1 \\ ks\neq ht}}^{\rho(k)} \left(\frac{z-\alpha_{ks}}{\alpha_{ht}-\alpha_{ks}}\right). \qquad (3.2)$$

Similarly for *r* a positive integer, we get

$$\sum_{t=1}^{\rho(h)} \frac{(r-1)!}{(r-t)!} (\log \alpha_h)^{r-t} \Delta_{i,ht} = \lim_{\substack{\alpha_{ks}\to\alpha_k \\ \text{all } ks}} \left(\prod_{k=1}^{m} \prod_{s=1}^{\rho(k)} \left(\alpha_{ks} \frac{\partial}{\partial \alpha_{ks}}\right)^{s-1} \right) \sum_{t=1}^{\rho(h)} (\log \alpha_{ht})^{r-1} D_{i,ht},$$

which by Lemma 2 becomes the coefficient of z^{i-1} in the polynomial

$$\lim_{\substack{\alpha_{ks}\to\alpha_k \\ \text{all } ks}} \Delta \sum_{t=1}^{\rho(h)} \frac{(\log \alpha_{ht})^{r-1}}{\alpha_{ht}^{n+1}} \prod_{k=1}^{m} \prod_{\substack{s=1 \\ ks\neq ht}}^{\rho(k)} \left(\frac{z-\alpha_{ks}}{\alpha_{ht}-\alpha_{ks}}\right). \qquad (3.3)$$

From Lemma 1 and the shape of the linear form *H*, we must get a *p*-adic upper bound for the expression

$$q_i := \sum_{h=1}^{m} \sum_{t=1}^{\rho(h)} \frac{(r-1)!}{(r-t)!} (\log \alpha_h)^{r-t} \frac{\Delta_{i,ht}}{\Delta}, \ (1 \le i \le M).$$

We have observed that q_i is exactly the coefficient of z^{i-1} in the polynomial

$$Q(z) = \lim_{\substack{\alpha_{ks}\to\alpha_k \\ \text{all } ks}} \sum_{h=1}^{m} \sum_{t=1}^{\rho(h)} \frac{(\log \alpha_{ht})^{r-1}}{\alpha_{ht}^{n+1}} \prod_{k=1}^{m} \prod_{\substack{s=1 \\ ks\neq ht}}^{\rho(k)} \left(\frac{z-\alpha_{ks}}{\alpha_{ht}-\alpha_{ks}}\right).$$

At this point, we could of course derive a *p*-adic upper bound for the coefficients q_i directly from the shape of Q. However, a bound obtained in this way is weak and untidy. To obtain a clean and strong bound, we resort to the use of interpolation. Neglecting the limit for a moment, $Q(z)$ is exactly the polynomial of degree $M-1$ such that

$$Q(\alpha_{ht}) = \frac{(\log \alpha_{ht})^{r-1}}{\alpha_{ht}^{n+1}}, 1 \le h \le m; 1 \le t \le \rho(h). \qquad (3.4)$$

Taking the quantities α_{ht} as formally distinct, these conditions determine Q. We suppose that the distinct quantities α_{ht} lie (p-adically) arbitrarily close to the α_h $(1 \le h \le m)$. Still neglecting the limit in $Q(z)$, we write it as an interpolation series

$$Q(z) = b_{11} + b_{12}(z-\alpha_{11}) + b_{13}(z-\alpha_{11})(z-\alpha_{12}) + \ldots + b_{m\rho(m)}(z-\alpha_{11})\ldots(z-\alpha_{m,\rho(m)-1}) \quad (3.5)$$

By the conditions (3.4) defining *Q*, and by similar derivation as in Laohakosol and Pitman [1], we can represent the interpolation coefficients b_{ht} as Schnirelman integrals

$$b_{ht} = \int_{1,R} \frac{(\log z)^{r-1}(z-1)dz}{z^{n+1}(z-\alpha_{11})\cdots(z-\alpha_{ht})} \quad (1 \le h \le m, 1 \le t \le \rho(h)),$$

where the integrals are taken along the circle with center 1 and radius *R* with $p^{-1/(p-1)} < R < 1$. Here, the lower bound for *R* guarantees that all α_{ij} 's lie inside the circle, and the upper bound ensures that the point *O* lies outside. By uniform convergence (see [4]) of the series defining the integrals, the integrals all remain well-defined when the relevant limit is taken and indeed we can drop any implicit assumption that the α_h be distinct. We require by Lemma 1 to find an upper bound for the quantities

$$\left|q_i\right|_p \quad (1 \le i \le M).$$

Using the fact that $|\alpha_j|_p = 1$, from the equation (3.5), we have for $1 \le i \le M$

$$|q_i|_p = \max_{ht} |b_{ht}|_p = \max_{ht} \left| \int_{1,R} \frac{(\log z)^{r-1}(z-1)dz}{z^{n+1}(z-\alpha_{11})\cdots(z-\alpha_{ht})} \right|_p$$

$$\le \frac{R^{r-1}R}{1 \cdot R^{\rho(1)+\ldots+\rho(m)}} = R^{r-M},$$

because $|z-\alpha|_p = |(z-1)+(1-\alpha)|_p = R$. To get optimal bounds, we consider two separate cases.*Case* $r > M$. Since the inequality

$$\left|q_i\right|_p \le R^{r-M} \quad (i = 1,\ldots,M)$$

holds for all R satisfying $p^{-1/(p-1)} < R < 1$, taking here the limit as $R \to p^{-1/(p-1)}$, we have in this case

$$|q_i|_p \le R^{(M-r)/(p-1)} \quad (i = 1,\ldots,M).$$

Case $r \le M$. In this case we take the limit as $R \to 1$ to get

$$\left|q_i\right|_p \le 1 \quad (i = 1,\ldots,M).$$

Hence, by Lemma 1, there exists a rational integer *v* such that $1 \le v \le M$ and

$$\left|E(n+v)\right|_p \ge \begin{cases} p^{(r-M)/(p-1)} \left|E^{(r-1)}(0)\right|_p & \text{if } r > M, \\ \left|E^{(r-1)}(0)\right|_p & \text{if } r \le M. \end{cases}$$

We observe, moreover that by taking $r = 1$ (and so $r \le M$), and replacing n by $n-u$ in (3.3), we obtain the expression (3.2). Consequently, the corresponding linear forms are

$$H' = \sum_{h=1}^{m} \sum_{t=1}^{\rho(h)} \alpha_h^u u^{t-1} a_{ht} = E(u),$$

$$q_i' = \sum_{h=1}^{m} \sum_{t=1}^{\rho(h)} \alpha_h^u u^{t-1} \frac{\Delta_{i,ht}}{\Delta} \quad (i = 1,\ldots,M),$$

and the interpolation coefficients b_{ht}' take the form

$$b'_{ht} = \int_{1,R} \frac{(z-1)dz}{z^{n+1}(z-\alpha_{11})\cdots(z-\alpha_{ht})} \quad (1 \le h \le m, 1 \le t \le \rho(h))$$

with the same *R* as above. By the same arguments as for the case of q_i, we see that

$$\left|q'_i\right|_p \le 1 \quad (i = 1,\ldots,M).$$

Hence, we have proved

Theorem 1. *Let* $\alpha_1,\ldots,\alpha_m$ *be distinct elements of* $\mathbb{C}_p$ *satisfying*

$$|\alpha_j - 1|_p < p^{-1/(p-1)} \quad (j = 1,\ldots,m).$$

Denote by E the exponential polynomial

$$E(z) = \sum_{k=1}^{m} \sum_{s=1}^{\rho(k)} a_{ks} z^{s-1} \alpha_k^z \quad (|z|_p \le 1),$$

where $\rho(1),\ldots,\rho(m)$ *are non-negative integers with sum M, and* a_{ks} *are constants in* $\mathbb{C}_p$ *not all zero. Then for integers* $n \ge 0$ *and* $r \ge 1$, *we have*

$$\max_{n+1\le v\le n+M} \left|E(v)\right|_p \ge \begin{cases} p^{(r-M)/(p-1)} \left|E^{(r-1)}(0)\right|_p & \text{if } r > M, \\ \left|E^{(r-1)}(0)\right|_p & \text{if } r \le M, \end{cases}$$

and for any rational integer $u \le n$, *we have*

$$\max_{n+1\le v\le n+M} |E(v)|_p \ge |E(u)|_p .$$

An immediate consequence is the following

Corollary 1. *Let the notation be as in Theorem 1. Then*

$$\max_{n+1\le v\le n+M} \left|\sum_{k=1}^{m} a_k \alpha_k^v\right|_p \ge \left|a_1 + \ldots + a_m\right|_p .$$

Before proceeding to our next result, we make the following remarks.

Remarks.

1. Corollary 1 is another version of *p*-adic Turán's theorem. In this *p*-adic case, since $|\alpha_j|_p = 1$ for all *j*, the distinction between the two main theorems of Turánin the classical case (see [5]) disappears.

2. The condition that $|\alpha_j - 1|_p < p^{-1/(p-1)} = 1$ for all *j* is necessary to make α_j^z a well-defined analytic function of *z* with $|z|_p \le 1$. It seems restrictive if one only aims at proving Corollary 1; indeed in Theorem 3 of Laohakosol and Pitman [1], there is no such restriction. However, by a result of Cassels [6] there are infinitely many *p*-adic fields $\mathbb{Q}_p$ for which all α_j's $(j = 1,\ldots,m)$ can be embedded as *p*-adic units, i.e. $|\alpha_j|_p = 1$ for all *j*. Moreover being *p*-adic units, by a well-known result (see [7]), there exists a positive integer *d* such that

$$|\alpha_j^d - 1|_p < p^{-1/(p-1)} \quad (j = 1,\ldots,m).$$

Consequently, by considering α_j^d instead of α_j, we have an abundant supply of *p*-adic fields to work with.

3. It should be observed that the estimates in the *p*-adic case here are much easier to compute than the corresponding ones in the classical case; as a by-product we do not have to bound the values of *r* from above to get an optimal bound as in the classical case (see [2]). As to the values of *n* in Theorem 1, the condition $n \ge 0$ is mainly imposed so that the determinants involved are non-zero.

4. The bounds obtained in Theorem 1 and Corollary 1 cannot in general be improved as the following examples show.

(i) Let $p \neq 2$, and let

$$E_1(z) = 1-(1+p)^z.$$

Then

$$\max_{0+1\le v\le 0+2} \left| E_1(v) \right|_p = \max\left(|\, p \,|_p, |\, p^2+2p \,|_p \right) = |\, p \,|_p$$
$$= \left| \log(1+p) \right|_p = \left| E_1'(0) \right|_p = \left| E_1^{(2-1)}(0) \right|_p .$$

(ii) Let $p \neq 2$, and let

$$E_2(z) = (1+p)^2 + (1-p)^z.$$

Then

$$\max_{0+1\le v\le 0+2} \left| E_2(v) \right|_p = 1 = |\, 1+1 \,|_p .$$

Next, we prove

Theorem 2. *Let $\alpha_1,\ldots,\alpha_m$ be distinct elements in $\mathbb{C}_p$ satisfying*

$$\left|\alpha_j - 1\right|_p < p^{-1/(p-1)} \quad (j=1,\ldots,m).$$

Let E be the exponential polynomial

$$E(z) = \sum_{k=1}^{m} \sum_{s=1}^{\rho(k)} a_{ks} z^{s-1} \alpha_k^z \quad (\left|z\right|_p \le 1),$$

where $\rho(1),\ldots,\rho(m)$ are non-negative integers with sum M, and a_{ks} $(1\le k\le m, 1\le s\le \rho(k))$ are constants in $\mathbb{C}_p$ not all zero. Further, let

$$\delta = \min_{\substack{1\le j,h\le m \\ j\neq h}} \left|\alpha_h - \alpha_j\right|_p ,$$
$$\rho = \max_{1\le k\le m} \rho(k).$$

Then if n is a nonnegative integer, we have, for each ht $(1\le h\le m, 1\le t\le \rho(h))$,

$$\max_{n+1\le v\le n+M} \left|E(v)\right|_p \ge \left|a_{ht}\right|_p \delta^{3m^2\rho^2/2-5m\rho/2+2} p^{-m\rho(\rho-1)/2(p-1)}.$$

Remark The value of δ, though non-zero, is usually very small because

$$0 < \delta \le |\, \alpha_h - \alpha_j \,|_p = |\, (\alpha_h - 1) - (\alpha_j - 1) \,|_p < p^{-1/(p-1)} \ , h \neq j.$$

Proof Here, we consider the linear form *H* in Lemma 1 to be a linear polynomial in one variable

$$H(y_{ht}) = y_{ht}$$

for a certain index *ht*. By Lemma 1, we need an upper bound for $\left| \Delta_{i,ht} / \Delta \right|_p$ because

$$\max_{1\le v\le M} \left| E(n+v) \right|_p \ge \left| a_{ht} \right|_p \cdot \max_{1\le v\le M} \left|\Delta / \Delta_{i,ht}\right|_p .$$

As pointed out in [2], the shape of this last polynomial is quite complicated, and we have no hope of using interpolation to derive a neat bound. Therefore, we instead compute directly a *p*-adic lower bound for Δ and an upper bound for $\Delta_{i,ht}$. To obtain a *p*-adic upper bound for $\Delta_{i,ht}$, we note the following:

- first, a *p*-adic upper bound for the coefficients of z^j $(1 \le j \le M)$ in $\prod_{k=1}^{m}\prod_{\substack{s=1\\ks\neq ht}}^{\rho(k)}\left(\frac{z-\alpha_{ks}}{\alpha_{ht}-\alpha_{ks}}\right)$ is $\delta^{-m\rho+1}$;
- second, by the shape of *D*, and $\left|\alpha_j\right|_p = 1$ for all j, we get $\left|D/\alpha_{ht}^{n+1}\right|_p \le 1$.

Thus, a *p*-adic upper bound for the coefficients (of z^j) in $D\alpha_{ht}^{-n-1}\prod_{k=1}^{m}\prod_{\substack{s=1\\ks\neq ht}}^{\rho(k)}\left(\frac{z-\alpha_{ks}}{\alpha_{ht}-\alpha_{ks}}\right)$ is $\delta^{-m\rho+1}$.

Now each partial derivative $\alpha\frac{\partial}{\partial\alpha}$ increases the *p*-adic upper bound for the coefficients at most by a factor of $1/\delta$. Therefore, a *p*-adic upper bound for the coefficients is

$$\prod_{k=1}^{m}\prod_{\substack{s=1\\ks\neq ht}}^{\rho(k)}\delta^{-m\rho+1-s+1} \le \delta^{(-m\rho+2)(m\rho-1)}\prod_{k=1}^{m}\delta^{-\rho(k)(\rho(k)+1)/2}$$

$$\le \delta^{(-m\rho+2)(m\rho-1)}\delta^{-\rho(\rho+1)m/2} = \delta^{-\rho^2(m^2+m/2)+5m\rho/2-2}.$$

Now from the shape of Δ in equation (3.1), we have

$$\left|\Delta\right|_p \ge \prod_{k=1}^{m}\prod_{s=1}^{\rho(k)}\left(p^{(-s+1)/(p-1)}\delta_k^{\rho(1)+\cdots+\rho(k-1)}\right)$$

$$\ge \prod_{k=1}^{m}\left(p^{-(\rho(k)-1)/2(p-1)}\delta^{\rho(1)+\cdots+\rho(k-1)}\right)^{\rho(k)} \ge \delta^{m(m-1)\rho^2/2}p^{-m\rho(\rho-1)/2(p-1)}.$$

Combining these estimates, the required result follows.

An immediate consequence of Theorem 2 is the following:

Corollary 2. *Let the notation be as in Theorem 2. Then for some positive integer* h $(1 \le h \le m)$, *we have*

$$\max_{n+1\le v\le n+m}\left|\sum_{k=1}^{m}a_k\alpha_k^v\right|_p \ge \left|a_h\right|_p\delta^{(3m^2-5m+4)/2}.$$

References

[1] Laohakosol, V. and Pitman, J., 1981. Applications of *p*-adic interpolation to exponentialpolynomials and sum of powers. *Journal of Australian Mathematical Society*, (Ser. A) 30,419-437.

[2] van der Poorten, A.J., 1970. Generalisations of Turán's main theorems on lower bounds for sums of powers. *Bulletin of the Australian Mathematical Society*, 2, 15-37.

[3] van der Poorten, A.J., 1976. Some determinants that should be better known. *Journal of Australian Mathematical Society*, (Ser. A) 21, 278-288.

[4] Adams, W.W., 1966. Transcendental numbers in the *p*-adic domain, *American Journal of Mathematics*, 88, 279-308.

[5] Turán's, P., 1953. *Eine neue Methode in der Analysis und deren Anwendungen* Akademiai Kiado: Budapest.

[6] Cassels, J.W.S., 1976. An embedding theorem for fields. *Bulletin of the Australian Mathematical Society*, 14, 147-168.

[7] Amice, Y., 1959. Analyse *p*-adiques. *Seminaire Delange-Pisot*, 1, 63.

Current Applied Science and Technology Vol. 18 No. 2 May-August 2018
DOI: 10.14456/cast.2018.3

Antioxidant and Antihyperglycemic Activities of Four Edible Lentinus Mushrooms

Wimolpun Rungprom*

Department of Chemistry, Faculty of Science and Technology,
Phranakhon Si Ayutthaya Rajabhat University, Ayutthaya, Thailand

Received: 4 July 2017, Revised: 5 July 2018, Accepted: 13 July 2018

Abstract

Four Lentinus mushrooms: *Lentinus edodes*, *Lentinus polychrous, Lentinus sajor-caju,* and *Lentinus squarrosulus* were investigated for their chemical compositions as well as their antioxidants and hyperglycemic activities. The chemical composition of Lentinus mushrooms contained total phenolic and total flavonoid contents, normally used as an indirect measurement of antioxidant capacity. Scavenging activity on DPPH radicals and FRAP assays were used for confirming antioxidant activity while assays of α-glucosidase inhibitory activity were used for evaluating antihyperglycemic activity in these mushroom extracts. The highest amount of total phenolic content (TPC) displayed in the extract of *L. squarrosulus* which correlated well with antioxidant properties of mushroom extracts indicated by DPPP and FRAP assays. It is firstly reported herein on α-glucosidase inhibitory activity in Lentinus mushrooms, in which *L. polychrous* revealed the highest inhibitory activity (IC_{50} value 39.59±0.01 μg/mL) and correlated well with total flavonoid compound.

Keywords: α-glucosidase inhibitor, *Lentinus edodes*, *Lentinus polychrous, Lentinus sajor-caju L. squarrosulus*, antihyperglycemic, antioxidation

1. Introduction

Nowadays, mushrooms are not only intended to satisfy consumers and provide essential nutrients, but also to prevent disease and improve their physical and mental well-being. Edible mushrooms characteristically contain many different bioactive compounds such as polysaccharide, amino acid, glycolipid, terpenoid, and so on with highly diverse biological activities like anticancer, antibacterial, antifungal and immunomodulatory potential [1, 2]. Some advantages of using edible mushrooms over plants as sources of bioactive compounds are that mushrooms can be produced in much less time, and can be manipulated to produce optimal quantities of active compounds [3-5]. Apart from the research of potent α- glucosidase inhibitors from alternative sources such as fungi and others microorganisms, Lentinus mushrooms which were identified as rich sources of nutrients and popular consumption in Thailand were selected for this study. Four Lentinus mushrooms: *L. edodes*, *L. polychrous, L. sajor-caju* and *L. squarrosulus* belong to Family Polyporaceae, are recognized as many as 40 species over the world [6,7]. Chemical composition and the potential of antioxidant activity of the four Lentinus mushrooms and the effect of extract on the activity of α–glucosidase were investigated in this study.

*Corresponding author: E-mail: rwimon@aru.ac.th

2. Materials and Methods

2.1 Materials

All four Lentinus mushrooms which have fully cap of fruiting body or were in harvest stage were cultivated in local mushroom farm in Amphor U-thai, Phranakhon Si Ayutthaya, Thailand and preserved in cellophane bags with air tight conditions. Taxonomic identification was done following the description of Pegler [8]. Mushroom specimens were deposited at Herbarium of Science and Technology Center, Phranakhon Si Ayutthaya Rajabhat University, Thailand.

2.2 Extraction

The fruiting bodies of these four edible Lentinus mushrooms (500 g) were collected, cleaned and air-dried before grinding and soaking in the extraction solvent for 24 h. Each mushroom was stirred with 80% ethanol (250 mLx4) at 25°C for 24 h, and then filtered through Whatman filter paper No.4. The ethanol extract was then evaporated under reduced pressure to yield ethanolic extracts. The dried extracts were resuspended in ethanol and stored at 4 °C for analyses of total flavonoid contents and α-glucosidase.

2.3 Total phenolic compound analysis

The total phenolic contents of the extract were determined using a modified version of the Folin-Ciocalteu method [9]. The extract (0.1 ml) was mixed with 50 µl of 2 N Folin Ciocalteu reagent, and allowed to stand for 3-5 min at room temperature before adding 0.3 ml of 20% Na_2CO_3 to the mixture. After leaving for 15 min at room temperature, 1 ml of distilled water was added. The absorbance was measured at 725 nm using a UV-spectrometer. Total phenolic was quantified by calibration curve obtained from measuring the absorbance of gallic acid standard. The concentration was expressed as mg of gallic acid equivalents per gram of extract [10].

2.4 Total flavonoid contents analysis

The total flavonoid content of the extract was determined according to the colorimetric method as described by Moreno *et al* [11]. Each extract (0.5 ml) was added to test tubes containing 0.1 ml of 10% $Al(NO_3)_3$ (w/v), 1 M of CH_3COOK and 4.3 ml of 80% ethanol. After incubation for 40 min at room temperature, the absorbance was determined at 415 nm. The total flavonoid content was expressed in milligrams of quercetin equivalents (QE) per gram of extract.

2.5 DPPH assay

The DPPH (2, 2-diphenylpicrylhydrazyl) assay [12] was used to determine the free radical scavenging activity of mushroom extracts. Each mushroom extract in ethanol was mixed with 1 ml of methanolic solution containing DPPH radicals, resulting in a concentration of 0.2 mM DPPH. The mixture was shaken vigorously and left to stand for 30 min in dark condition, and the absorbance was then measured at 517 nm. The DPPH free radical scavenging activity was expressed in the percentage inhibition which was calculated by $[(A_0-A_1)/A_0] \times 100$, where A_0 is the absorbance without the sample, and A_1 is the absorbance with the sample.

2.6 FRAP assay

The reducing power was recorded while FRAP (Ferric reducing antioxidant power assay) was determined according to the method described by Benzie and Strain [13] with some modifications by Jeong *et al*. [14]. The stock solutions included 300 mM acetate buffer, pH 3,6,10 mM TPTZ (2, 4, 6-tripyridyl-s-triazine) solution in 40 mM HCl, and 20 mM $FeCl_3.6H_2O$ solution. The fresh working solution included 40 mM HCl, 20 mM TPTZ solution, and 2.5 ml $FeCl_3.6H_2O$ solution and was warmed at 37 °C. The mushroom tested sample was then mixed with 0.5 ml extracts and allowed to react with FRAP solution for 30 min in dark condition. The colored product (Ferrous

tripyridyltriazine complex) was undertaken at 539 nm absorbance. The standard curve was linear between 25 and 800 nM Trolox (6-hydroxyl-2,5,7,8-tetramethylchroman-2-carboxylic acid). The results were expressed in mM TE (Trolox equivalent antioxidant capacity) perform of dried mushrooms.

2.7 α-Glucosidase assay

An inhibitory effect against α-glucosidase (from baker's yeast) was performed using the modified protocol previously reported [15-17]. Briefly, the α-glucosidase (0.1 U/mL) and substrate (1 mM *p*-nitrophenyl-α-D-glucopyranoside) were dissolved in 0.1 M phosphate buffer, pH 6.9. A 10 μL of test compound (1 mg/mL in DMSO) was incubated with 40 μL of α-glucosidase at 37 ºC for 10 min. A 50 μL substrate solution was then added to the reaction mixture and incubated at 37 ºC for additional 20 min. The reaction was terminated by adding 100 μL of 1 M Na_2 CO_3. Enzymatic activity was quantified by measuring the absorbance at 405 nm (Bio-Red microplate reader model 3550 UV). The percentage inhibition was calculated by $[(A_0-A_1)/A_0] \times 100$, where A_0 is the absorbance without the sample, and A_1 is the absorbance with the sample. The IC_{50} value was determined from a plot of percentage inhibition versus sample concentration. Acarbose was used as a standard control and the experiment was performed in triplicate.

2.8 Data Analysis

The concentrate of tested compounds required to inhibit 50% of the α-glucosidase activity under the assay conditions was determined from dose-response curves and defined as IC_{50} value. Each value means SD of triplicate determinations. Mean separation within columns was done by Duncan's multiple range test at 0.1% level and significant differences of these data were calculated using analysis of variance (ANOVA).

3. Results and Discussion

The ethanolic extract yields from four Lentinus mushrooms were 3.11±0.001, 4.45±0.003, 3.20±0.004 and 1.99±0.006 mg/g dried weight mushroom in *L. edodes*, *L. polychrous, L. sajor-caju* and *L.squarrosulus*, respectively, as shown in Figure 1. The extract yields were in agreement with the finding of previous report by Attarat and Phermthai [4].

The ethanolic extracts of Lentinus mushrooms were analyzed for the total phenolic content (TPC) and total flavonoid content (TFC). Phenolic and flavonoid exhibited a wide range of biological effects such as antioxidation, antibacterial, antiinflammatory and antihyperglycemic. In this study, TPC used as indirect testing of antioxidant capacity in Lentinus mushrooms extracts. Total phenolic and flavonoid compounds in Lentinus mushrooms extracts are presented in Table 1.

The extract of *L. squarrosulus* contained the highest amount of TPC at 300.5±0.6 mg GAE/g. The finding was very similar to that of previous report [4] and for TFC, it was firstly reported in Lentinus mushrooms with *L. Polychrous* presenting the highest amount of TFC at 120.9±0.2mg QE/g. In addition, TPC of mushroom extract was also used as an indirect measure of antioxidant capacity that was further revised by different assays as DPPH and FRAP assays. Thus, the antioxidant properties as percentage inhibition of DPPH of Lentinus mushroom extracts were showed in Figure 2.

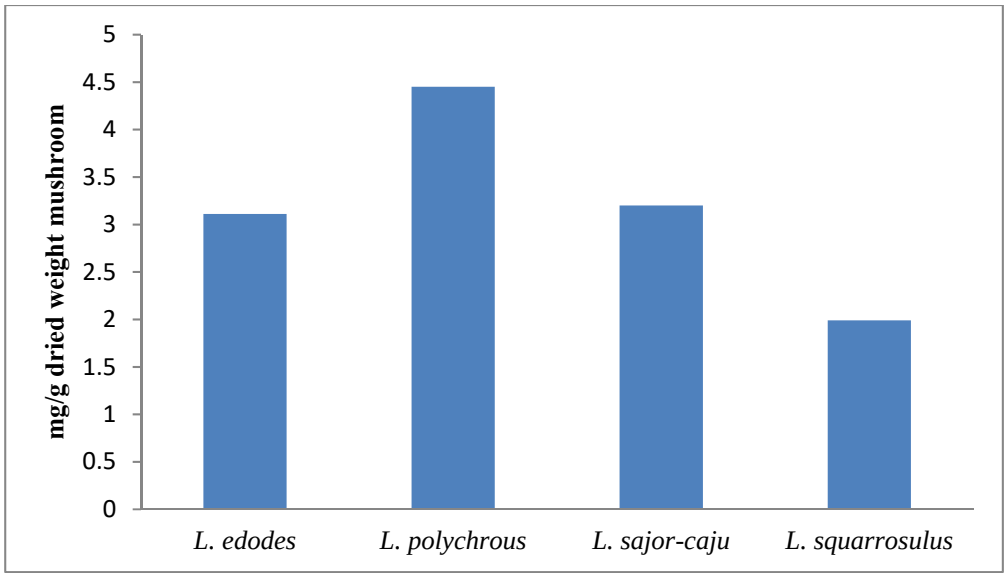

Figure 1. The ethanolic extract yields from four Lentinus mushrooms

Table 1. Total phenolic and total flavonoid contents in extracts of Lentinus mushrooms

Species	TPC* (mg GAE/g)	TFC** (mg QE/g)
L. edodes	140.1±0.2c	62.8±0.1c
L. polychrous	120.1±0.1d	120.9±0.2a
L.sajor-caju	196.0±0.3b	112.2±0.4b
L. squarrosulus	300.5±0.6a	19.18±0.6d

*Total phenol content analysed as gallic acid equivalent mg/g of extract, values are averages of triplicates.
**Total flavonoid content analysed as quaercetin equivalent mg/g of extract, values are averages of triplicates.
Note Different letters within the same column means significantly different ($P \leq 0.1$)

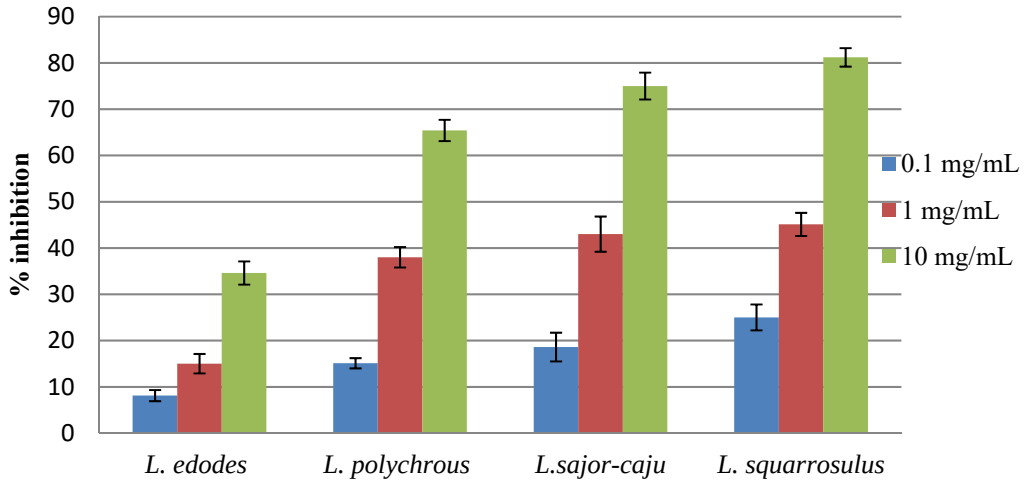

Figure 2. Percentage inhibition of DPPH radical of Lentinus mushrooms

Among the Lentinus mushroom extracts, *L. squarrosulus* showed the highest percentage inhibition of DPPH in all concentrations which were dose-dependent inhibition. At a concentration of 1.0 mg/mL the percentage inhibition of DPPH of *L. polychrous, L. sajor-caju and L. squarrosulus* was about 38, 43 and 45.1%, respectively.

The FRAP assay was expressed by comparison of micromolar of trolox equivalent per gram dried mushroom as shown in Figure 3. The extract of *L. squarrosulus* showed 94.1 μM TE/g dried mushroom suggesting that it was more potent antioxidant than other extracts. This data was correlated with TPC and DPPH assays.

Additionally, the antihyperglycemic properties were evaluated in Lentinus mushroom extracts which were carried out by α-glucosidase inhibitory activity as shown in Table 2. Acarbose was used as the positive control in the treatment of diabates millitus as α-glucosidase inhibitor. The extracts of *L. polychrous and L. squarrosulus* revealed α- glucosidase inhibitory activities with IC_{50} 39.59±0.01 and 46.24±0.02 at 10 mg/mL while the extracts of *L. edodes* and *L. sajor-caju* revealed α- glucosidase inhibitory activities less than 30%.

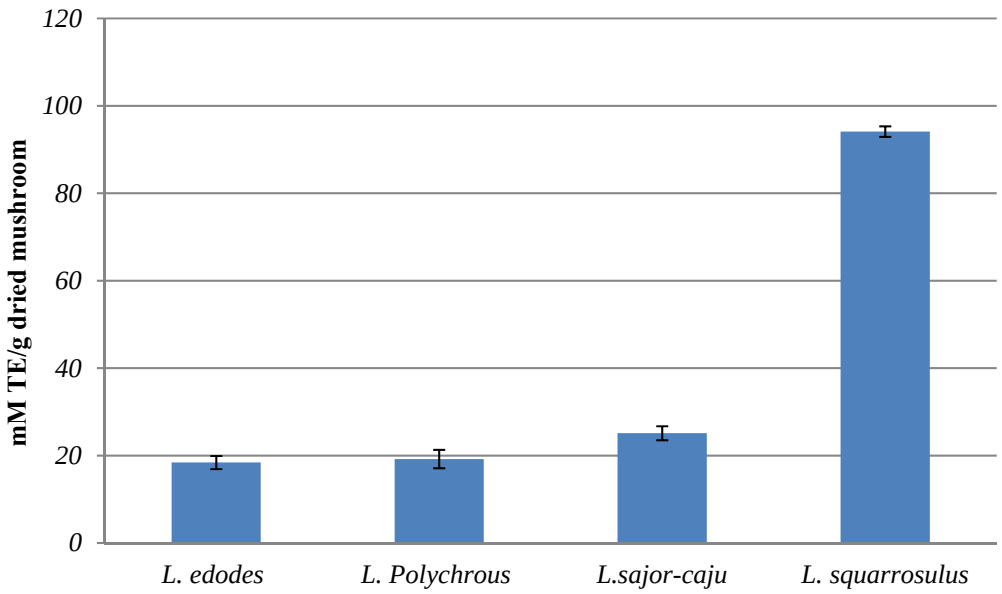

Figure 3. FRAP assay, expressed in μM Trolox equivalent antioxidant capacity

Table 2. Inhibitory activity of α- Glucosidase in Lentinus mushrooms

Extract	IC_{50} (μg/mL)*
L. edodes	NI
L. polychrous	39.59±0.01
L. sajor-caju	NI
L. squarrosulus	46.24±0.02
Acarbose	52.29

*NI= No inhibition, inhibitory effect less than 30% at 10 mg/mL.

4. Conclusions

Four Lentinus mushrooms: *L. edodes*, *L. polychrous L.* sajor-caju and *L. squarrosulus* contained high amount phenolic compounds which were antioxidants that correlated well with DPPH and FRAP assays. Both assays used a similar mechanistic basis, the electrons were transferred from antioxidant in order to reduce an oxidation reaction. However, the evaluation of these antioxidants has to be confirmed by other assays. This research firstly reported on α- glucosidase inhibitory activity in Lentinus mushrooms, in which *L. polychrous* gave the highest inhibitory activity with IC_{50} value of 39.59±0.01 μg/mL. Two mushrooms, *L. polychrous* and *L. squarrosulus* were highly effective in antioxidation and antihyperglycemia. In addition, the highest total flavonoid contents of *L. Polychrous* showed highest α-glucosidse inhibitory activity, indicating the correlation of flavonoids to α-glucosidase activity. Therefore, the richness of bioactive components in these mushrooms make them appropriate for functional food and nutritional supplements.

5. Acknowledgements

This work was supported by the Commission of Higher Education, CHE IG Project and Rajabhat Phranakhon Si Ayutthaya Research Fund.

References

[1] Lui, Y.T., Sun, J., Luo, Z.U., Rao, Z.Q., Su, Y.J., Xu, R.R. and Yang, Y.J., 2012. Chemical composition of five wild edible mushrooms collected from southwest China and their antihyperglycemic and antioxidant activity. *Food and Chemical Toxicology,* 50, 1238-1244.

[2] Ayodele, S.M., and and Idoko, M.E., 2011. Antimicrobial activities of four wild edible mushrooms in Nigeria. *International Journal of Science and Nature*, 2, 1, 55-59.

[3] Ren, L., Hemar, Y., Perera, C.O., Lewis, G., Krissansen, G.W. and Buchanan, de K,P., 2014. Antibacterial and antioxidant activitis of aqueous extract of eight edible mushrooms, *Bioactive Carbohydrates and Dietary Fibre*, 3, 41-51.

[4] Attarat, R., and Phermthai, T., 2015. Bioactive compounds in three edible Lentinus mushrooms, *Walailak Journal of Science and Technology*, 12(6), 491-504.

[5] Sharma, S.K. and Atri, N.S., 2014. Nutraceutical composition of wild species of genus *Lentinus* Fr. from northern India. *Current Research in Environmental&Applied Mycology,* 4, 11-32.

[6] Ayodele, S.M. and Idoko, M.E., 2011. Antimicrobial activities of four wild edible mushrooms in Nigeria. *International Journal of Science and Nature*, 2(1), 55-59.

[7] Ren, L., Hemar, Y., Perera, C.O., Lewis, G., Krissansen, G.W. and Buchanan. de K, P., 2014. Antibacterial and antioxidant activitis of aqueous extract of eight edible mushrooms, *Bioactive Carbohydrates and Dietary Fibre*, 3, 41-51.

[8] Pegler, D.N., 1983. The genus *Lentinus*: A new monograph. *Kew Bulletin Additional Series X*, 10,1, 281, Royal Botany Garden, Kew.

[9] Taga, M.S., Miller, E.E. and Pratt, D.E., 1984. Chai seed as a source of natural lipid antioxidants, *Journal of American Oil Chemistry Society*, 61, 928-31.

[10] Jeong, H.J., Kim, J. S., Hyun, T.K., Yang, J.F., Kang, H.H., Cho, J.C., Yeom, H.M. and Kim, J.M., 2013. In vitro antioxidant and antidiabetic activities of *Rehmannia glutinosa* tuberous root extracts, *Science Asia*, 39, 605-609.

[11] Moreno, M.I., Isla, M.I., Sampietro, A.R. and Vattuone, M.A., 2000. Comparison of the free radical scavenging activity of propolis from several regions of Argentina, *Ethnopharmacol*, 71, 109-114.

[12] Bloise, M.S., 1958. Antioxidant determination by the use of stable free radicals, *Nature*, 181, 1199-2000.

[13] Benzie, I.F.F. and Strain, J.J., 1996. The ferric reducing ability of plasma (FRAP) as a measure of "antioxidant power": the FRAP assay, *Analytical Biochemistry*, 239, 70-76.

[14] Jeong, H.J., Kim, J. S., Hyun, T.K., Yang, J.F., Kang, H.H., Cho, J.C., Yeom, H.M. and Kim, J.M., 2013. In vitro antioxidant and antidiabetic activities of *Rehmannia glutinosa* tuberous root extracts, *Science Asia*, 39, 605-609.

[15] Phuwapraisirisan, P., Puksasook, T., Jong-aramruang, J. and Kokpol, U., 2008. Phenylethyl cinnamides: A new series of α-glucosidase inhibitors from the leaves of *Angle marmelos*, *Bioorganic & Medicinal Chemistry Letters*, 18, 4956-4958.

[16] Wikul, A., Damsud, T., Kataoka, K. and Phuwapraisirisan, P., 2012. (+)-Pinoresinol is a putative hypoglycemic agent in defatted sesame (*Sesamum indicum*) seeds though inhibiting α-glucosidase. *Bioorganic & Medicinal Chemistry Letters*, 22, 5215-5217.

[17] Worawalai, W., Wacharasindhu, S. and Phuwapraisirisan, P., 2012. Synthesis of new *N*-substituted aminoquercitols from naturally available (+)-*proto*-quercitol and their α-glucosidase inhibitory activity. *Medicinal Chemistry Communications*, 3, 1466-1470.

Current Applied Science and Technology Vol. 18 No. 2 May-August 2018
DOI: 10.14456/cast.2018.4

Characterization, Functionality and Antioxidant Activity of Water-Soluble Proteins Extracted from *Bombyx mori* Linn.

Niphattha Chatsuwan, Yuporn Puechkamut and Praphan Pinsirodom*

Faculty of Agro-Industry, King Mongkut's Institute of Technology Ladkrabang, Ladkrabang, Bangkok, Thailand

Received: 10 July 2018, Revised: 20 July 2018, Accepted: 1 August 2018

Abstract

The yield of water-soluble protein extracted from silkworm pupae, *Bombyx mori* Linn. (WSPB) was 3.96% by wet weight basis. The major amino acids found in WSPB were glutamic acid, which was the most abundant, followed by histidine, phenylalanine and glycine in that order. The electrophoretic study revealed that proteins with MW of 37, 64 and 75 kDa were the major protein components in WSPB. Based on FTIR analysis, WSPB remained its structural integrity. The surface hydrophobicity, free and total sulfhydryl group contents were 3.52, 22.17 μmol/g and 23.08 μmol/g, respectively. WSPB was highly solubilized in the pH range of 5-11. WSPB exhibited poor emulsifying properties and foaming capacity but the foam stability was comparable to bovine serum albumin (BSA). WSPB had high antioxidant potential, based on DPPH$^{\bullet}$, ABTS$^{\bullet+}$ and FRAP assay. Therefore, protein from silkworm pupae is a potential source of antioxidant and can be served as an ingredient in processed foods to enhance its desired functionality and nutritional value.

Keywords: Characterization, Functionality, Antioxidant activity, Water-soluble protein, Edible insect, *Bombyx mori* Linn.

1. Introduction

Silkworm pupae (*Bombyx mori* Linn.) are considered a good food source for humans because of their high nutritional value [1]. They have been consumed in many Asia countries including Thailand, China, Korea, Japan and India. Silkworm pupae are the main by-product of the silk industry and constitute 60% of dry cocoon weight after extracting threads [2]. The nutritional value of silkworm pupae is rich in lipids (20.1% wt) and protein (12% wt), exhibiting the high levels of essential amino acids such as valine, methionine and phenylalanine [3]. Several studies have shown that silkworm pupae contain 45 to 55% protein (18 amino acids, including 8 essential amino acids) on a dry matter basis. Four kinds of protein components have been identified in silkworm pupae which albumin was found to be the highest at 27.24%, followed by glutelin at 23.72%, prolamine at 11.82% and globulin at 4.21%, respectively [4]. The hydrolysate of albumin was determined with the highest angiotensin-converting enzyme (ACE) inhibiting effect, followed by globulin. Inhibiting ACE could be decreased hypertension, which recognized as a serious risk factor for cardiovascular diseases [4]. This means that it is a good-quality protein source and a good source of bioactive peptides [4, 5].

*Corresponding author: Tel.: +66-2329-8000 ext. 7250 Fax: +66-2329-8526
E-mail: praphan.pi@kmitl.ac.th

Proteins can be added to foods to improve their functional properties such as solubility, emulsifying and foaming properties [6]. Park *et al.* [7] also determined the effects of adding flour made from silkworm pupae to meat batter. They found that combining the flour with transglutaminase improved the physicochemical properties of meat batter. Kim *et al.* [8] found that adding *B. mori* pupae flour to emulsion sausages increased their cooking yield and hardness. *B. mori* pupae have many biomedical advantageous for humans including controlling blood glucose level, improving male sexual function and enhancing memory [9, 10]. Wu *et al.* [1] postulated that animal proteins may have other health benefits, in addition to energy and nutritional functions, including enzyme (ACE) antioxidant activity and free radical-scavenging. Generally, *B. mori* are well known, easily obtained and a favorite in Thailand and are reported to be high in minerals, fatty acids and protein [11, 12]. The aim of this investigation was therefore to study on the characteristics, functional properties and antioxidant activities of water-soluble proteins from silkworm pupae (*B. mori*), in order to determine whether they are a good source of protein that could be extracted and used as a food ingredient.

2. Materials and Methods

2.1 Protein extraction

Frozen silkworm pupae (*B. mori*) was obtained from a commercial supplier (Mr. BUC FOOD, Ayutthaya, Thailand) was blended with cold water (4°C) at a ratio of 1:4 w/v for 15 min using blender (MMB54G5S, BOSCH, Germany) and stirred overnight at 4°C, to ensure that the proteins were dissolved. The suspension was centrifuged at 12,500 g for 30 min at 4°C. After centrifugation, the sample was separated to 3 layers. The top layer was fat layer. The middle layer contained water soluble protein fraction. The bottom layer was undissolved components. Then, the middle layer, containing water soluble protein fraction was collected, freeze-dried and referred to as "water-soluble protein from *B. mori*: WSPB". Extraction was performed in triplicate and the protein content of the extract was determined by Kjeldahl method [13].

2.2 Yield and efficiency of extraction

The yield of WSPB was calculated as a percentage of the weight of WSPB powder in comparison with the weight of *B. mori* before extraction and was calculated as follows:

Yield (%) = (weight of WSPB (g) / weight of sample (g)) × 100.

Extraction efficiency was calculated as a percentage of the total protein extracted from *B. mori* of WSPB in comparison with the content of total protein content in *B. mori* in which determined by Kjeldahl method [13]. The extraction efficiency of WSPB was calculated as follows:

Extraction efficiency (%) = (total extracted protein of WSPB (g) / total protein content of *B. mori* (g)) × 100.

2.3 Characterization of WSPB

2.3.1 Amino acid analysis

The amino acid composition of WSPB was determined by The Central Instrument Facility at Mahidol University, Bangkok, Thailand. The analysis was performed using HPLC (Waters Alliance 2695 with heater, Jasco FP2020 fluorescence detector (EX: 250 and EM: 395 nm)) with a Hypersil gold column C18 (4.6×150 mm, 3µm) at 35°C. Amino acid standards (Sigma-Aldrich, USA) were used for calibration.

2.3.2 Sodium dodecyl sulfate-polyacrylamide gel electrophoresis (SDS-PAGE)

SDS-PAGE was performed according to the method of Laemmli [14] with slight modifications. The samples (3 g) were mixed with 27 mL of 5% SDS, heated at 85°C for 1 h, then centrifuged at 8,500

g for 5 min using a centrifuge (5804 R Eppendorf, Germany) to remove undissolved debris. The supernatant was collected and mixed at 1:1 (v/v) ratio with the sample buffer (0.5 M Tris–HCl, pH 6.8, containing 4% (w/v) SDS, 20% (v/v) glycerol and 0.3% (w/v) bromophenol blue) for non-reducing condition and in the presence of 10% (v/v) β-ME for reducing condition. Samples (15 µg protein, determined by Biuret method) were loaded onto a polyacrylamide gel made of 10% separating gel and 4% stacking gel and subjected to electrophoresis at a constant current of 20 mA/gel, using an electrophoresis apparatus (AE-6440, Atto Co., Tokyo, Japan). After electrophoresis, gels were fixed with a mixture of 50% (v/v) methanol and 10% (v/v) acetic acid for 45 min, followed by staining with 0.05% (w/v) Coomassie Blue R-250 in 15% (v/v) methanol and 5% (v/v) acetic acid for overnight with constant shaking. Finally, gels were destained with the mixture of 30% (v/v) methanol and 10% (v/v) acetic acid until clear background was obtained. The molecular weight protein standard markers, using Precision Plus Protein™ Unstained Standard (10-250 kDa) (Bio-Rad, CA, USA) were run in the same manner used to estimate the molecular weight of proteins. Gels were imaged using a scanner (MFC-L2700DW, Brother, UK) and band intensities were quantified with the public domain digital analysis software, ImageJ (ImageJ 1.51t, National Institutes of Health, Bethesda, USA).

2.3.3 Fourier transform infrared spectroscopy (FTIR)

FTIR spectrum of WSPB was determined by Scientific Instrument Centre at King Mongkut's Institute of Technology Ladkrabang, Bangkok, Thailand. The analysis was performed using a Nicolet Model 6700 FT-IR Spectrometer (Thermo Scientific, Germany). Spectrum was acquired at a resolution of 4 cm^{-1} and the measurement range was 4000–400 cm^{-1} at room temperature. Automatic signals were collected in 32 scans and evaluated against a background spectrum recorded from the clean, empty cell at 25°C.

2.3.4 Determination of surface hydrophobicity

Surface hydrophobicity of the WSPB samples was determined using a fluorescence probe 1-anilino-8-naphathalenesulfonate (ANS) following the method described by Malik *et al.* [15] with some modifications. WSPB was prepared at concentrations in the range of 0.05-0.5 mg/mL with a phosphate buffer (0.1 M, pH 7). 20 µL of ANS (8.0 mM in phosphate buffer 0.01 M, pH 7) was added to 4 mL of WSPB solution, vortexed and kept in the dark for 15 min. Relative fluorescence intensity (RFI) of both the buffer (blank) and each protein solution (from the lowest to the highest concentration) was measured using a fluorescence spectrometer (F-2700, Hitachi, Japan) at 390 nm (excitation wavelength) and 480 nm (emission wavelength), with a scanning speed of 5 nm s^{-1}. RFI of each dilution bank was subtracted from corresponding protein solution with the fluorescence probe ANS to obtain the net RFI. The initial slope of the plot of standardized net RFI values versus % protein concentration was expressed as surface hydrophobicity (H_o).

2.3.5 Determination of free and total sulfhydryl group content determination

The method used for determination of the sulfhydryl group content of WSPB was adopted from Malik *et al.* [15] with some modifications. The protein solution (0.5% w/v) was prepared using a standard buffer pH 8.0 (0.086 M Tris, 0.09 M glycine and 4 mM Na_2EDTA) for free sulfhydryl group determination and a denaturing buffer (standard buffer plus 8 M urea and 0.5% w/v sodium dodecyl sulfate) for total sulfhydryl group determination. The samples were then incubated at room temperature for 30 min. and the mixture was centrifuged (12,500 g for 20 min) prior to collecting the supernatant for determination. To each 4 mL aliquot of supernatant, 0.1 mL Ellman's reagent solution (5,5-dithiobis (2-nitrobenzoic acid): DTNB) (4 mg DTNB/mL buffer) was added, rapidly mixed and allowed to stand for 15 min. The solution was then read at 412 nm in an UV-Vis spectrophotometer (UV-1800, Shimadzu, Japan) against a blank. The blank was prepared by mixing 4 mL of the respective buffer with 0.1 mL of Ellman's reagent. In order to calculate micromoles of SH/g of protein, a molar extinction coefficient of 1.36×10^4 M^{-1} cm^{-1} was used.

2.3.6 Color measurement

The color of WSPB powder was determined using the Colour Quest XE colorimeter (Hunter Lab., Hunter Assoc. Laboratory, USA). The setting for the illuminant was D_{65} source and the observer was standard 10°. Calibration of the instrument was conducted with black and white calibration tiles. WSPB powder was filled in a cuvette quart path length 25 mm, and three observations were measured and expressed as CIE L^* (lightness), a^* (redness), and b^* (yellowness) with 5 readings/samples.

2.4 pH measurement

WSPB (1 g) was mixed with 9 mL of distilled water and stirred at 100 rpm for 10 min. The pH value of the mixture was measured at room temperature in triplicate using an electronic pH meter (FE-20, Mettler-Toledo Instruments Co., Ltd., Switzerland).

2.5 Determination of protein functional properties

2.5.1 Protein solubility

Protein solubility was measured according to the method of Nalinanon *et al.* [16] with slight modifications. The solubility of WSPB was determined at pH values from 1 to 11. Briefly, 50 mg of WSPB was dispersed in 8 mL of distilled water and the pH of the mixture was adjusted to 1, 2, 3, 4, 5, 6, 7, 8, 9, 10 or 11 using 1 M HCl or 1 M NaOH. The dispersion was stirred for 30 min at room temperature and then the volume was adjusted to 10 mL and centrifuged at 6,000 g for 10 min. The supernatant was collected and subjected to protein determination using Biuret method. Bovine serum albumin was used as a protein standard. Total protein content in the sample was determined from the soluble portion of the sample in 0.5 M NaOH and relative solubility of protein sample was calculated as follows:

Relative solubility (%) = (protein content in supernatant/ total protein content in sample) × 100

2.5.2 Emulsion activity index (EAI) and emulsion stability index (ESI)

The EAI and the ESI were determined according to the method of Pearce and Kinsella [17], with slight modifications. 2 mL of soybean oil and 6 mL of protein solution (5 mg/mL) were homogenized at 20,000 rpm for 1 min. An aliquot of the emulsion (50μL) was pipetted from the bottom portion of the container at 0 and 10 min after homogenization and subsequently diluted 100-fold using 0.1% sodium dodecyl sulfate (SDS) solution. Each sample was mixed thoroughly for 10 s using a vortex mixer. A_{500} of the resulting dispersion was measured using a spectrophotometer (UV-1800, Shimadzu, Japan). EAI and ESI were calculated as follows:

$$EAI\ (m^2/g) = (2\times 2.303\times A\times DF)/l\Phi C$$

where $A = A_{500}$, DF = dilution factor (100), l = path length of cuvette (m), Φ = oil volume fraction and C = protein concentration in aqueous phase (g/m^3)

$$ESI\ (min) = (A_0\times t/\Delta A)$$

where $\Delta A = A_0 - A_{10}$ and t = 10 min.

2.5.3 Foaming capacity (FC) and foam stability (FS)

FC and FS of WSPB solution was determined as described by Nalinanon *et al.* [16] with slight modification. Sample (35 mL), with 5 mg/mL protein concentration, was transferred into a 100-mL cylinder. The solutions were homogenized at 16,000 rpm for 1 min at room temperature (about 25°C) and the samples were allowed to stand for 0 and 60 min. FE and FS were then calculated using the following equations:

$$FC\ (\%) = V_T/V_0 \times 100$$
$$FS\ (\%) = V_{60}/V_0 \times 100$$

where V_T is total volume after whipping, V_0 is the original volume before whipping, and V_{60} is total volume after leaving at room temperature for 60 min.

2.6 Determination of antioxidant activity

2.6.1 DPPH radical scavenging activity

DPPH radical scavenging activity was measured following the method of Murakami *et al.* [18] with a slightly modification. Briefly, The reaction mixture contained 5.4 mL of WSPB at different concentration and 0.6 mL of 0.8 mM DPPH in 95% ethanol. The mixture was incubated at room temperature for 30 min in dark, and then the absorbance at 517 nm was measured using a spectrophotometer (UV-1800, Shimadzu, Japan). The control was prepared in the same manner excepted that distilled water was used instead of the sample. The percentage of DPPH· scavenging activity of the sample was calculated as:

$$\text{Scavenging activity (\%)} = (1\text{-}A_{sample}/A_{control}) \times 100$$

where $A_{control}$ is the absorbance of the assay without sample and A_{sample} is the absorbance in the presence of the WSPB.

The result was expressed as the IC_{50} value. The IC_{50} (concentration providing 50% inhibition) value was calculated from the plotted graph of scavenging activity against the concentrations of the sample.

2.6.2 ABTS radical scavenging activity

ABTS radical scavenging activity was measured following the method of Rice-Evans *et al.* [19] with a slightly modification. The ABTS radical ($ABTS^{\bullet+}$) was produced by reacting 7.4 mM ABTS stock solution with 2.45 mM potassium persulphate at a ratio of 1:1 (v/v). The mixture was allowed to react for 12-16 h at room temperature in the dark. This working solution of $ABTS^{\cdot+}$ solution was diluted with 95% ethanol, in order to obtain an absorbance of 0.700 ± 0.020 at 734 nm. The reaction mixture contained 0.15 mL of WSPB at different concentrations and 2.85 mL of $ABTS^{\cdot+}$ solution. The mixture was incubated at room temperature for 6 min in dark. Then, the absorbance at 734 nm was measured using a spectrophotometer (UV-1800, Shimadzu, Japan). The control was prepared in the same manner excepted that distilled water was used instead of the sample. The percentage of $ABTS^{\cdot+}$ scavenging activity and IC_{50} of the sample was calculated in the same manner as described in section 2.6.1.

2.6.3 Ferric reducing antioxidant power (FRAP)

FRAP was determined by the method described by Benzie and Strain [20]. Briefly, the FRAP reagent was freshly prepared by mixing of 10 mM 2,4,6-Tri(2-pyridyl)-s-triazine (TPTZ) solution in 40 mM HCl, 20 mM $FeCl_3.6H_2O$ solution and 300 mM acetate buffer, pH 3.6 (1:1:10 *v*/*v*/*v*). A sample (0.1 mL) was mixed with 3mL of FRAP reagent and the mixture was left at room temperature for 8 min in the dark. The absorbance was measured at 593 nm using a spectrophotometer (UV-1800, Shimadzu, Japan). The blank was prepared in the same manner, except that distilled water was used instead of the sample. A standard curve was prepared using Trolox in the range of 20-120 µg. The activity was expressed as µg Trolox equivalent (TE)/g protein.

2.7 Statistical analysis

All results were performed in triplicate. Data were presented as means ± standard deviation and a probability value of <0.05 was considered significant. For pair comparison, T-test was used. SPSS statistic program (SPSS 11.0 for Windows, SPSS Inc., Chicago, USA) was used for data analysis.

3. Results and Discussion

3.1 Yield and characteristics of WSPB

The yield and some physicochemical characteristics of water-soluble protein from *B. mori* (WSPB) are shown in Table 1. The silkworm pupae was simply extracted with distilled water. The yield of the resultant freeze-dried counterpart or WSPB was 3.62% based on wet weight basis. Kim *et al.* [8] reported that the yield of defatted silkworm pupae flour was about 35.84% (dry weight), which composed of ground whole insect without fat. The difference is probably due to different preparation and extraction procedures. According to the total protein content of *B. mori* (6.04%) determined by Kjeldahl method, the extraction efficiency of WSPB was calculated to be 65.62%, indicating high efficacy of protein extraction. The protein extraction method using water in the present work is low cost, environmental friendly and practical of use in large scale of protein extraction.

The pH of WSPB was 6.64, which was slightly higher than that reported for untreated silkworm pupae flour (pH 6.43) [8]. This might be due to the difference in the source or cultivation of the silkworms. The color of WSPB expressed as *L**, *a** and *b** values was 75.21, 2.11 and 24.67, respectively, presenting a bright-light reddish-yellow color. However, a general observation of the visible color of WSPB powder tended to be bright yellow. The predominant pigment of silkworm pupae is melanin, which can be black, brown or yellow in color [21]. Kim *et al.* [8] dried silkworm pupae at high temperature, which might be one cause for the color to be darker (*L** = 42.95) in their experiments compared to this result.

Table 1. Yield and physicochemical characteristics of water-soluble protein from *B. mori* (WSPB)

		WSPB[†]
Yield (%)		3.96±0.14
Extraction efficiency (%)		65.62±2.29
pH		6.64±0.01
Color	*L**	75.42±0.17
	*a**	2.22±0.11
	*b**	24.70±0.13
Free sulfhydryl content (μmol/g)		22.18±0.05
Total sulfhydryl content (μmol/g)		23.08±0.07
Surface hydrophobicity (H_0)		3.52±0.03

[†]Mean ± SD from triplicate determinations.

The total sulfhydryl content and free sulfhydryl content of WSPB were 23.08 and 22.18 μmol/g, respectively. It was suggested that WSPB may have a good reducing power as a function of –SH group. The surface hydrophobicity (H_o) of WSPB was 3.52±0.03, which was lower than previously reported by Azagoh *et al.* [22] who found surface hydrophobicity of the mealworm beetle larvae (*Tenrbrio molitor*) to be 102.5. Higher surface hydrophobicity was also previously found in soy protein isolate [23] and soluble protein from *T. molitor* larvae meal [22]. They explained that aggregating proteins are more hydrophobic and hydrophobic zones are buried inside the structure of proteins. Elias *et al.* [24] proposed that amino acids in protein including those with sulfhydryl groups (methionine and cysteine) or aromatic ring (tryptophan, tyrosine, and phenylalanine) contain a hydrogen atom that can interact with free radicals. With high free sulfhydryl content and low surface hydrophobicity, WSPB could be easily extracted into water fraction and might also ready to modify its structure to have better functionality as desired.

3.2 Amino acid composition

The amino acid composition of WSPB is presented in Table 2. WSPB composed of 15 amino acids of which 7 are essential amino acids and 8 nonessential amino acids. The predominant essential amino acids were histidine, lysine, threonine and valine and the predominant nonessential amino acids were glutamic acid, proline, glycine and tyrosine. Glutamic acid, histidine, proline and glycine were the major amino acid found in WSPB with descending amount in order. Rao [25] also reported that glutamic acid was the most abundant amino acid in silkworm larvae. These results are similar to those reported by Wu *et al.* [1] for *B. mori*, although, the level of amino acid content was lower when compared to those reports of Rao [25] and Longvah *et al.* [26]. These differences might be due to differences in the extraction method and source of insects. Generally, protein functionality and bioactivity govern by its amino acid composition as well as amino acid sequence [27]. In addition, the total hydrophobic amino acid, including isoleucine, leucine, methionine, phenylalanine, valine, alanine, glycine and proline of WSPB was calculated to be 333 residues/1000 residues, indicating that WSPB had slightly low molecular hydrophobicity.

Table 2. Amino acid composition of water-soluble protein from *B. mori* (WSPB) (residues/1000 residues)

Amino acids	WSPB (residues/1000 residues)
Essential amino acids	
Histidine	129
Isoleucine	29
Leucine	36
Lysine	54
Methionine	ND
Phenylalanine	23
Threonine	53
Tryptophan	ND
Valine	50
Nonessential amino acids	
Alanine	52
Arginine	37
Aspartic/Asparagine	62
Cysteine	ND
Glutamic/Glutamine	210
Glycine	66
Proline	77
Serine	59
Tyrosine	53

ND is not detectable.

3.3 SDS-PAGE

Protein pattern and molecular weight distribution of WSPB were analyzed by SDS-PAGE using 10% separating gel under reducing and non-reducing conditions as shown in Figure 1. There was a wide range of molecular weights in the WSPB ranging from lower 20 kDa to 250 kDa. Four major groups of protein bands under reducing condition were found to be 50-75 kDa, 37-50 kDa, 25-37 kDa and less than 25 kDa with the observed protein bands at 37 kDa, 45 kDa, 64 kDa, 75 kDa and 80 kDa being abundant. Four major groups of protein bands under non-reducing condition were found to be over 150 kDa, 50-100 kDa, 37-50 kDa and less than 25 kDa with the observed protein band intensity 37 kDa, 64 kDa and 75 kDa being abundant. The protein patterns of WSPB under non-reducing condition were difference from reducing condition. The absence of protein bands with molecular weight over 250 kDa and lower band intensity of three major bands in WSPB under non-reducing condition and with the presence of protein bands with 80 kDa, 54 kDa and 45 kDa under reducing condition indicated that WSPB contained disulfide bonds. Wang *et al.* [4] reported four major protein components in silk worm pupae, including albumin (97.4 kDa, 61.4 kDa, 44.4 kDa and 26.7 kDa), glutelin (200 kDa and 15 to 60 kDa), globulin (130.0 kDa and 26.8 kDa) and prolamin (15.3 to 46 kDa).

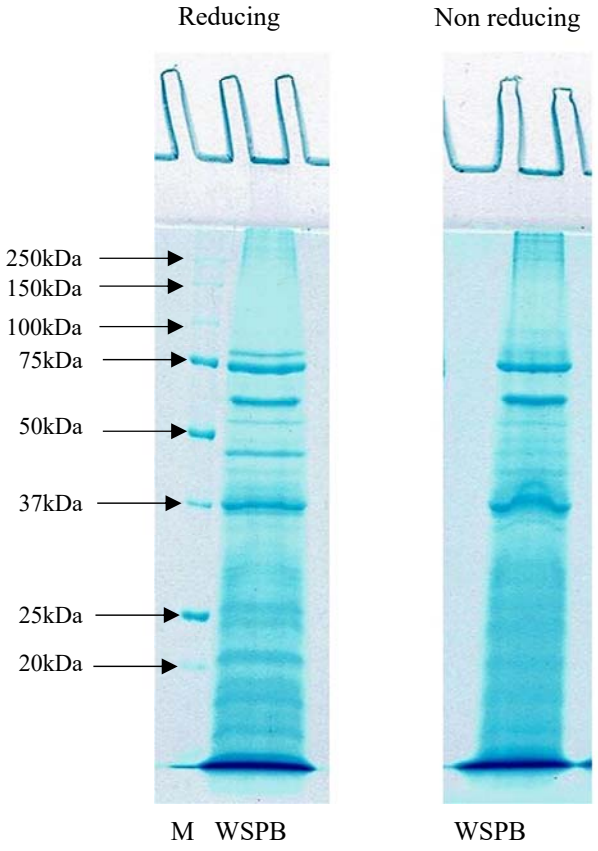

Figure 1. SDS-PAGE patterns of water-soluble protein from *B. mori* (WSPB) under reducing and non-reducing conditions. M denotes standard molecular weight protein markers.

3.4 Fourier-transform infrared (FTIR) spectrum of WSPB

The FTIR spectrum of WSPB is depicted in Figure 2. The result showed that WSPB had three characteristic amide bands representing amide *B* (2900–3200 cm^{-1}), amide *I* (1600–1700 cm^{-1}) and amide *III* (1200–1400 cm^{-1}). This result was in accordance with those previously reported in silkworm pupae protein modified by ultrasound or micronization techniques [28]. The major peaks were found at wavenumbers of 2924.47, 1609.58, and 1398.30 cm^{-1} for amide *B*, amide *I* and amide *III*, respectively. Amide *B* corresponded to asymmetric stretch vibration of =C–H as well as $–NH_3^+$ and amide *I* bands originated from C=O stretching vibrations coupled to N–H bending vibrations, CN stretch and CCN deformation [29]. Amide *III* represented the combination peaks between N–H deformation and C–N stretching vibrations and was involved with the triple helical structure of protein [30]. As a result, WSPB remained its structural integrity after extraction.

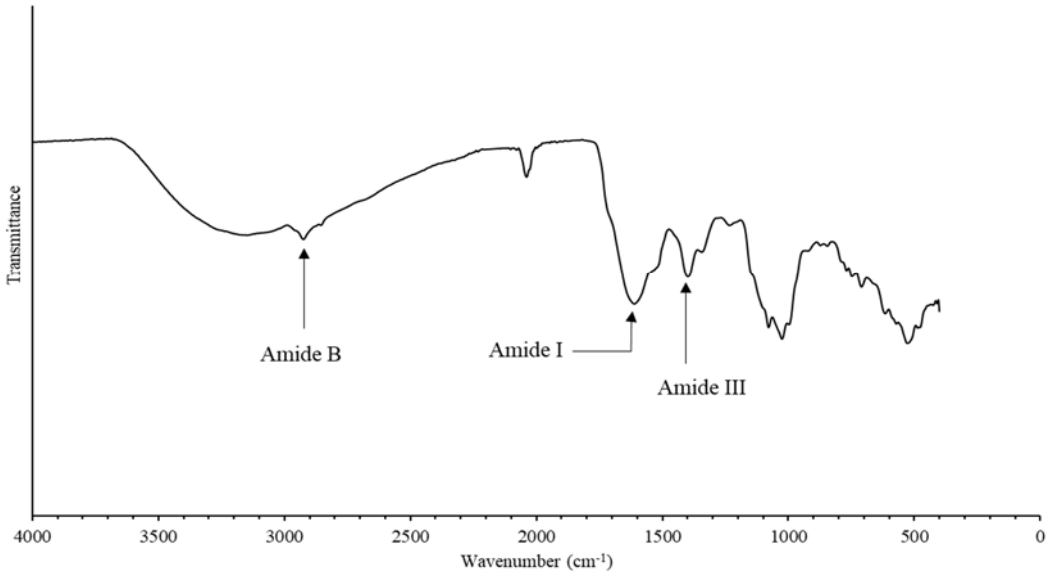

Figure 2. Fourier transform infrared spectrum of water-soluble protein from *B. mori* (WSPB)

3.5 Functional properties of WSPB

The solubility of WSPB in the pH range of 1-11 was depicted in Figure 3. The result showed that WSPB was highly solubilized more than 80% in the pH range of 5-11, indicating that the protein in silkworm pupae can be solubilized at neutral to alkaline pH. At acidic pH, the solubility of WSPB was generally low (< 40%). The lowest solubility was found in the pH range of 3-4, indicating isoelectric pH (pI) of WSPB. Wang *et al.* [4] reported that the pIs of albumin, globulin, glutelin and prolamin of silk worm protein were 2.5, 2.7, 4.0 and 4.5, respectively. This was due to a reduction in electrostatic repulsive forces between the proteins, leading to protein aggregation [22]. This effect is similar to those reported for several legumes, animal protein and protein isolates [22, 31, 32].

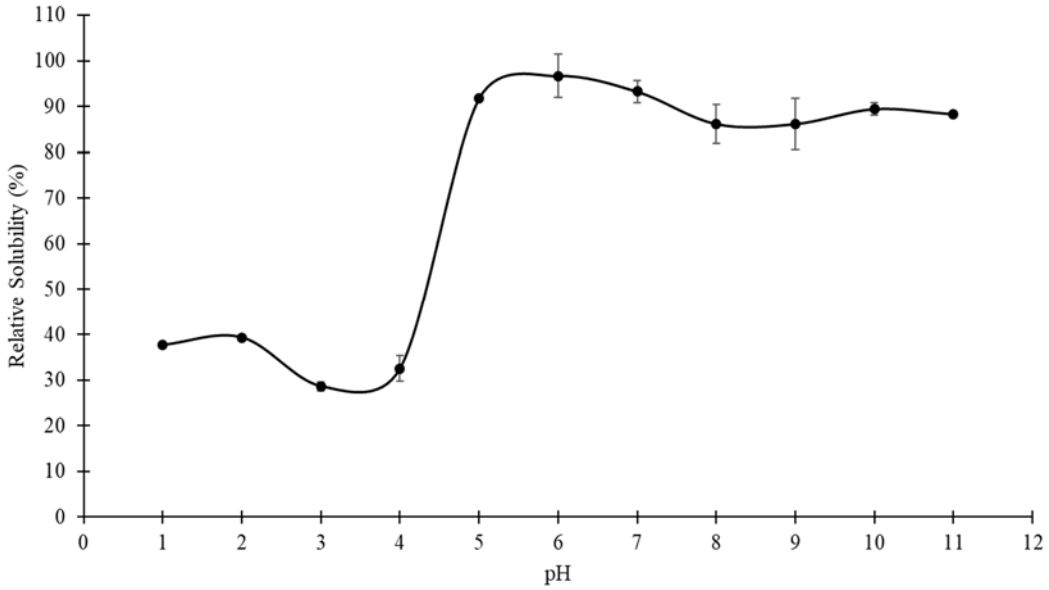

Figure 3. Relative solubility (%) of water-soluble protein from *B. mori* (WSPB) as affected by different pHs.

Emulsifying and foaming properties of WSPB are shown in Table 3. The emulsion activity index (EAI) and emulsion stability index (ESI) of WSPB were 25.09 m^2/g and 21.15 min, respectively. The EAI and ESI of WSPB were significantly lower than bovine serum albumin (BSA) ($p<0.05$). The differences between the emulsion activity and emulsion stability are related to the amphiphilicity of the protein surface, protein contents (soluble and insoluble) and other components [6].

Table 3. Emulsifying and foaming properties of water-soluble protein from *B. mori* (WSPB) and bovine serum albumin (BSA) [†]

Functional properties	WSPB	BSA
Emulsion activity index (EAI) (m^2/g)	$25.09\pm1.34^{b*}$	295.24 ± 2.30^{a}
Emulsion stability index (ESI) (min)	21.15 ± 0.22^{b}	38.55 ± 0.77^{a}
Foam capacity (FC) (%)	9.29 ± 1.01^{b}	81.23 ± 7.27^{a}
Foam stability (FS) (%)	93.46 ± 0.06^{a}	67.41 ± 2.95^{b}

[†] Mean ± SD from triplicate determinations.
[*] Different superscript letters in the same row indicate significant differences ($p<0.05$).

WSPB exhibited 9.29% and 93.46% for foam capacity (FC) and foam stability (FS), respectively. The FC of WSPB was low when compared with BSA (81.23%) ($p<0.05$). This might be due to the variation of molecular weights of protein component in WSPB, interrupting the formation of protein film at the lamellae of air bubble. The result was similar to those reported by Adebowale *et al.* [33] for whole giant cricket (*Gryllidae* sp.) powder that had a FC of 6%, and Omotoso [34] who reported the FC from *Cirina forda* as 7.1%. However, FS of WSPB was significantly higher than that of BSA

(67.41%) ($p<0.05$). Johnson and Zabik [35] explained that intermolecular protein-protein interaction enhances the cohesive nature of the film, therefore imparting stability and elasticity to the membrane. This interaction appears to be dependent on the presence of a high ratio of nonpolar/polar side chains in the protein [35] which was found in WSPB, according to its amino acid component. Zielińska *et al.* [6] reported the FC of *Gryllidae sigillatus* flour as 41% and FS was 34.67%. The differences between FC and FS of proteins may be due to their different compositions in different species and their different conformational characteristics [6]. The differences in FS is also probably due to components such as carbohydrates, which reduces protein-protein interactions and leads to formation of weak interfacial membranes that are unable to stabilize the foams [36].

3.6 Antioxidant activities

Antioxidant activities as determined by ABTS, DPPH and FRAP assays of WSPB are shown in Table 4. WSPB exhibited strong scavenging activity on DPPH and ABTS radicals with IC_{50} of 43.11 and 16.57 µg/mL, respectively. Wu *et al.* [1] reported that protein hydrolysates from larval instars of silkworm, obtained after digestion with gastrointestinal proteases, had $DPPH^{\bullet}$ scavenging capacity (IC_{50}) of 57.91 µg/mL. Pachiappan *et al.* [37] reported that silkworm pupae powder had $DPPH^{\bullet}$ scavenging capacity (IC_{50}) of 60.58 µg/mL. These reports found less effective on $DPPH^{\bullet}$ scavenging activity when compared with the present result (IC_{50} of 43.11 µg/mL). In contrast, the results had low potential on DPPH inhibition when compared with methanolic silkworm pupae extract from muga silkworm (*Antheraea assamensis*) (IC_{50} of 25.83 µg/mL as reported by Deori *et al.* [38]. Additionally, Zielińska *et al.* [36] reported that the antiradical activity against $DPPH^{\bullet}$ for the hydrolysates obtained after digestion of five edible insects ranged from 19.1 to 76.3 µg/mL. The antiradical activity against $ABTS^{\bullet+}$ (IC_{50}) ranged from 4.6 to 25.9 µg/mL [36]. The more stable products could be formed and the radical chain reaction terminated from these peptides since they are electron donors that could react with free radicals [39]. These results indicate that insect protein could be a good source of antioxidant peptides.

Table 4. Antioxidant activity of water-soluble protein from *B. mori* (WSPB)

Antioxidant assays	WSPB[†]
DPPH (IC_{50} µg/mL)	43.11±0.11
ABTS (IC_{50} µg/mL)	16.57±0.04
FRAP (µg TE/g protein)	54.20±0.13

[†] Mean ± SD from triplicate determinations

As per FRAP assay, WSPB also presented reducing power on Fe^{3+} of 54.20 µg TE/g protein. Bousopha *et al.* [40] reported that collagen hydrolysate from Pharaoh cuttlefish skin with 10-30% DH had ferric reducing power values of 23.50 to 26.50 µmolTE/g protein. The increase or decrease in ferric reducing power for protein hydrolysates may be related to the exposure of electron-dense amino acid side chain groups, such as polar or charged moieties during hydrolysis [41]. Chalamaiah *et al.* [42] reported that the reducing power of three carp roe protein hydrolysates increased with increasing concentrations. Compounds with higher reducing power were shown to have a better ability to donate electrons or hydrogen and serve as a significant indicator of their potential for use as an antioxidant [29]. The antioxidant activities of $DPPH^{\bullet}$, $ABTS^{\bullet+}$ and FRAP scavenging ability, appear to be dependent on the molecular weight of the peptide [42]. In addition, those with a low-molecular weight had lower antioxidant activity. This suggests that the hydrolysates obtained from some edible insect protein can be used as compounds that are able to donate electrons and thus show antioxidant activity.

4. Conclusions

B. mori could be a good source of protein. Its water-soluble protein fraction exhibited beneficial physicochemical and functional properties as well as high antioxidant activity. This edible insect protein can be used as an alternative food ingredient in many food applications.

5. Conflicts of interest

The authors declare that there is no conflict of interests regarding the publication of this article.

6. Acknowledgements

This work was supported by King Mongkut's Institute of Technology Ladkrabang. The authors would also like to thank Professor Dr. Anthony Keith Thompson, Visiting Professor at Faculty of Agro-Industry, King Mongkut's Institute of Technology Ladkrabang for invaluable suggestions and corrections.

References

[1] Wu, Q.-Y., Jia, J.-Q., Tan, G.-X., Xu, J.-L.and Gui, Z.-Z., 2011. Physicochemical properties of silkworm larvae protein isolate and gastrointestinal hydrolysate bioactivities. *African Journal of Biotechnology*, 10, 6145-6153.

[2] Hu, B., Li, C., Zhang, Z., Zhao, Q., Zhu, Y., Su, Z. and Chen, Y., 2017. Microwave-assisted extraction of silkworm pupal oil and evaluation of its fatty acid composition, physicochemical properties and antioxidant activities. *Food Chemistry*, 231, 348-355.

[3] Mishra, N., Hazarika, N.C., Narain, K. and Mahanta, J., 2003. Nutritive value of non-mulberry and mulberry silkworm pupae and consumption pattern in Assam, India. *Nutrition Research*, 23, 1303-1311.

[4] Wang, W., Wang, N., Zhou, Y., Zhang, Y., Xu, L., Xu, J., Feng, F. and He, G., 2011. Isolation of a novel peptide from silkworm pupae protein components and interaction characteristics to angiotensin I-converting enzyme. *European Food Research and Technology*, 232, 29-38.

[5] Yang, Y., Tang, L., Tong, L. and Liu, H., 2009. Silkworms culture as a source of protein for humans in space. *Advances in Space Research*, 43, 1236-1242.

[6] Zielińska, E., Karaś, M. and Baraniak B., 2018. Comparison of functional properties of edible insects and protein preparations thereof. *LWT - Food Science and Technology*, 91, 168-174.

[7] Park, Y.-S., Choi, Y.-S., Hwang, K.-E., Kim, T.-K., Lee, C.-W., Shin, D.-M. and Han, S.G., 2017. Physicochemical properties of meat batter added with edible silkworm pupae (*Bombyx mori*) and transglutaminase. *Korean Journal for Food Science of Animal Resources*, 37, 351.

[8] Kim, H.-W., Setyabrata, D., Lee, Y.J., Jones, O.G. and Kim, Y.H.B., 2016. Pre-treated mealworm larvae and silkworm pupae as a novel protein ingredient in emulsion sausages. *Innovative Food Science & Emerging Technologies*, 38, 116-123.

[9] Kim, M.-J., Hong, S.-J., Yang, J. and Kim, H.-K., 2007. Silkworm (*Bombyx mori* L.) reduces vasopressin expression in the hypothalamus of streptozotocin-induced diabetic mice. *Neurological Research*, 29, 72-77.

[10] Oh, H.-G., Lee, H.-Y., Kim, J.-H., Kang, Y.-R., Moon, D.-I., Seo, M.-Y., Back, H.-I., Kim, S.-Y., Oh, M.-R., Park, S.-H., Kim, M.-G., Jeon, J.-Y., Shin, S.-J., Ryu, K.-S., Chae, S.-W., Kim, O. and Park, J.-K., 2012. Effects of male silkworm pupa powder on the erectile dysfunction by chronic ethanol consumption in rats. *Laboratory Animal Research*, 28, 83-90.

[11] Hanboonsong, Y., Jamjanya, T. and Durst, P.B., 2013. *Six-legged livestock: edible insect farming, collection and marketing in Thailand*. [e-book] Bangkok: Food and Agriculture Organization of the United Nations Regional Office for Asia and the Pacific. Available through: http://www.fao.org/3/a-i3246e.pdf.

[12] Yhoung-Aree, J., Puwastien, P. and Attig, G.A., 1997. Edible insects in Thailand: An unconventional protein source? . *Ecology of Food and Nutrition*, 36, 133-149.

[13] A.O.A.C., 2000. *Official methods of analysis*. 16th ed. Washington, DC.: The Association of official analytical chemists.

[14] Laemmli, U.K., 1970. Cleavage of structural proteins during the assembly of the head of bacteriophage T4. *Nature*, 227, 680.

[15] Malik, M.A., Sharma, H.K. and Saini, C.S., 2017. High intensity ultrasound treatment of protein isolate extracted from dephenolized sunflower meal: Effect on physicochemical and functional properties. *Ultrasonics Sonochemistry*, 39, 511-519.

[16] Nalinanon, S., Benjakul, S., Kishimura, H. and Shahidi, F., 2011. Functionalities and antioxidant properties of protein hydrolysates from the muscle of ornate threadfin bream treated with pepsin from skipjack tuna. *Food Chemistry*, 124, 1354-1362.

[17] Pearce, K.N. and Kinsella, J.E., 1978. Emulsifying properties of proteins: evaluation of a turbidimetric technique. *Journal of Agricultural and Food Chemistry*, 26, 716-723.

[18] Murakami, M., Yamaguchi, T., Takamura, H. and Atoba T.M., 2004. Effects of thermal treatment on radical-scavenging activity of single and mixed polyphenolic compounds. *Journal of Food Science*, 69, FCT7-FCT10.

[19] Rice-Evans, C., Miller, N. and Paganga, G., 1997. Antioxidant properties of phenolic compounds. *Trends in Plant Science*, 2, 152-159.

[20] Benzie, I.F.F. and Strain, J.J., 1996. The ferric reducing ability of plasma (FRAP) as a measure of "antioxidant power": The FRAP assay. *Analytical Biochemistry*, 239, 70-76.

[21] Wittkopp, P.J. and Beldade, P., 2009. Development and evolution of insect pigmentation: Genetic mechanisms and the potential consequences of pleiotropy. *Seminars in Cell & Developmental Biology*, 20, 65-71.

[22] Azagoh, C., Ducept, F., Garcia, R., Rakotozafy, L., Cuvelier, M.E., Keller, S., Lewandowski, R. and Mezdour, S., 2016. Extraction and physicochemical characterization of *Tenebrio molitor* proteins. *Food Research International*, 88, 24-31.

[23] Wagner, J.R., Sorgentini, D.A. and Añón, M.C., 2000. Relation between solubility and surface hydrophobicity as an indicator of modifications during preparation processes of commercial and laboratory-prepared soy protein isolates. *Journal of Agricultural and Food Chemistry*, 48, 3159-3165.

[24] Elias, R.J., McClements, D.J. and Decker, E.A., 2005. Antioxidant activity of cysteine, tryptophan, and methionine residues in continuous phase β-lactoglobulin in oil-in-water emulsions. *Journal of Agricultural and Food Chemistry*, 53, 10248-10253.

[25] Rao, P.U., 1994. Chemical composition and nutritional evaluation of spent silk worm pupae. *Journal of Agricultural and Food Chemistry*, 42, 2201-2203.

[26] Longvah, T., Mangthya, K. and Ramulu, P., 2011. Nutrient composition and protein quality evaluation of eri silkworm (*Samia ricinii*) prepupae and pupae. *Food Chemistry*, 128, 400-403.

[27] Nalinanon, S., Benjakul, S. and Kishimura, H., 2010. Biochemical properties of pepsinogen and pepsin from the stomach of albacore tuna (Thunnus alalunga). *Food Chemistry*, 121, 49-55.

[28] Zhou, Z.-F., Ren, Z.-X., Yu, H.-Y., Jia, J.-Q. and Gui, Z.-Z., 2017. Effects of different modification techniques on molecular structure and bioactivity of *Bombyx mori* pupa protein. *Journal of Asia-Pacific Entomology*, 20, 35-41.

[29] Je, J.-Y., Lee, K.-H., Lee, M.H. and Ahn, C.-B., 2009. Antioxidant and antihypertensive protein hydrolysates produced from tuna liver by enzymatic hydrolysis. *Food Research International*, 42, 1266-1272.

[30] Muyonga, J.H., Cole, C.G.B. and Duodu, K.G., 2004. Characterisation of acid soluble collagen from skins of young and adult Nile perch (*Lates niloticus*). *Food Chemistry*, 85, 81-89.

[31] Bußler, S., Rumpold, B.A., Jander, E., Rawel, H.M. and Schlüter, O.K., 2016. Recovery and techno-functionality of flours and proteins from two edible insect species: Meal worm (*Tenebrio molitor*) and black soldier fly (*Hermetia illucens*) larvae. *Heliyon*, 2, e00218.

[32] Horax, R., Vallecios, M.S., Hettiarachchy, N., Osorio, L.F. and Chen, P., 2017. Solubility, functional properties, ACE-I inhibitory and DPPH scavenging activities of Alcalase hydrolysed soy protein hydrolysates. *International Journal of Food Science & Technology*, 52, 196-204.

[33] Adebowale, Y.A., Adebowale, K.O. and Oguntokun, M.O., 2005. Evaluation of nutritive properties of the large African cricket (*Gryllidae* sp). *Pakistan Journal of Scientific and Industrial Research*, 48, 274.

[34] Omotoso, O.T., 2006. Nutritional quality, functional properties and anti-nutrient compositions of the larva of Cirina forda (Westwood) (*Lepidoptera: Saturniidae*). *Journal of Zhejiang University SCIENCE B*, 7, 51-55.

[35] Johnson, T.M. and Zabik, M.E., 1981. Ultrastructural examination of egg albumen protein foams. *Journal of Food Science*, 46, 1237-1240.

[36] Zielińska, E., Baraniak, B., Karaś, M., Rybczyńska, K. and Jakubczyk, A., 2015. Selected species of edible insects as a source of nutrient composition. *Food Research International*, 77, 460-466.

[37] Pachiappan, P., Mohanraj, P., Mahalingam, C., Manimegalai, S., Swathiga, G. and Thangamalar, A., 2016. *In vitro* evaluation of antioxidant activity of bioproducts extracted from silkworm pupae. *Environment & We an International Journal of Science & Technology*, 11, 33-39.

[38] Deori, M., Boruah, D.C., Devi, D. and Devi, R., 2014. Antioxidant and antigenotoxic effects of pupae of the muga silkworm Antheraea assamensis. *Food Bioscience*, 5, 108-114.

[39] Jemi, l I., Jridi, M., Nasri, R., Ktari, N., Ben Slama-Ben Salem R., Mehiri, M., Hajji, M. and Nasri M., 2014. Functional, antioxidant and antibacterial properties of protein hydrolysates prepared from fish meat fermented by *Bacillus subtilis* A26. *Process Biochemistry*, 49, 963-972.

[40] Bousopha, S., Nalinanon, S. and Sriket, C., 2016. Production of collagen hydrolysate with antioxidant activity from Pharaoh cuttlefish skin. *Chiang Mai University Journal of Natural Sciences*, 15, 151-162.

[41] Zambrowicz, A., Pokora, M., Eckert, E., Szołtysik, M., Dąbrowska, A., Chrzanowska, J. and Trziszka, T., 2012. Antioxidant and antimicrobial activity of lecithin free egg yolk protein preparation hydrolysates obtained with digestive enzymes. *Functional Foods in Health and Disease*, 2, 487-500.

[42] Chalamaiah, M., Jyothirmayi, T., Diwan, P.V. and Dinesh Kumar, B., 2015. Antioxidant activity and functional properties of enzymatic protein hydrolysates from common carp (*Cyprinus carpio*) roe (egg). *Journal of Food Science and Technology*, 52, 5817-5825.

Current Applied Science and Technology Vol. 18 No. 2 May-August 2018
DOI: 10.14456/cast.2018.5

Development and Validation of RP-HPLC Method for the Dissolution Study of Bosentan in Bulk and in Pharmaceutical Dosage Form

Karunakaran Anandakumar[*1], Munusamy Jambulingam[1], Jayaprakash Rmaesh[1], Sebasthiar Josephine Subarla[1], Premkumar Sangeetha[1]and Murugesan Raja[2]

[1]Department of Pharmaceutical Analysis, Swamy Vivekanandha College of Pharmacy, Namakkal (Dt) Tamil Nadu, India
[2]Department of Pharmaceutics, Sri Ramakrishna Institute of Paramedical Sciences, College of Pharmacy, Coimbatore-641 044, Tamil Nadu, India

Received: 20 November 2017, Revised: 22 June 2018, Accepted: 4 July 2018

Abstract

A simple, sensitive, precise and accurate reversed phase high performance liquid chromatographic (RP-HPLC) method has been developed for the dissolution study of Bosentan in bulk and in pharmaceutical dosage forms. The method was developed using the mobile phase comprising of Triethylamine buffer pH adjusted to 2.5 with ortho phosphoric acid and acetonitrile in the ratio of 50:50 v/v over Waters Symmetry C_8 column (150 mm length x 4.6 mm i.d x 5 µm particle size) at temperature 40°C. The flow rate was 1.5 ml/ min and UV detection was at 266 nm. The retention time of Bosentan was 4.475 mins. The recovery was found to be 99.98 % which is demonstrative of accuracy of the protocol. Inter-day and intra-day precisions of the newly developed method were less than the maximum allowable limit (%RSD < 2) according to ICH guidelines. The method showed linearity in the concentration range of 35-210 µg/ ml with correlation coefficient (r^2) value of 0.9999. No interference was observed from the blank (dissolution medium) and placebo samples. Hence the method was specific for determination of % release of Bosentan tablets in dissolution study. In robustness study for dissolution condition there was no significant change was observed in % release after individually changing the dissolution parameters. Calculations for system suitability parameters met the acceptance criteria. The percentage drug release was found to be 99.41 % for marketed Bosentan tablet. Several trials were performed by changing the dissolution medium; the 1 % SLS dissolution medium shows successful drug release. All the validation parameters were within the acceptance range. Therefore, the method was found to be simple, precise, accurate, reproducible, sensitive and less time consuming and can be successfully applied for routine quality control and analysis and dissolution study of Bosentan in bulk and in pharmaceutical dosage form.

Keywords: Bosentan, RP-HPLC, Method development, Validation, ICH guidelines, Dissolution studies.

[*]Corresponding author: Tel.: +91 9443454675 Fax: +914288-234417
E-mail: anandkarunakaran@gmail.com

Current Applied Science and Technology Vol. 18 No. 2 May-August 2018
DOI: 10.14456/cast.2018.5

1. Introduction

Bosentan (BOS) is chemically, 4-tert-butyl-N-[6-(2-hydroxy-ethoxy)-5-(2-methoxy-phenoxy)-[2,2]-bipyrimidine-4-yl]-benzenesulfonamide (Figure 1). BOS is used to treat pulmonary artery hypertension [1] and to reduce number of digital ulcers [2]. BOS is an Endothelin receptor antagonist, which belongs to a class of highly substituted pyrimidine derivatives [3]. Endothelin-1 (ET-1) is a neurohormone, the effects of which are mediated by binding to ET_A and ET_B receptors in the endothelium and vascular smooth muscle. ET-1 concentrations are elevated in plasma and lung tissue of patients with pulmonary arterial hypertension, suggesting a pathogenic role for ET-1 in this disease. BOS is a specific and competitive antagonist at Endothelin receptor types ET_A and ET_B. BOS has a slightly higher affinity for ET_A receptors than for ET_B receptors. Inhibition of the ET receptors disrupts the intracellular pathway that leads to vasoconstriction thereby causing vasodilation. BOS is white to yellowish white powder, freely soluble in dimethylformamide, acetonitrile; soluble in ethanol and ethyl acetate, slightly soluble in isopropanol, and very slightly soluble in hexane, poorly soluble in water [4-8].

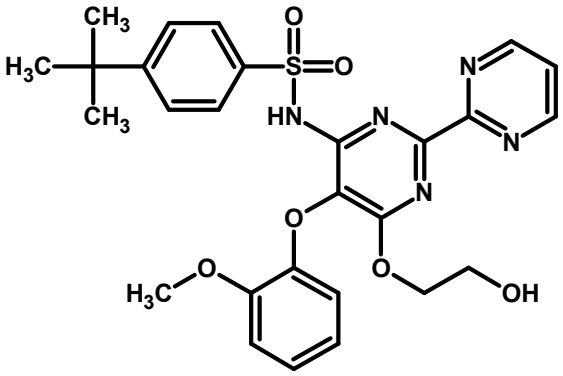

Figure 1. Chemical Structure of Bosentan

Literature survey revealed that few analytical methods have been reported for the estimation of BOS by UV-Visible spectroscopic methods [9-12] and RP-HPLC methods [13-18] Karnaker reddy *et al*. [13] reported RP-HPLC method development and validation of BOS drug present in tablets using methanol : potassium dihydrogen orthophosphate buffer pH 7.8 (60:40 % v/v) as mobile phase, at a flow rate of 0.8 ml/ min at 220 nm, Rt 3.702 mins. Muralidharan *et al*. [14] reported a simple RP-HPLC method for the estimation of BOS in tablet formulation using Acetonitrile: 10 mM ammonium acetate buffer pH 4.5 (70:30 % v/v) as mobile phase at a flow rate of 1 ml/ min at 265 nm, Rt 3.702 mins. Sujatha *et al*. [15] reported a new validated RP-HPLC method for the estimation BOS in tablet dosage form using phosphate buffer pH 4.0 and Acetonitrile (30: 70 % v/v) as mobile phase at a flow rate of 1 ml/ min at 270 nm, Rt 3.54 mins. Lavudu *et al*. [16] reported a determination of Bosentan in pharmaceutical dosage forms by HPLC using ammonium pH 5.0 : Acetonitrile (70:30 % v/v) as mobile phase at a flow rate of 1 ml/ min at 220 nm, Rt 1.986 mins. Kalaichelvi and Jayachandran [17] reported RP-HPLC method for Bosentan using phosphate buffer pH 5 : Acetonitrile (45:55 % v/v) as mobile phase at a flow rate of 1 ml/ min at 270 nm, Rt 5.7 mins. Lavudu *et al*. [18] reported an application of spectrophotometry and HPLC for Bosentan using methanol and ammonium buffer (60:40 % v/v)

as mobile phase at a flow rate of 1.0 ml/ min, λmax 227 nm, Rt 2.449 mins. Stability indicating HPLC [19-21] and HPTLC [22] methods were reported for the estimation of BOS. Also impurity profiling by RP-HPLC [23], determination of residual solvents by headspace gas chromatography [24, 25], determination of BOS in rat plasma by UFLC-MS/MS [26] method were reported. Literature survey revealed that there was no such simple RP-HPLC method for the dissolution study of BOS in bulk and pharmaceutical dosage form. Therefore, development of a simple RP-HPLC method for dissolution study of BOS is highly desirable. Hence, the aim of the present study was to develop a simple and rapid RP-HPLC method for dissolution study of BOS in bulk and in pharmaceutical dosage form and to validate the method according to ICH guidelines [27].

2. Materials and Methods

2.1 Chemicals and reagents

Working standard of BOS USP was obtained from Par Formulation Pvt Ltd. The marketed formulation was obtained from the local market. HPLC grade acetonitrile and methanol was procured from Fisher scientific (Hyderabad, India) and ortho phosphoric acid, triethylamine, sodium lauryl sulfate, sodium dihydrogen phosphate, sodium hydroxide of AR grade were purchased from Rankem (Hyderabad, India) and Merck (Mumbai, India). High purity water was obtained by using Millipore Milli-Q water purification system (Billerica, USA). The buffer was prepared by dissolving 1 ml of triethylamine in 1,000 ml of Milli-Q water and the pH was adjusted to 2.5 with orthophosphoric acid. One percentage of SLS was prepared by dissolving 10 gm of sodium lauryl sulfate in 1000 ml of Milli-Q water.

2.2 Instrumentation and chromatographic conditions

High Performance Liquid Chromatographic system (Waters Alliance, USA), equipped with an auto sampler and PDA detector was used for the analysis. The data was recording using Empower 3 software. Dissolution apparatus (Distek, USA) was used for the dissolution study of BOS. Analytical reversed phase C_8 (Waters Symmetry column, 150 mm length x 4.6 mm i.d x 5 µm particle size) was used for the separation. Mobile phase consisting of a mixture of triethylamine buffer adjusted pH to 2.5 with orthophosphoric acid and acetonitrile 50:50 v/ v was delivered at a flow rate of 1.5 ml/ min with PDA detection at 266 nm. The mobile phase was filtered through 0.45 µm membrane filter, sonicated and degassed before use. The column temperature was 40 ˚C.

2.3 Method development and optimisation of chromatographic conditions

Mobile phase comprising of different solvent composition were tried to achieve optimum separation. The mobile phase consisting of Triethylamine buffer, pH-adjusted to 2.5: Acetonitrile in the ratio of 80:20, 70:30, 60:40 and 50:50 % v/ v were tried. In the ratio of 80:20 % v/v and 70:20 % v/v the Bosentan peak was not eluted properly. At 60:40 % v/v the peak shape was good but slightly tailing was observed. At 50:50% v/v Bosentan was eluted with sharp peak and obeyed system suitability parameters. Finally, triethylamine buffer pH was adjusted to 2.5 with ortho phosphoric acid and acetonitrile (50:50 v/ v) was selected as an appropriate developing medium which gave good separation and met acceptable system suitability parameters.

2.4 Selection of column oven temperature:

The Study was started with initial stage column temperature maintained at ambient, and then increased slowly up to 40 °C. At 40°C good peak shape, peak symmetry and better separation was observed. The peak shape and peak symmetry was good at 40 °C than the ambient temperature. Hence, 40 °C temperature was selected for further analysis.

2.5 Preparation of standard solution
Standard stock solution of BOS was prepared by dissolving 35 mg of BOS in 25 ml of methanol in 25 ml volumetric flask. The solution was sonicated for 5 min. Five ml of the above stock solution was diluted to 50 ml with 1 % SLS to get a concentration range of 140 µg/ ml.

2.6 Preparation of sample solution
BOS tablet powder equivalent to 35 mg was accurately weighed and transferred into 25 ml volumetric flask, dissolved and make up the volume with methanol. The resulting solution was sonicated for 15 minutes and filtered through Whatman filter paper No. 41 to obtain the concentration of 1400 µg/ ml. Five ml of the above solution was transferred into 50 ml volumetric flask, dissolved and made up the volume with 1 % SLS to get a final concentration of 140 µg/ ml.

2.7 Dissolution study
Dissolution test for BOS formulation was performed in the dissolution system (n = 6), dissolution apparatus No II (paddle). The media used was 1 % SLS. The temperature of the bath was maintained at 37^0C and speed of the paddle was set at 50 rpm. The aliquots of sample were withdrawn up to 60 min in different time intervals, and filtered through 0.45 µ PVDF membrane filtered and injected into HPLC system.

3. Results and Discussion

All of the analytical parameters for the proposed method were determined according to the International Conference on Harmonization (ICH) guidelines.

3.1 Selection of wavelength
10 µg/ ml of BOS standard solution was scanned between 200-400 nm. The λmax was detected at 266 nm and this wavelength was fixed for analysis.

3.2 Optimization of chromatographic conditions
Mobile phase comprising of different solvent composition were tried to achieve optimum separation. The mobile phase consisting of Triethylamine buffer pH adjusted to 2.5: Acetonitrile in the ratio of 80:20, 70:30, 60:40 and 50:50 % v/ v were tried. In the ratio of 80:20 % v/v and 70:20 % v/v the Bosentan peak was not eluted properly. At 60:40 % v/v the peak shape was good but slight tailing was observed. At 50:50 % v/v Bosentan was eluted with sharp peak and obeyed system suitability parameters. Finally, triethylamine buffer pH adjusted to 2.5 with orthophosphoric acid and acetonitrile (50:50 v/v) was selected as an appropriate developing medium which gave good separation and met acceptable system suitability parameters.

3.3 Linearity
Linearity of the method was confirmed by constructing calibration graph. Seven solutions having concentrations of 35, 70, 112, 140, 168, 196 and 210 µg/ ml were prepared. Then 20 µl from each solution was injected using auto sampler and the analyses were monitored at 266 nm. The procedure was repeated for six times. The method was found to be linear in the concentration range of 35-210 µg/ ml with the correlation coefficient of 0.9999 which were found to be within the accepted range of guidelines and represented a good linear relationship of the newly developed method. The slope and intercept of the calibration curve was found to be 21908.463 and 4229.138, respectively. The LOD and LOQ were found to be 207.5537 µg/ ml and 628.9505 µg/ml, respectively. The calibration curve is shown in Figure 2.

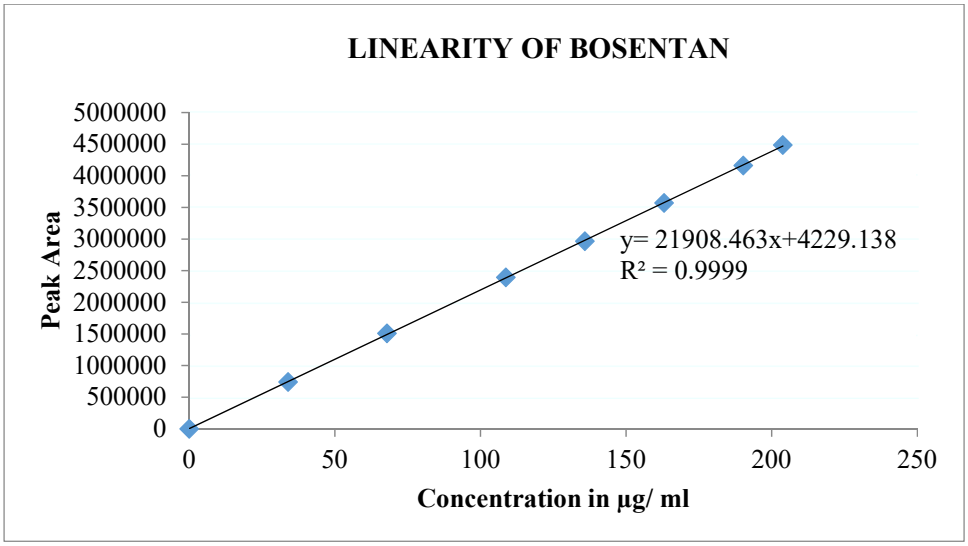

Figure 2. Linearity plot of Bosentan

3.4 Precision3

3.4.1 Repeatability

Repeatability of the method was done by using the different analysis of the dissolution sample for six times. The results are shown in Table 1.

Table 1. Repeatability studies

Sample No	Mean Peak Area*	% Release*	Average % Release	% RSD
1	2995113	98.3	98.93	0.43
2	3017075	99.0		
3	3023718	99.2		
4	3016147	99.0		
5	3032621	99.5		
6	3005952	93.6		

Remark: *Mean of six observations

3.4.2 Intermediate precision

Intermediate precision was done by intraday and inter day analysis of dissolution sample was done for three times in the same day and one time for three consecutive days. This is shown in Table 2.

Table 2. Intermediate precision

Parameters	% Release*	SD	% RSD
Intraday	99.69	0.1969	0.19
	99.74	0.2014	0.20
	99.97	0.1739	0.17
Inter day	99.32	0.1234	0.15
	99.62	0.1523	0.13
	99.53	0.1230	0.15

Remark: *Mean of six observations.

3.4.3 Reproducibility:

Reproducibility of the method was done by using the different analysts and different instruments. The dissolution sample was analysed with different analysts and the results are shown in Table 3.

Table 3. Reproducibility studies

Sample No	Analyst 1		Analyst 2	
	Peak area	% Release	Peak area	% Release
1	2995113	98.3	3215897	100.1
2	3017075	99.0	3186967	99.2
3	3023718	99.2	3149781	98.0
4	3016147	99.0	3205632	99.8
5	3032621	99.5	3186839	99.2
6	3005952	98.6	3204993	99.7
Mean		98.9		99.3
%RSD		0.43		0.74

Remark: *Mean of six observations

3.5 Detection Limit

The detection limit of an individual analytical procedure is the lowest amount of analyte in a sample which can be detected but not necessarily quantitated as an exact value.

Based on the Standard Deviation of the Response and the Slope:

The detection limit (DL) was expressed as equation (1):

$$DL = \frac{3.3\ \sigma}{S}$$

Where, σ = the standard deviation of the response
S = the slope of the calibration curve
The slope S may be estimated from the calibration curve of the analyte.

3.6 Quantitation Limit:

The quantitation limit of an individual analytical procedure is the lowest amount of analyte in a sample which can be quantitatively determined with suitable precision and accuracy.

Based on the Standard Deviation of the Response and the Slope:
The quantitation limit (QL) was expressed as equation (2):

$$QL = \frac{10\,\sigma}{S}$$

Where, σ = the standard deviation of the response
S = the slope of the calibration curve
The slope S may be estimated from the calibration curve of the analyte.

3.7 Accuracy

Accuracy of the method was confirmed by recovery studies. The accuracy was expressed by calculating the percent recovery of the analyte from dissolution sample and % RSD was calculated. To evaluate the accuracy of the proposed method, successive analysis of four different concentrations of 25 %, 50 %, 100 % and 150 % standard BOS were carried out using proposed method. The recovery studies were performed in triplicate. The percentage recovery and % RSD were found to be 99.9638 % and 0.0516 %, respectively. This indicates that there was no interference due to excipients used in formulation. Hence, the proposed method was found to be accurate (Table 4).

Table 4. Accuracy of the method for the determination of Bosentan

Spiked level	Amount Added * (mg)	Amount Recovered* (mg)	Peak Area*	% Recovery	Mean (%) Recovery	SD	% RSD
25 %	30.042	29.993	730938	99.83	99.96	0.05	0.05
25 %	30.119	30.119	734019	100.00			
25 %	30.139	30.139	734518	100.00			
50 %	60.307	60.300	1469540	99.99			
50 %	60.220	60.187	1466788	99.95			
50 %	60.278	60.237	1467998	99.93			
100 %	120.595	120.590	2938812	100.00			
100 %	120.846	120.843	2944988	100.00			
100 %	120.759	120.661	2940543	99.92			
150 %	181.173	181.165	4415051	100.00			
150 %	181.057	181.045	4412127	100.00			
150 %	181.134	181.088	4413178	99.97			

Remark: *Mean of six observations.

3.8 Specificity

For the specificity study, the blank, placebo, standard and sample solution were prepared and injected for the determination of interference in the retention time of BOS peak. No interference from blank and placebo was observed at the retention time of the BOS. Therefore, it was concluded that the method was specific and can assess unequivocally the analyte of the interest in the presence of possible interference. The chromatograms for the blank, placebo, standard and sample are shown in Figure 3.

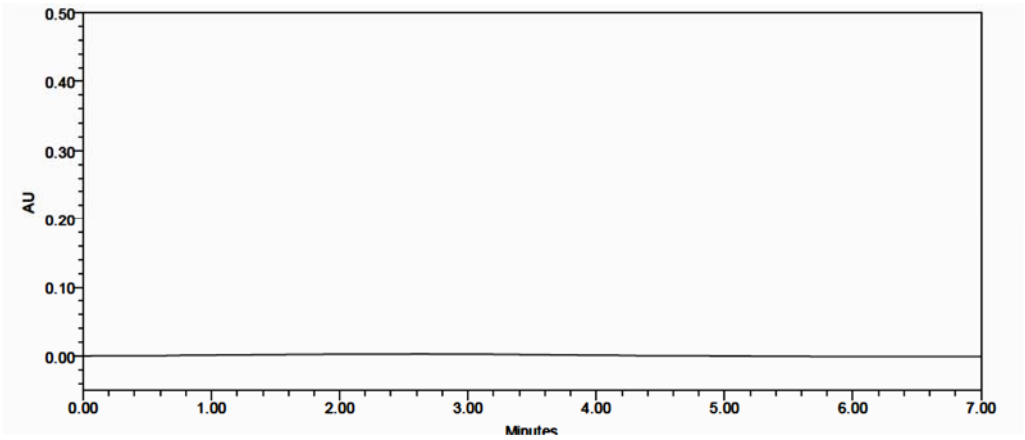

(a)

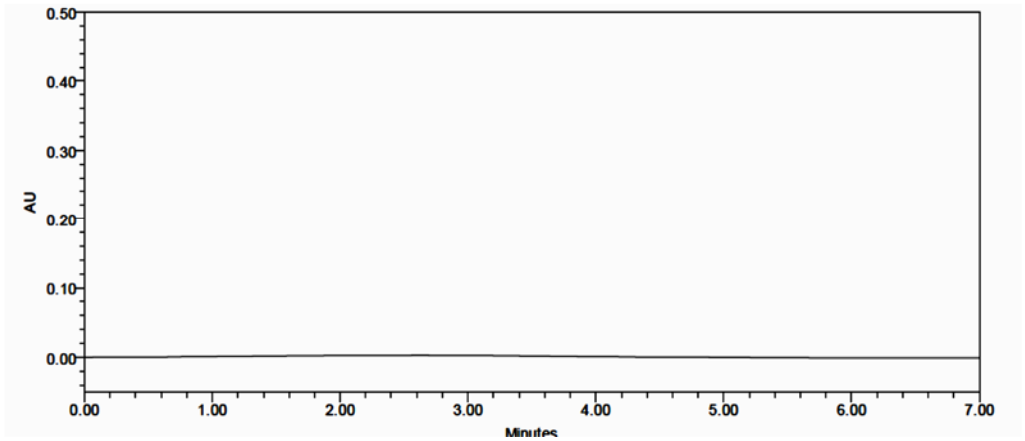

(b)

Figure 3. Chromatogram (a) blank, (b) placebo, (c) standard, (d) sample

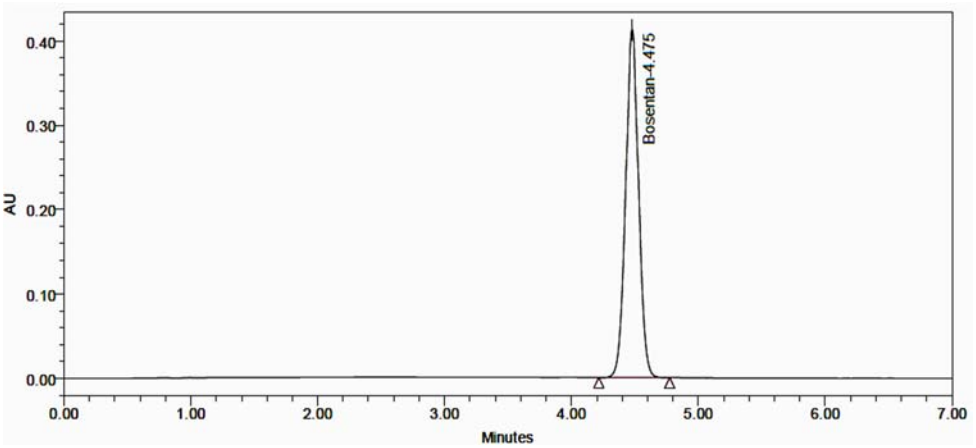

(c)

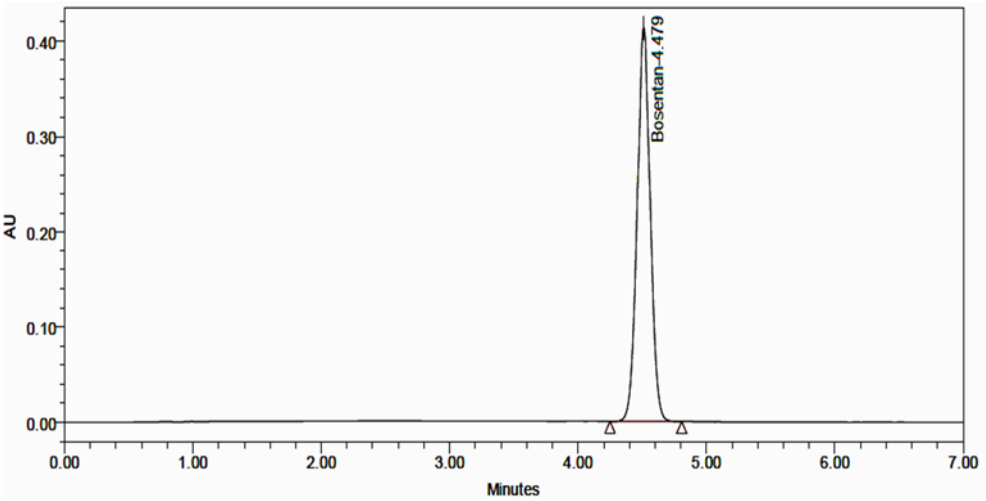

(d)

Figure 3. Chromatogram (a) blank, (b) placebo, (c) standard, (d) sample (cont.)

3.9 System suitability test

System suitability test was used to verify the precision/ reproducibility of the system that is adequate for the analysis to be performed. Parameters such as theoretical plates, tailing factor and reproducibility (% RSD for peak area of five replicates) were determined and compared against specifications. Five replicate injections of standard BOS solution were run using HPLC. Theoretical plate and tailing factor were determined. The theoretical plates were found to be 7829 and tailing factor was found to be 0.97 which were found to be within the limit (Table 5).

Table 5. System suitability parameters

S. No	Parameter	Obtained value	Acceptable limit
1	Retention time (min)	4.475	-
2	Theoretical plates	7829	>2000
3	Tailing factor	0.97	< 2
4	%RSD	0.3115	< 2

3.10 Robustness

Robustness of the method was checked by making slight changes in chromatographic and dissolution conditions like mobile phase ratio, pH of buffer, flow rate, temperature, medium volume, medium strength, and rpm. It was observed that there were no marked changes in the chromatograms, which demonstrated that the developed RP-HPLC method was found to be robust (Table 6).

Table 6. Robustness

Parameter		Retention Time*	Peak area*	% RSD	USP Tailing
Flow Rate	1.35 ml/ min	5.156	3313367	0.06	0.91
	1.65 ml/ min	4.247	2708208	0.08	0.91
Column Temp	35^0C	4.770	2978422	0.10	0.92
	45^0C	4.541	2975434	0.13	0.90
Mobile phase	48:52	4.007	2968468	0.05	0.92
	52:48	5.476	2973257	0.15	0.90
Normal Buffer pH	2.3	4.677	2961037	0.06	0.91
	2.7	4.820	2957455	0.04	0.91
Wavelength	264	4.474	2987501	0.44	0.91
	268	4.480	3013954	0.43	0.91
Strength of Medium	0.8% SLS	4.476	2994092	0.97	0.91
	1.2% SLS	4.483	3013470	0.69	0.91
Volume of Medium	882 ml	4.473	3050004	1.16	0.91
	918 ml	4.478	2941830	1.49	0.91
RPM	48	4.471	3000895	0.56	0.91
	52	4.479	3041987	0.38	0.91

Remark: *Mean of six observations

3.11 Filter study

A filter study was performed to determine the suitability of filter used and to determine the amount of filtrate to be discarded before a sample solution was collected for analysis. The peak area found in the filtered fractions of sample solution was comparable to the peak area found in the centrifuged portion of sample solution. There was no significant difference in peak area between different volumes filtered. Therefore the 0.45 µm PVDF and Nylon filter were suitable for use and the discarding of 4 ml of sample solution as filtrate as stated in the method (Table 7).

Table 7. Filter Study

Sample Name	Peak Area	% Difference
Centrifuged (10 min @ 3500rpm)	3002048	NA
0.45µ PVDF filtered, 3 ml discarded	3008720	0.2200
0.45µ PVDF filtered, 4 ml discarded	3009031	0.2300
0.45µ PVDF filtered, 5 ml discarded	3013272	0.3700
0.45µ PVDF filtered, 6 ml discarded	3011554	0.3100
0.45µ Nylon filtered, 3 ml discarded	3002468	0.0100
0.45µ Nylon filtered, 4 ml discarded	3008625	0.2100
0.45µ Nylon filtered, 5 ml discarded	3015016	0.4300
0.45µ Nylon filtered, 6 ml discarded	3005939	0.1200

3.12 Dissolution

The method was applied to dissolution study of BOS. The percentage drug release was found to be 99.41 % for Bosentan tablet 125 mg and 99.99 % for Marketed Bosentan Tablet 125 mg. Several trials were performed by changing the dissolution medium, the 1% SLS dissolution medium showed successful drug release. The results are shown in Table 8.

Table 8. Determination of percentage release in marketed formulation

Injection	Label claim (mg)	% Drug Release
Tracleer 125 mg	125 mg	99.99 %
Bosentas	125 mg	99.98%
Lupibos	125 mg	98.64%

3.13 Solution stability

The stability of both standard and sample solutions was studied by observing the peak areas of both the drugs. The amount calculated at different time intervals was within the acceptable limit. The results indicate that the solutions were stable up to 48 hours. The stability data is illustrated in Table 9.

Table 9. Solution stability of sample at room temperature

Time	Peak Area*	Retention Time	% Release*	% Difference
Initial	2995113	4.481	98.3	NA
24 h	2990682	4.483	98.1	0.14
48 h	2983104	4.485	97.9	0.40

3.14 Comparison of the developed method with the reported methods

Lavudu *et al*. [16, 18] reported two methods for the estimation of BOS by RP-HPLC but the retention times were found to be 1.986 mins and 2.449 mins, respectively. When calculating capacity factor, it was low and the separation was not good. Hence, the developed method had more advantageous than the reported methods. Karnakar reddy *et al.* [13] selected the detection wavelength as 220 nm. But the λmax of BOS was more than 265 nm. Hence, the detection was not clearly done in the reported method. The developed method was validated accordance with ICH guidelines and met all the acceptance criteria. The system suitability parameters calculated also in the accepted range. Hence the developed method can be used for the effective routine quality control analysis and dissolution study of BOS in bulk, tablet dosage form and in dissolution medium.

4. Conclusions

A simple, precise, accurate and reproducible RP-HPLC method has been developed and validated for the quantitative determination of Bosentan in the dissolution sample. A complete dissolution of BOS could be achieved after 45 min using apparatus II (paddle) at 50 rpm in 900 ml of dissolution medium (1 % Sodium lauryl sulphate). Based on the above studies, it was concluded that the developed RP-HPLC method was specific, accurate, precise, rugged, robust and linear over the concentration range. The report obtained in the validation parameter met the respective acceptance criteria. The results were statistically validated. Hence, the developed method can be used for routine quality control analysis and dissolution study of Bosentan in bulk and in pharmaceutical dosage form.

5. Acknowledgements

The authors are very much thankful to Dr. G. Murugananthan, Principal, Swamy Vivekanandha College of Pharmacy, Elayampalayam, Tiruchengode for his support and also thank to the management for providing the necessary facilities to carry out this research work.

References

[1] Kluwers, W., 2006. A to Z Drug Facts. Missouri: Facts & Comparisons a Wolters Kluwer business.
[2] https://livertox.nih.gov/Bosentan.htm/ dated 15.10.2017.
[3] www.rxlist.com/tracleer-drug/warnings-precautions.htm/ dated 15.10.2017.
[4] www.drugbank.ca/drugs/DB00559/ dated 15.10.2017.
[5] https://www.drugs.com/cdi/bosentan.html/ dated 15.10.2017.
[6] http://www.chemspider.com/Chemical-Structure.94651.html/ dated 15.10.2017.
[7] Sweetmar, S.C., 2011. Martindale: The complete Drug Reference. USA: Pharmaceutical Press.
[8] https://en.wikipedia.org/wiki/Bosentan.htm/ dated 15.10.2017.
[9] Maryadele, J., Heckelman, P.E. eds., 2006. The Merck Index. USA: Merck Research Laboratories.
[10] Ashok kumar, A., Anil kumar, A. and Gouri sankar, D., 2011. Development, estimation and validation of Bosentan in bulk and in its pharmaceutical formulation by UV-Visible spectroscopic method. *Int. J. Pharm and Bio Science,* 2(2), 225-230.

[11] Narendra, A., Deepika, D. and Mathrusriannapurna, M., 2012. New spectrophotometric method for the determination of Bosentan an anti-hypertensive agent in pharmaceutical dosage form. *Eur. J. Chem.,* 9 (2), 700-704.
[12] Shaik, M., Saidulu, P., Tejaswini, I.S. and Annapurna, U., 2014. Development of new validated analytical methods for the estimation of bosentan in bulk and pharmaceutical dosage form by UV spectrophotometry. *W. J. of Pharm. Res.,* 3(4), 509-516.
[13] Karnaker reddy, T., Younus, M.D., Ravindra reddy, Y., Ashwini kumar, G. and Sravan, S., 2011. RP-HPLC method development and validation of Bosentan drug present in tablets. *Int. J. Pharm. Tech.*, 2(3), 577-587.
[14] Muralidharan, S. and Kumar, J.R., 2012. Simple estimation of Bosentan in tablet formulation by RP-HPLC. *Ame. J. Anal. Chem.*, 3, 715-718.
[15] Sujatha, K., Palavan, C. and Seshagiri Rao, J.V.L.N., 2013. A new validated RP-HPLC method for the estimation of Bosentan in tablet dosage forms. *Ame. J. Pharm. Tech.,* 3 (4), 675-680.
[16] Lavudu, P., Rani, A.P., Chander, P. and Sekaran, C.B., 2013. Determination of Bosentan in pharmaceutical dosage forms by high performance liquid chromatography. *Int. J. Drug Del.*, 5(2), 146-151.
[17] Kalaichelvi, R. and Jayachandran, E., 2013. Estimation of Bosentan in pure and tablet dosage form by RP-HPLC. *Int. J. Pharm. Chem. Scien.*, 2(2), 837-840.
[18] Lavudu, P., Rani, A.P., Sekaran, C.B., Ramesh, A. and Kumar, A., 2014. Application of spectrophotometry and high performance liquid chromatography for the analysis of Bosentan in pharmaceutical dosage form. *Chem. Sci. Transaction.*, 3(4), 1242-1253.
[19] Khan, M.A., Sinha, S., Todkar, M., Parashar, V. and Swamy Reddy, K., 2012. Development and validation of a stability indicating analytical method for the related substances of Bosentan drug substance by HPLC. *Ame. J. Scien. Ind. Res.*, 3(2), 69-80.
[20] Rizwan, S.H., GirijaSastry, V. and Imad, Q., 2015. Stability indicating method development and validation of Bosentan in bulk drug and formulation by RP-HPLC method. *Int. J. Pharm. Tech. Res.*, 8(4), 569-579.
[21] Lakshmi Madhuri, B., Yadav, S. and Rao, J., 2016. RP HPLC stability indicating method development and validation for the determination of Bosentan in bulk and pharmaceutical dosage form. *Der Pharma Lett.*, 8(2), 487-495.
[22] Marolia, B.P., Shailesh Shah, A., Kunjan Bodiwala, B., Pintu Prajapati, B. and Hemakshi Jariwala, P., 2015. Development and validation of stability indicating HPTLC method for estimation of Bosentan monohydrate in tablet dosage form. *J. Pharm. App. Sci.*, 2(1), 29-35.
[23] Nataraj, K.S., Narasimharaju Raju, G.N.V.S., Srinivas Rao, A., Sai Kumar, S.V., Divya, S., and Alekhya, K., 2015. Method development and validation for impurity profiling of Bosentan monohydrate using a novel RP-HPLC method. *E. J. Pharm. Med. Res.*, 2(3), 526-544.
[24] Sivasaikiran, B., Nayudamma Chowdary, Y., Sreelakshmi, V., Shrivastava, S.K., and Pugazhendhy, S., 2014. Development and validation of a headspace gas chromatographic method for determination of residual solvents in Bosentan monohydrate. *Int. J. Pharm. Tech Res.*, 6(2), 421-427.
[25] Paul Richard, M., Haseena, S., Swarnalatha, G., Vanitha, C., Vijayakumar, B., Prakash, M., 2015. Development and validation of a headspace gas chromatographic method for determination of residual solvents in Bosentan monohydrate pure drug. *Asian J. Pharm. Res.*, 5 (1), 29-36.
[26] Atila, A., Ozturkb, M.; Kadioglua, Y., Halici, Z., Turkana, D., Yaylac, M. and Und, H., 2014. Development and validation of UFLC–MS/MS method for determination of Bosentan in rat plasma. *J. Pharm. Bio-med Anal.*, 97, 33-38.

[27] ICH, Q2 (R1), 2005. Harmonized tripartite guideline validation of analytical procedure, text and methodology, pp.4-5. Retrieved from http:// www.ich.org/ fileadmin/ public website/ ICHproducts/ guidelines/ quality/ Q2 R1 Guideline. pdf. 15.10.2017

Current Applied Science and Technology Vol. 18 No. 2 May-August 2018
DOI: 10.14456/cast.2018.6

UV Shielding Properties of Cellulose/TiO_2 Composite Film

Kittiya Plermjai[1], Weerachon Phoohinkong[1], Sorapong Pavasupree[2], Wanichaya Mekprasart[1], Wisanu Pecharapa[1] and Kanokthip Boonyarattanakalin[1*]

[1]College of Nanotechnology, King Mongkut's Institute of Technology Ladkrabang, Bangkok, Thailand
[2]Department of Materials and Metallurgical Engineering, Faculty of Engineering, Rajamangala University of Technology Thanyaburi, Pathumthani, Thailand

Received: 4 November 2017, Revised: 12 January 2018, Accepted: 4 July 2018

Abstract

Cellulose/TiO_2 composite film was prepared for UV shielding applications. Cellulose was extracted from sugarcane bagasse by ball milling process. The cellulose/ TiO_2 composite film with different concentrations of cellulose showed a synergic feature of optical transparency and UV-blocking. The crystalline structure of cellulose was characterized by X-ray diffraction (XRD). The treated cellulose has higher crystallinity than the untreated cellulose. Fourier transform infrared spectroscopy (FT-IR) analysis shows the evidence of chemical treatment hemicellulose and lignin removal from sugarcane bagasse. The optical properties were measured by UV-Vis spectrometer, the results of TiO_2 and cellulose solution correspond to UV-A and UV-C absorbance regions with high transparent of cellulose composite films. The revealed results are essential for UV protecting materials application.

Keywords: nanocellulose composite, TiO_2, UV-shielding, ball milling

1. Introduction

Cellulose is the most abundant resource material on earth. Cellulose is natural, renewable and biodegradable polymers [1, 2]. It is a linear homo-polysaccharide composed of $(1 \rightarrow 4)$ linked D-glucose units. Cellulose can be found in wood, cotton, rice straws, and sugarcane bagasse [2-5]. Sugarcane bagasse is a residue from sugar and alcohol industries. Many industries have used sugarcane bagasse as a raw material for electronic sensor, paper production, fermented products, and packaging [3]. In general, sugarcane bagasse contains 40-50% cellulose, 25-35% of hemicellulose and 18-24% of lignin [3, 5]. Various methods, such as acid hydrolysis, ionic liquid treatment, enzymatic hydrolysis and mechanical treatment, can be used to obtain cellulose. As a mechanical treatment, ball milling is a top-down technique from micro to nano-scale materials. Ball milling is widely used for the preparation of nanoparticles because of its simple operation, use of relatively inexpensive equipment, and its broad applicability to most types of biomass [6-7].

*Corresponding author: E-mail: kanokthip.bo@kmitl.ac.th

Hybrid inorganic/organic materials constitute a new class of functional nano-composites that exhibit high optical, thermal, and mechanical properties due to synergistic effects [8-9]. Natural cellulose is a linear polymer of β-(1→4)-D-glucopyranose with abundant surface hydroxyl groups forming plentiful inter- and intra-molecular hydrogen bonds. These hydroxyl groups provide suitable substrate for metal oxide incorporation onto the cellulose surface. Moreover, the extensive hydrogen bond network builds up a defined hierarchical order of supra-molecular organization for providing a chamber with the formation of inorganic nano-materials. Incorporation of TiO_2 to polymer casting solution could greatly affect the morphologies and properties of the resulting composite. Consequently, a wide range of applications can be obtained such as antimicrobial, anti-fungal, UV protective or self-cleaning properties. TiO_2 is a promising metal oxide that is extensively utilized in many industrial processes due to its stability, biocompatibility, non-toxicity and low cost [5–8].

In this work, cellulose was extracted from sugarcane bagasse by ball milling with mild acid hydrolysis and cellulose/TiO_2 composite films were prepared for an ultraviolet protecting material candidate.

2. Materials and Methods

2.1 Materials

Sugarcane bagasse was collected from plantations located at Sing Buri province, Thailand and used as a starting source of cellulose. Other reagents used were sulfuric acid, sodium hydroxide and hydrogen peroxide.

2.2 Methods

2.2.1 Isolation of cellulose

For extraction of cellulose, sugarcane bagasse was dried in sunlight and then cut into small pieces. The cut bagasse was milled into a powder. The bagasse powder (100 g) was dewaxed using 5% (v/v) sulfuric acid solution (2000 mL) for 2 h with constant stirring at 60 °C. The water-soluble components were removed with 50% (v/v) ethanol solution. The dewaxing process was repeated for 4 times. The residue was consequently washed with distilled water until the pH of the washed water became neutral. This step was conducted to remove lignin. In order to remove hemicellulose, the residual was bleached using 24% hydroogen peroxide and 4% sodium hydroxide solution with mechanical stirring at 60 °C for 2 h, filtered, and washed with distilled water to neutrality. After that, the slurry of 1% (wt/wt) purified cellulose in water was processed by grinding with ball milling process with the two different diameters size of zirconia balls (2 and 5 mm), in which the ball to material weight ratio was 3:1. The milling was performed for 24 h at 275 rpm with distilled water. The product was filtered and washed with distilled water until the pH of the washing water became neutral

2.2.2 Preparation of cellulose and cellulose/TiO_2 composite films

For preparing cellulose and cellulose/TiO_2 composite films, poly vinyl alcohol (PVA) was used for solution preparation. The 5% (wt/wt) PVA solution was prepared by dissolving in distilled water. Cellulose (0.05, 0.5, and 1% (wt/wt)) was added to the PVA solution. The stirring was performed at 80 °C for 2 h. After that, the mixed precursor was dispersed by sonication for about 5 min. For the preparation of cellulose/TiO_2 composite films, the 0.01% (wt/wt) TiO_2 solution was prepared by dispersed it in distilled water then added to the 5% (wt/wt) PVA solution using mechanical stirrer for 1 h. After that cellulose of 0.05, 0.5, and 1% (wt/wt) was added to the PVA/TiO_2 solution then stirring

at 80 °C for 2 h and the resulting mixture was dispersed by sonication for 5 min. The final suspension was casted in PET plates and dried at 55 °C for 4 h to remove water before characterization.

2.3 Characterization

The chemical constituents of sugarcane bagasse and cellulose composite were investigated by FTIR spectroscopy (Thermo Scientific Nicolet 6700). The FTIR spectra were recorded in the region between 4000 and 400 cm^{-1}. The crystalline structure and phase identification of the cellulose composites were investigated by X-ray diffraction (Rigaku, Smartlab). The optical transmittance of the prepared films was measured from 200 to 700 nm using UV-Vis spectrometer (PG, T90+).

3. Results and Discussion

3.1 FTIR spectroscopic analysis

FTIR spectra of sugarcane bagasse and extracted cellulose are shown in Figure 1. Accordingly, all samples have three main absorbance regions (Figure 1(a)) in the ranges of 800-1200 cm^{-1}, 1200-1800 cm^{-1} and 2500-3900 cm^{-1} which are assigned to different vibrations mode of various functional groups as observed in Figure 1(b)-(d). The peak at 832 cm^{-1} indicates the bending vibration of the arene C-H bond in lignin. The peak was not found after the bleaching and extracted cellulose by ball-milling in sample (3) and (4). The peak at 897 cm^{-1} in sample (3) and (4) is associated with β-glycosidic linkages between glucose units in cellulose/hemicellulose [10]. This characteristic peak was not found in lignin structure (sample (1) and (2)) indicating that the bleached and extracted samples contain greater amount of cellulose and hemicellulose. The strong peaks observed in the spectra of all samples between the ranges of 1034, 1051 and 1160 cm^{-1} are related to the C-O stretching of cellulose, in plane aromatic C-H deformation vibration of lignin, and C-O antisymmetric stretching vibration of glucosidic ring in cellulose/hemicellulose and pyranose ring C-O-C asymmetric stretching of cellulose/hemicellulose, respectively [12]. The peak at 1105 cm^{-1} can be assigned to the C-O-C glucosidic ring vibration in cellulose. The absorption peaks at 1200 cm^{-1} is O-H deformation vibration mode of cellulose, while the 1240 cm^{-1} peak is aryl C-O out of plane stretching vibration in lignin. After bleaching process, the lignin peaks are not found in samples (3) and (4), revealing the complete removal of lignin. The absorption peaks at 1320 cm^{-1} which are present in all samples are assigned to CH_2 wagging. The peak at 1365 cm^{-1} and 1450 cm^{-1} correspond to the bending vibrational mode of C-H and C-O bonds in polysaccharide aromatic rings and the C-H asymmetric deformations, respectively [10 - 12]. The peak at 1513 cm^{-1} is derived from vibration mode of C=C aromatic ring skeletal in lignin. After bleaching process and extraction in sample (3) and (4), this characteristic peak of lignin vanished. The peak at around 1600 cm^{-1} in raw bagasse and dewaxed sample is due to C=O stretching vibration. This peak also disappears in extracted and blenched samples. The wide absorbance peak at around 1634 cm^{-1} in the extracted and blenched samples is associated with absorbed water in cellulose. Moreover, the peak positioned at 1728 cm^{-1} is correlated to C=O stretching vibration of carboxylic group of lignin and hemicellulose [10-12]. The cellulose samples after bleaching process do not have the peak at 1728 cm^{-1}, indicating that lignin and hemicellulose are totally removed from sugarcane bagasse [13-15]. The absorption peak at around 2900 cm^{-1} is due to the C-H stretching vibration. The broad peak at around 3340 cm^{-1} is attributed to the O-H stretching vibration of the OH groups.

From the FTIR analysis, it is shown that sample (1) and (2) contain lignin and hemicellulose. After bleaching process with hydrogen peroxide solution and extraction of cellulose by ball-milling, the characteristic peak of hemicellulose and lignin vanished. The cellulose was purified by chemical and mechanical treatments to remove of lignin and hemicellulose during cellulose isolation process.

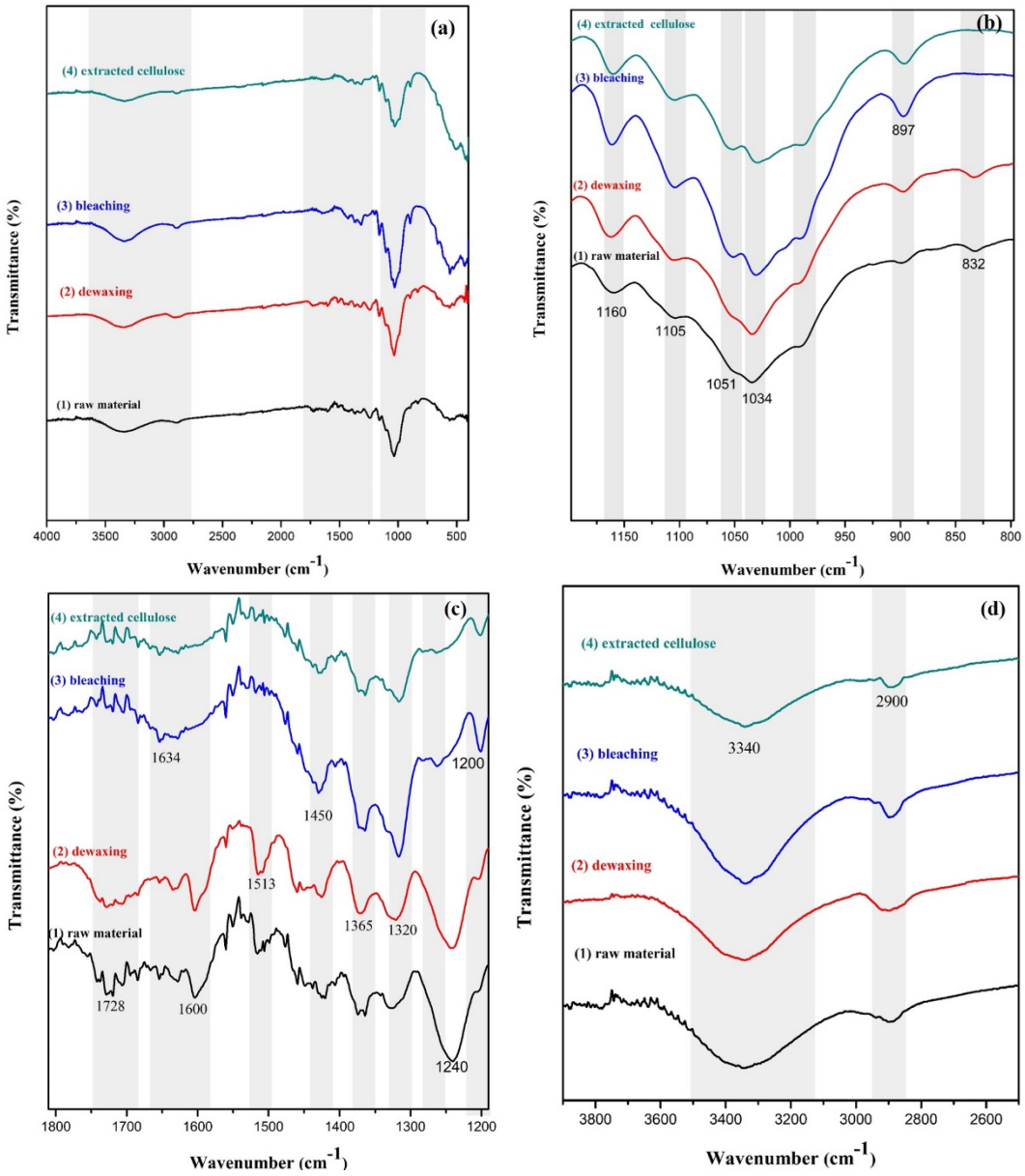

Figure 1. (a) FTIR spectra of lignocellulose, (b) FTIR spectra in the region between (800-1200 cm^{-1}), (c) between (1200-1800 cm^{-1}) and between (2500-3900 cm^{-1}).

3.2 X-ray diffraction

X-ray diffraction was used to analyze the cellulose structure and crystalline. There are several polymorphs of cellulose (I, II, III and IV). Typically, cellulose in natural such as trees, plants, tunicates, algae, and bacteria is cellulose I polymorph with monoclinic and triclinic structures. The

XRD pattern of cellulose I contains the main diffraction peaks at 2θ are around 16.5°, 22.5° and 34.5° which correspond to the (110) (200) and (004) lattice planes [16]. The XRD results were shown in Figure 2 in which sample (a) is untreated cellulose and sample (b) is treated cellulose by ball-milling 24 h. There are two main peaks at 16.5°, 22.5° in the XRD pattern of untreated cellulose with broadening base peak due to the amorphous nature. After the cellulose was treated by bleaching and ball-milling process, the flat base line in (110) and (200) peaks with the small peak at 2θ = 34.5° are observed. From the XRD results, it can be summarized that the bleaching and ball-milling processes increased the crystallinity of cellulose because the hydrolysis in bleaching process removed the amorphous lignin and hemicellulose [11, 17].

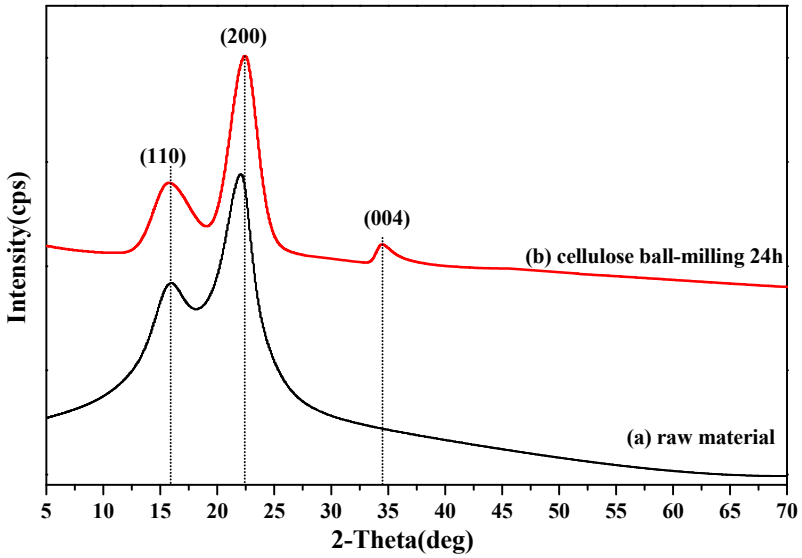

Figure 2. XRD patterns of (a) sugarcane bagasse, (b) cellulose ball-milling 24 h

3.3 Transmittance

The UV absorbance spectra of TiO_2 and cellulose solution were measured from 200 to 700 nm. The absorbance of TiO_2 and cellulose solution shown in Figure 3 exhibits its UV-blocking ability. The strong absorbance peak at around 200 nm and 350 nm of cellulose and TiO_2 solution correspond to UV-C and UV-A regions, respectively. UV-Vis spectra in transmission mode was recorded for PVA/cellulose without TiO_2 and PVA/cellulose with TiO_2 composite films with different concentrations of cellulose (0.05, 0.5 and 1 wt %). The results of transmittance were shown in Figure 4. Bare PVA/cellulose without TiO_2 and PVA/cellulose with TiO_2 composite films have rather high transparency in visible region implying that these films are able to transmit visible light while shielding UV radiation. As the same time, when increasing the concentration of cellulose composite films, the UV transmittance decreased (Figure 4). Meanwhile, as the film was incorporated with TiO_2-P25 nanoparticles, their transparencies in UV region ranging from 250-350 nm drastically decreased but their values in visible region insignificantly decreased. The feature can be related to the typically strong UV absorbance character of cellulose and TiO_2.

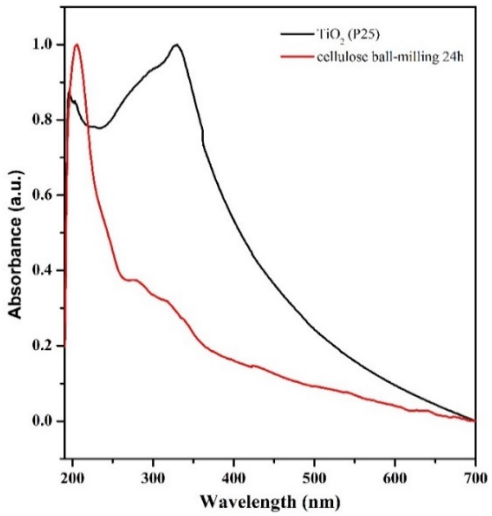

Figure 3. The UV absorbance spectra of TiO_2 and cellulose solution.

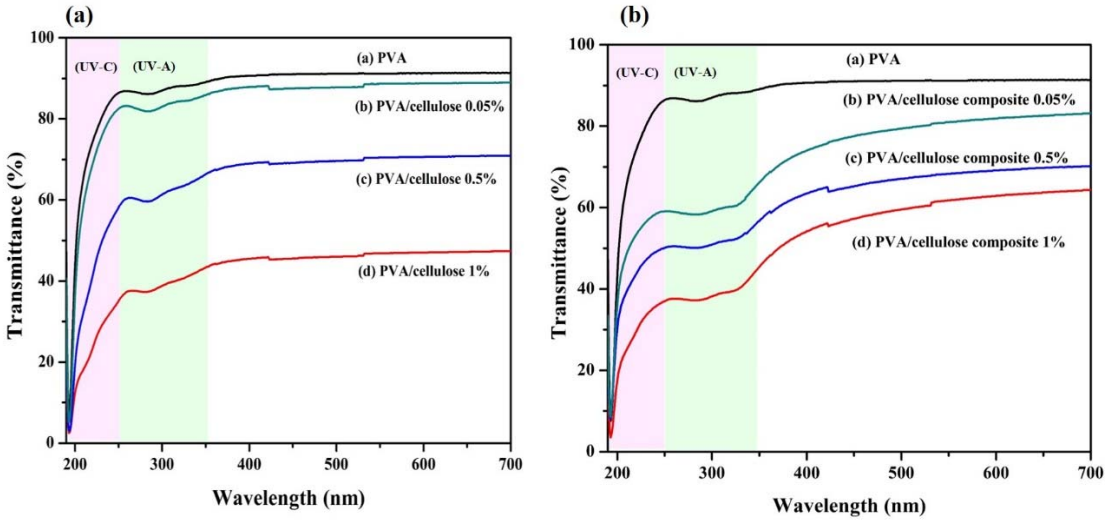

Figure 4. UV-Vis spectra of PVA/cellulose films (a) and PVA/cellulose composite films (b)

4. Conclusions

In this study, cellulose was successfully isolated from sugarcane bagasse by ball-milling process and acid leaching. The FTIR spectra analysis shows that the chemical treatment could remove most of hemicellulose and lignin from the sugarcane bagasse as shown by the disappearance of characteristic peaks of hemicellulose and lignin. The XRD pattern revealed that the treated cellulose by bleaching and ball-milling process has a higher crystallinity than the untreated cellulose. The absorbance regions of of TiO_2 and cellulose solution correspond to UV-A and UV- C while the optical transparency of cellulose composite films are high transmittance.Thus the composite films

have the optical properties of UV protecting with high transparency. Under these conditions, the obtained results show that the cellulose composite films could be applied for the realization of transparent, low-cost, lightweight, and flexible substrates in UV-blocking fields.

5. Acknowledgements

This work has partially been supported by the National Council of Thailand (Grant No 488072) and College of Nanotechnology, King Mongkut's Institute of Technology Ladkrabang.

References

[1] Salas, C., Nypelö, T., Abreu, C.R., Carrillo, C. and Rojas, O., 2014. Nanocellulose properties and applications in colloids and interfaces. *Current Opinion in Colloid and Interface Science*, 19, 383-396.

[2] Li, W., Yue, J. and Liu, S., 2012. *Ultrasonics Sonochemistry*, 19, 479-485.

[3] Mandal, A. and Chakrabarty, D., 2011. Isolation of nanocellulose from waste sugarcane bagasse (SCB) and its characterization. *Carbohydrate Polymers*, 86, 1291-1299.

[4] Habibi, Y., Lucia, L.A. and Rojas, O., 2010. Cellulose nanocrystals: Chemistry, self-assembly, and applications. *Chemical Reviews*, 110, 3479-3500.

[5] Oliveira, F.B.d. *et al.*, 2016. Production of cellulose nanocrystals from sugarcane bagasse fiber and pith. *Industrial Crops and Products,* 93, 48-57.

[6] Phanthong, P., Guan, G., Ma, Y., Hao, X. and Abudula, A., 2016. Effect of ball milling on the production of nanocellulose using mild acid hydrolysis method. *Journal of the Taiwan Institute of Chemical Engineers*, 60, 617-622.

[7] Zhao, H., Kwak, J.H., Wang, Y., Franz, J.A., White, J.M., and Holladay, J.A., 2006. Effects of crystallinity on dilute acid hydrolysis of cellulose by cellulose ball-milling study. *Energy and Fuels*, 20, 807-811.

[8] Julkapli, N.M. and Bagheri, S., 2017. Progress on nanocrystalline cellulose biocomposites. *Reactive and Functional Polymers*, 112, 9-21.

[9] Morawski, A. W., Kusiak-Nejman, E., Przepiórski, J., Kordala, R. and Pernak, J. 2013. Cellulose-TiO_2 nanocomposite with enhanced UV-Vis light Absorption. *Cellulose,* 20(3), 1293-1300.

[10] Ouyang, X., Wang, W., Yuan, Q., Li, S., Zhang, Q. and Zhao, P., 2015, Improvement of lignin yield and purity from corncob in the presence of steam explosion and liquid hot pressured alcohol. *RSC Advances*, 5, 61650-61656.

[11] Rahimi Kord Sofla, M., Brown, R.J., Tsuzuki, T. and Rainey, T.J. 2016. A comparison of cellulose nanocrystals and cellulose nanofibres extracted from bagasse using acid and ball milling methods. *Advances in Natural Sciences: Nanoscience and Nanotechnolo*gy, 7(3),1-9.

[12] Alemdar, A. and Sain, M., 2008. Isolation and characterization of nanofibers from agricultural residues - wheat straw and soy hulls. *Bioresource Technology*, 99, 1664-1671.

[13] Mandal, A. and Chakrabarty, D., 2011. Isolation of nanocellulose from waste sugarcane bagasse (SCB) and its characterization, *Carbohydrate Polymer*s, 86, 1291-1299.

[14] Sain, M. and Panthapulakkal, S., 2006. Bioprocess preparation of wheat straw fibers and their characterization. *Industrial Crops and Products,* 23, 1-8.

[15] Li, W., Wu, Q., Zhao, X., Huang, Z, Cao, J., Li, J., and Liu, S., 2014. Enhanced thermal and mechanical properties of PVA compositesformed with filamentous nanocellulose fibrils. *Carbohydrate Polymers*, 113, 403-410.

[16] Moon, R.J., Martini, A., Nairn, J., Simonsen, J. and Youngblood, J., 2011. Cellulose nanomaterials review: Structure, properties and nanocomposites. *Chemical Society Reviews*, 40, 3941-3994.

[17] Wu, R-L., Wang, X-L., Wang, Y-Z., Bian, X-C. and Li, F., 2009. Cellulose/soy protein isolate blend films prepared via room-temperature ionic liquid. *Industrial and Engineering Chemistry Research*, 48, 7132-7136.

Current Applied Science and Technology Vol. 18 No. 2 May-August 2018
DOI: 10.14456/cast.2018.7

A New Type of Dilute Magnetic Semiconductor: Saturation Magnetization Dependence on Level of Nonmagnetic Ion Doping

Prissana Robkhob[1], Sirikanjana Thongmee[1], I-Ming Tang[2*]

[1]Department of Physics, Faculty of Science, Kasetsart University, Bangkok, Thailand
[2]Computational & Applied Science for Innovation Clusters (CLASSIC)
Faculty of Science, King Mongkut's University of Technology, Thonburi, Thailand

Received:13 April 2018, Revised:18 July 2018, Accepted: 1 August 2018

Abstract

By definition, a dilute magnetic semiconductor is a II-IV or III-V semiconductor in which some of the nonmagnetic ions are replaced by magnetic ions. Defects due to Zn vacancies in ZnO nano particles (NP's) can induce virtual magnetic moments in this semiconduct or making it a room temperature ferro magnet. The systematic changes in the magnetic behaviors of ZnO NP's doped with non magnetic Al, Ag, Mg and Sb ions are observed. The changes are usually explained in terms of the increased stability of the zinc vacancies when the vacancies are a part of new impurity complexes formed when the impurity ions substitute for the zinc ions. In most cases, this explains the increases in the saturation magnetizations as more nonmagnetic impurities are substituted into the ZnO NP's.

Keywords: ZnO nanoparticles, Zn vacancies, Virtual magnetic moments, Hysteresis Loops, DFT calculations.

1. Introduction

Dilute magnetic semiconductors [1] or DMS's are semiconductors in which some of the nonmagnetic ions are replaced by magnetic ions. At the present time, the main examples are (Ga, M)As, (Ga, Mn)P and (Ga, Mn)N [2]. To be useful, the semiconductors must undergo a ferromagnetic transition above room temperature. The Curie temperature T_c of (Ga, Mn) As is $T_C \sim$ 170 K while (Ga, Mn) P and (Ga, Mn) N have T_C's of approximately 400 K and 940 K, respectively [3]. To help in the search for new DMS, Coey *et al.* [4] have calculated the T_C of possible new DMS created by the doping of the II-IV semiconductors with different magnetic TM impurities. The magnetic properties of the TM ions are due to the presence of unpaired electrons in the magnetic transition metal ions. The electron orbiting in one direction will create a magnetic moment in one direction, while the electron orbiting in the other direction will create a magnetic moment in the opposite direction. If the electrons are paired, the two magnetic moments will cancel out.

*Corresponding author: E-mail: fscimt@ku.ac.th

For $T \geq T_C$ a spontaneous magnetic field will arise in the DMS. This field will cause the electric current, which consists of both spin up and spin down electrons, to split into two currents, one consisting of a current of one spin and the other of the opposite spin. In other words, the magnetic field lowers the energies of the spin down electrons, and increased the energies of the spin up electrons; resulting in a current of spin down electrons and another of spin up electrons. The level of the energy gap of the semiconductor can be raised or lowered by adjusting a bias field. This could result in the filtering of one of the components of the current, allowing only currents of one spin direction to pass through. This phenomenon is needed in spintronics devices [5] where information is not only contained in the charges stored but also in the spins of the electrons stored.

The world of magnetism was turned upside down when Venkatesan *et al.* [6] observed magnetism in the dielectric oxide HfO_2 nanoparticles (NP's). Neither the Hf^{4-} nor the O^{2-} ions have unpaired electrons and according to Hund's rule, they should not have magnetic moments. Sundarssan *et al.,* [7] have stated that ferromagnetism is a universal feature of NP's of otherwise nonmagnetic oxides such as CeO_2, Al_2O_3, ZnO, TiO_2 and In_2O_3. All of these oxides are also the II-VI semiconductors. Anisotropic ferromagnetism has been observed in one of these oxide NP's, ZnO when doped with 5 atomic % Sc, Ti, V, Fe, Co or Ni by Venkatesan *et al.* [8]. Anghei *et al.* [9] have observed ferromagnetism in ZnO NP's doped with Cr and Mn. These reported behaviors of ZnO NP's doped with magnetic TM impurities makes them dilute magnetic semiconductors (DMS).

Our interests in this paper are the doping of ZnO NP's with nonmagnetic TM ions and other ions which do not possess unpaired electrons. We are interested in the ions Sb, Ag, Al and Mg. We begin by noting that ZnO NP's would be expected to be nonmagnetic since neither Zn^{2+} ions and O^{2-} ions (like the Hf^{4+} ions and O^{2-} ions in HfO_2 NP's) have unpaired electrons, but ferromagnetism has been observed in ZnO NP's. Hong *et al.,* [10] have observed ferromagnetism in the undoped semiconducting oxide TiO_2, $HfO_2$and In_2O_3nano films. Since the bulk form of these three oxides are diamagnetic, they proposed that the room temperature ferromagnetism observed are due to either defects caused by oxygen vacancies or zinc vacancies when the thin films were formed. Rainey *et al.* [11] proposed that these defects were also responsible for the room temperature ferromagnetism in ZnO. There was a large effort to determine which defect was responsible for the RTM. This was done experimentally by looking for correlations between the presence of RTM and whether there was oxygen or zinc defects present. Many of the early studies came to the conclusion that the oxygen vacancies were connected to the appearance of RTM [12, 13].

Using first principle density functional theory (DFT), Wang *et al.* [14] found that the introduction of vacancies at the Zn sites in the wurtzite structure of the ZnO crystal into the DFT calculations produced virtual energy levels located around the vacancy sites into which the 2*p* orbital electrons of the neighboring oxygen ions could occupy. The spin polarized configurations of these electrons had a lower energy than the nonspin polarized configuration. This meant that the formation of a virtual magnetic moment was favored. Peng *et al.* [15] developed the d^o model of magnetism in the DMS. Working against the formation of the virtual magnetic moment was the extreme instability of the zinc vacancy itself. DFT calculations have shown that the life time of V_{Zn} (designation of a zinc vacancy) can be stabilized by having the zinc vacancy be part of the impurity complex formed when impurities are doped into the ZnO NR's.

Wang *et al.* [14] studied the effects of doping LI, Mg or Al into ZnO NP's. Their DFT calculations found the magnetic moments on the zinc vacancies were 1.91, 1.5 or 0.92 μ_B when the zinc vacancies were part of the impurity complexes V_{Zn} + Li_{Zn}, V_{Zn} + Mg_{Zn}, or V_{Zn} + Al_{Zn}, respectively (X_{Zn} denoting a X ion replacing the Zinc ion at one of its sites). Lu *et al.* [16] studied the effects of substituting a group V element (N, Sb, As and P) into the ZnO NP's. They believed that the stability of the ferromagnetic phase arises from the *p-p* and the *p-d* and Zn-2*d* orbital and it would decrease with the increase in the dopant atomic number due to the lower electronegativity of the dopant ions. Thus the FM stability induced by the formation of the X_{Zn} + nV_{Zm} complex decrease in the order N <Sb< As < P because of the delocalization of the O-2*p* orbital of the dopant ions. 'n'

is the number which insure the charge neutrality of the substitution. Limpijumnong *et al.* [17] found that the formation energy of the As_{Zn}+ $2V_{Zn}$complex (1.59 eV) is lower than that of the Sb_{Zn} + $2V_{Zn}$ complex (2.00 eV). Tian *et al*. [18] obtained direct experimental evidences for the importance of the Sb_{Zn} + $2V_{Zn}$ complex to the properties of the Sb-doped ZnO NP's.

Thus the physics behind the increase in the magnetizations of the doped ZnO NP's with magnetic or nonmagnetic impurities are different. The changes in the magnetic properties of ZnO NP's when doped with magnetic ions are due to the increases in the number of magnetic ions while the changes due to the doping with nonmagnetic ions are due to the increases in the stability of the zinc vacancies when they are part of a impurity complex. To gain more insights into this facet, we have looked at the changes in the magnetic properties of ZnO NP's when the number of nonmagnetic ions replacing the Zn ions in the NP's are systematically changed. As pointed out by Ventekasen *et al.* [6] and by Peng *et al.* [15] the observation of ferromagnetism in a series of materials which do not contain ions with partially filled *d* or *f* bands is a challenge to the theory of magnetism. Peng *et al.,* further asked "*whether the observed magnetismis an intrinsic property of the host material or an extrinsic property depending sensitively on the type of dopant used to induce the magnetization."* We have performed some magnetization studies to help gain more insights into these new types of DMS.

2. Materials and Methods

The various doped ZnO nanorods (NR's) were fabricated using the standard hydrothermal method. To fabricate the Sb dopedNC's, stoichiometric amounts of (Zn $(NO_3)_2{\cdot}6H_2O$) and $SbCl_3$ were weight out to yield $Zn_{1-x}Sb_xO$ NP's (x = 0.05 0.15, 0.25 and 0.30) and mixed together in an aqueous solution. The pH was adjusted to 10 by the addition of NaOH. Each solution was then placed separately into a Teflon-lined auto cave and heated to 150° C for 20 hrs. To fabricate the Ag doped NR's, stoichiometric amounts of $(Zn(NO_3)_2{\cdot}6H_2O)$ and $Ag(NO_3)_2$ were weight out to yield $Zn_{1-x}Ag_xO$ NP's (x = 0.03, 0.04 and 0.05) and the same procedure was repeated except that the temperature of the auto cave was set at 180º C. For the Al doped NR's, stoichiometric amounts of $(Zn(NO_3)_2{\cdot}6H_2O)$ and $Al(NO_3)_2$ were weight out to yield $Zn_{1-x}Al_xO$ NP's (x = 0.01, 0.02 →0.01) and the last process was repeated. For the Mg doped NC's, stoichiometric amounts of (Zn $(NO_3)_2{\cdot}6H_2O$) and Mg $(NO_3)_2$ were weight out to yield $Zn_{1-x}Mgb_xO$ NP's (x = 0.01, 0.02, 0.03, 0.04 and 0.05) and the previous process was repeated. When the concentration of Zn^{2+} and $(OH)^-$ ions in the each of the solution placed in the auto cave reached the critical super saturation value of ZnO, ZnO nanoparticles began to form. During the rest of the time in the auto cave, the remaining Zn^{2+}, (OH) and the various impurity ions would be deposited on the (001) face of wurtzite structure of the initial ZnO nanocrystals resulting in the formation of nanorod shaving a hexagonal structure.

3. Results and Discussion

The magnetizations of the various nonmagnetic doped ZnO NR's were measured at room temperature using either a vibrating sample magnetometer or a SQUID magnetometer located in the Department of Material Science, Faculty of Engineering, National University of Singapore. From the hysteresis loops of $Zn_{1-x}Sb_xO$ (x = 0.0, 0.05, 0.15, 0.25 and 0.30) we extracted the values of the saturation magnetizations. This was done by subtracting the diamagnetic contribution to the magnetization. The results taken from Nakarungsee *et al*. [19] are plotted in Figure 1. In Figure 2, we have plotted the values of the saturation magnetization of Zn1-xAgxO (x = 0.0, 0.1, 0.2, 0.3, 0.4

and 0.5) taken from Robkhob *et al*. [20]. The dependences of the saturation magnetizations of the two are quite different. For the Sb doped ZnO NR's, the saturation magnetization decreases as more nonmagnetic Sb ions are substituted in, while the saturation magnetization increases as more nonmagnetic Ag ions are substituted in. This latter behavior is keeping with the assumption that the magnetizationis due to the increased stability of the Zn vacancies when it becomes part of an impurity complex $Ag_{Zn} + 2V_{Zn}$.

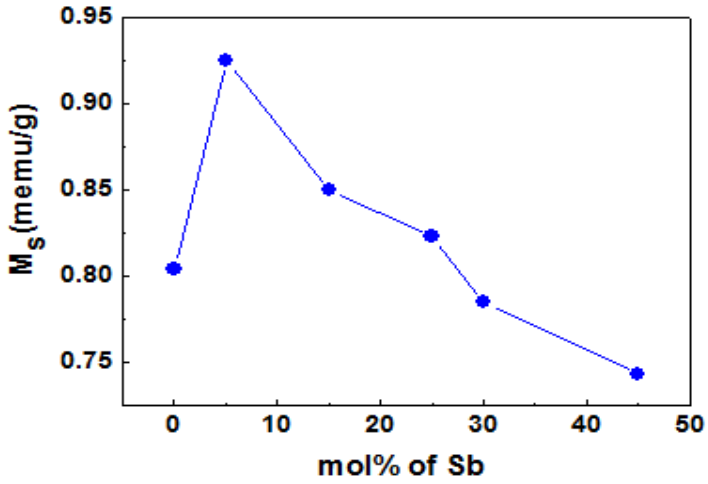

Figure 1. Dependence of the saturation magnetization of $Zn_{1-x}Sb_xO$ NR's on the level of Sb doping. The replacement of the Zn ions by the non-magnetic Sb ions leads to increase in M_S. The increase is not a systematic one, i.e., the increase in M_S is not a systematic one.

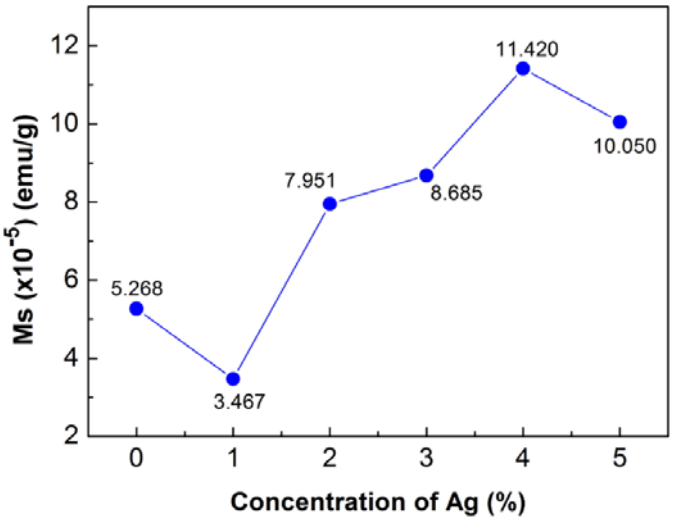

Figure 2. Dependence of the saturation magnetization of $Zn_{1-x}Ag_xO$ NR's on the level of Ag doping. The increase in the M_S is explained as being the result of the increase stability of the Zn vacancies when they are part of an impurity complex made up of Zn vacancy defect the defect arising from the replacement of Zn ion by an Ag ion.

To clarify this, we measured the saturation magnetization of Al doped ZnO NR's, $Zn_{1-x}Al_xO$ (x = 0.0 → 0.1 in steps of 0.01) and plotted the results [21] in Figure 3. Ignoring the saturation value of $Zn_{0.95}Al_{0.05}O$ NR's, the saturation magnetizations of $Zn_{1-x}Al_xO$ NR's tend to increase as more Al isdoped in until concentration of the Al ions reaches x = 0.07. This behavior is consistent with the explanation used to explain the behavior of the saturation magnetization of $Zn_{1-x}Ag_x0$ $Zn_{1-x}Ag_x0$, the substitution of the nonmagnetic ions stabilized the Zn vacancies. To gain more insight in these new types of DMS, we have fabricated Mg doped $Zn_{1-x}Mg_xO$ (x = 0.02. 0.046, 0.054 and 0.07). The hysteresis loops of the $Zn_{1-x}Mg_xO$ were taken with a VSM at room temperature. From these loops, we obtained the saturation magnetization of each of the Mg doped ZnO NR's. The saturation magnetization are plotted on Figure 4. As is seen, as x increases from 0.046 to 0.07, the saturation magnetizations increase in line with the behaviors seen in Figures 2 and 3. The behavior of M_S for the Sb doping and the magnetization values which do not follow the general increase in the magnetization of the other (Al, Ag and Mg) doped ZnO NR's, may reflect the point raised by Peng *et al.* [15] that the observed properties may be an extrinsic property which depends on the type of dopant used to induce magnetization and whose nature is not understood.

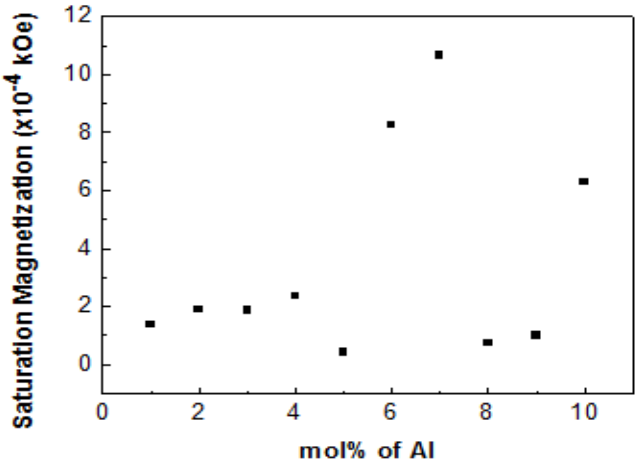

Figure 3. Dependence of the saturation magnetization of $Zn_{1-x}Al_xO$ NR's on the level of Al doping. Since the dependences of M_S on the level of substitution of one nonmagnetic ion (Zn) by another nonmagnetic Ag ions are quite defferent, the change in M_S due to the replacement of a Zn ion by a third nonmagnetic ions (Al) was done to see which behavior is the typical behavior and which is atypical. Except for the x = 0.05 NP, the saturation magnetization is seen to increase as x is increased from x = 0.01 to 0.07, meaning that the behavior due to Ag doping is the typical one, i.e., the increase in M_S in the increase stability of the Zn vacancies when other nonmagnetic ions are substituted for the Zn ions.

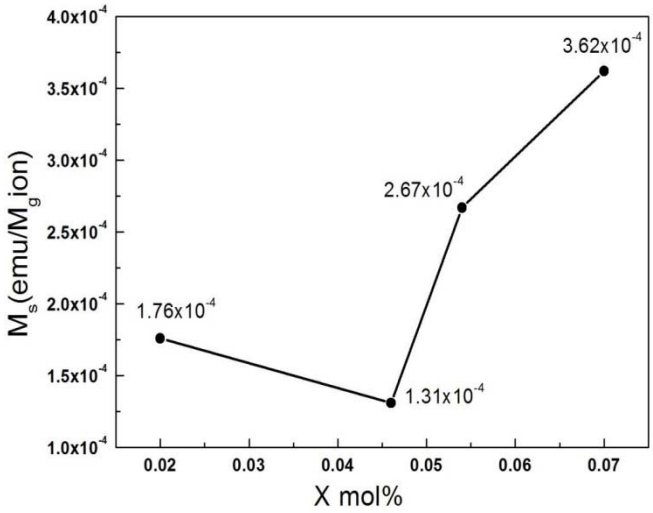

Figure 4. Dependence of the saturation magnetization of $Zn_{1-x}Mg_xO$ NR's on the level of Mg doping. If the increase in the M_S as additional nonmagnetic ions replaces the nonmagnetic Zn ions is a general feature of the new class of dilute magnetic semiconductors, the same behavior would be ex-pected if another nonmagnetic ion is used. The Mg ions are another nonmagnetic ions. As we see, the saturation magnetization increases as more Mg ions replace the Zn ions.

4. Conclusions

According to the definition of Dilute Magnetic Semiconductors (DMS), the doped ZnO NR's which we are studying are not dilute magnetic semiconductors since the impurities being substituted for the nonmagnetic Zn ions are not magnetic ions. They are nonmagnetic ions, so that the systems we are studying do not fit the definition of DMS. Complicating matters the magnetism observed in ZnO NP's are due to defects, missing Zn ions, i.e., vacancies. The magnetic moments are virtual moments which arise when virtual energy levels of the virtual electronic statesformed about the missing Zn ions are occurred by a pair of electrons from the neighboring oxygen ions in the wurtzite structure ZnO NP's. This virtual magnetic moment are magnetic since theoreticalbcalculations show that the spin polarized configuration of the electrons in the virtual atom have a lower energy than that of the non spin polarized configuration. This makes them real leading to real consequences so virtual reality becomes real. Thus, our virtual DMS become real DMS and should be further studied to see if they have real applications.

5. Acknowledgements

IMT would like to acknowledge the financial support provide to him by the King Mongkut's University of Technology, Thonburi through the 55thAnniversary Commemorative Fund. PR wouldlike to thank the Thailand Research Fund (TRF) for a Royal Golden Jubilee PhD Fellowship.

ST would like to acknowledge financial support from the Faculty of Science, Kasetsart University and Kasetsart University Research and Development Institute.

References

[1] Furdyne, J.J., 2010. Dilute magnetic semiconductors. *J. Appl. Phys.*, 64, R29.
[2] Dietl, T., Ohno, H., Matsukura, F., Cibert, J. and Ferrand, D., 2000. Zener Model Description of Ferromagnetism in Zinc-Blende Magnetic Semiconductors. *Science,* 287, 1019.
[3] Dietl, T. and Ohno, H., 2014. Dilute Ferromagnetic Semiconductors Physics and Spintronics Structures. *Rev. Mod. Phys.,* 86, 187.
[4] Coey, J.M.D., Venkatesan, M. and Fitzgerald, C.B., 2005. Donor impurity exchange in dilute ferromagnetic oxides, *Nature Materials,* 41, 173-179.
[5] Zutic, I., Fabian, J. and Das Sarma, S., 2004. Spintronics: Fundamentals and Applications, *Rev. Mod. Phys.*,76, 323.
[6] Venkatesan, M., Fitzgerald, C.B. and Coey, J.M.D., 2004. Unexpected magnetism in a dielectric oxide. *Nature,* 430, 630.
[7] Sundaresan, A., Bhargavi, R., Rangarajan, N., Siddesh, U. and Rao, C.N.R., 2006. Ferromagnetism as a universal feature of nanoparticles of otherwise nonmagnetic oxides. *Phys. Rev., B*, 74, 161306.
[8] M. Venkatesan, M., C.B. Fitzgerald, C.B., J.G. Lunney, J.G., J.M.D. Coey, J.M.D., 2004. Anisotropic ferromagnetism in substituted zinc oxide. *Phys. Rev. Lett.,* 93, 177206.
[9] Anghei, J., Thurber, A., Tenne, D.A., Hanna, C.B. and Punnoose, A., 2010. Correlation between saturation magnetization, bandgap and lattice volume of transition metal (M =Cr, Mn, Fe, Co or Ni) doped Zn1-xMxO nanoparticles. *J. Appl. Phys.,* 107, 09E314.
[10] Hong, N.H., Sakai, J., Poirot, N. and Brize, V., 2006. Room-temperature ferromagnetism observed in undoped semiconducting and insulating oxide thin films. *Phys. Rev., B*, 73, 132404.
[11] Rainey, K., Chess, J., Eixenberger, J., Tenne, D.A., Hanna, C.B. and Punnoose, A., 2014. Defect induced ferromagnetism in undopedZnO nanoparticles. *J. Appl. Phys.,* 115, 17D727.
[12] Liu, W., Li, W., Hu, Z., Tang, Z. and Tang, X., 2011. Effect of oxygen defects on ferromagnetic of undoped ZnO. *J. Appl. Phys.,* 110, 013901
[13] Gao, D., Zhang, Z., Fu, J., Xu, Y., Qi, J. and Xue, D., 2009. Room temperature ferromagnetism in pure ZnO nanoparticles. *J. Appl. Phys.,*105, 113928.
[14] Wang, Q.J., Wang, J.B., Zhong, X.L., Tan, Q.H., Hu, Z. and Zho, Y.C., 2012. Magnetism mechanism in ZnO and ZnO doped with nonmagnetic elements X (X = Li, Mg, and Al): A first-principles study. *Appl. Phys. Lett*. 100, 132407.
[15] Peng, H.W., Xiang, H.J., Wei, S.H., Li, S.S., Xia, J.B. and Li, J.B., 2009. Origin and enhancement of hole-induced ferromagnetism in first-row d0 semiconductors. *Phys. Rev. Lett.,* 102, 017201.
[16] Lu, Y.B., Dai, Y., Guo, M., Yu, L. and Huang, B.B., 2013. Investigation of magnetic properties induced by Group V elements in doped AnO. *Phys. Chem. Chem. Phys*., 15, 5208.
[17] Limpijumnong, S., Zhang, S.B., Wei, S.H. and Park, C.H., 2004. Doping by large size mismatched impurities: The microscopic origin of arsenic or antimony doped zinc oxide. *Phys. Rev. Lett.,* 15, 155504.
[18] Tian, S., Zeng, D., Xie, C. and Zhao, X., 2014. Direct experimental evidence for SbZn + 2VZn complex as the important defect in the Sb-doped ZnOnanocrystals, *Material Letters,* 116, 363.
[19] Nakarungsee, P., Chen, G.S., Herng, T.S., Ding, J., Tang, I.M. and Talabthong, Thongmee, S., 2016. Sb substitution into ZnO nano-compoisite: Ferromangetic behavior. *JMMM,* 397, 79.
[20] Robkhob, P., Herng, T.S., Dingm J., Tang, I.M. and Thongmee, S., 2017. Magnetic behavior of ZnO nanorods doped with silver (Ag^{3+}) ions. *J. Nanosci. & Nanotech,* 17, 5631.
[21] Yingsamphancharoen, T., Nakarungsee, P., Herng, T.S., Ding, J. and Tang. I.M., 2016. Ferromagnetic behavior due to Al^{3+} doping into ZnO nanorods. *JMMM,* 419, 274.

Instructions for Authors

Current Applied Science and Technology journal contains research reports, articles concerning development work, reviews of the literature and research activities. The objectives are to publish and promote research contributions and innovative work in fields associated with applied science and technology. An electronic journal is provided on the website (https://www.tci-thaijo.org/index.php/cast/index). The Editors reserve the right to require revision of the submitted manuscript as a condition for final acceptance.

The institute and the editorial board claim no responsibility for the contents or views expressed by the authors of individual articles. Copying is allowed provided that acknowledgement is made. All articles submitted for publication will be assessed by a group of distinguished

Ethics:

The journal is committed to maintaining the high level of integrity in the content published and has a Conflict of Interest policy in place. The journal uses plagiarism detection software to screen the submissions. If plagiarism is found, the COPE guidelines on plagiarism will be followed.

Page Charge: Free

Submission of Manuscripts:

Manuscripts must be written in English and submitted online. Manuscripts are to be reviewed (double blinded) by at least 3 referees specializing in relevant fields. Revised manuscripts have to be sent online.

All manuscripts should be submitted to: https://www.tci-thaijo.org/index.php/cast/index

Contact:

Editor of Current Applied Science and Technology
King Mongkut's Institute of Technology Ladkrabang
1 Soi Chalongkrung 1, Ladkrabang District,
Bangkok 10520, Thailand
Tel: 662-329-8136
Fax: 662-329-8221
Email: cast@kmitl.ac.th

Manuscript Preparation Guide:

General: Manuscripts must be typewritten using *Microsoft Word for Windows,* single-spaced with margin set-up (in page set up menu) as follows (see also the document template):

Top Margin 1.5"	Bottom Margin 1.5"
Left Margin 1.5"	Right Margin 1.5"

Good quality printouts using A4 paper size are required. Format should be a single column. Times New Roman font type is required. Font sizes for various text functions are as follows:

Text functions	Size *	Typeface
Title	14 (CT)	Bold
Author and co-authors	11 (CT)	Normal
Address for correspondence	11 (CT)	Normal
Abstract and main text	10 (LJ)	Normal
Section heading and number including "Abstract", "Acknowledgement", "References"	12 (CT)	Bold
Subsection heading and number	11 (LJ)	Bold

* CT = Center Text, LJ = Left Justified.

The corresponding author should be noted (included a Fax number and E-mail address) and indicated with an asterisk. Full postal addresses must be given for all co-authors, keyed to names (if required) by superscripted Arabic numbers.

Paper Length: Should not normally exceed 10 pages including figures and tables
Spelling: American English
Abstract: Should not exceed 250 words
Keywords: Should not exceed 8 keywords
Text: Authors are requested to use the following order when typing:-

All research reports (Full Length or Short Reports): Title, Authors, Affiliations, Abstract, Keywords, Introduction (in reserch papers this must be confined to relevant matters, and must not be a general review of cognate literature), Materials and Methods, Results and Discussion, Conclusions, Acknowledgements, References.

Reviews and Discussion Papers will be considered in any format appropriate to the purposes of the authors, although adherence to the general guidelines described above is encouraged.

Line Art Figures: Figures can be drawn using several packages such as Win Draw®, Auto CAD®, Corel Draw®, VISIO® etc.

Photographs: Actual size photographs are acceptable. However, they can also be put into a text stream using a good-resolution scanner. All photographs must be clear when printed in monochrome.

Graphs: Several packages available today can produce attractive and professional graph presentation. Some also provide curve-fitting function, which can be useful. However, two-dimensional bar charts are preferred. All graphs must be clear in monochrome printing.
Equations and complex expressions: Math CAD®, Math Writer® and Equation Editor® (included in Microsoft Word®) are acceptable for presentation of this type of material.

Citations: Citations in the text should be denoted by numbers between square brackets (i.e. [1, 2], [1-3], [1, 3-8]…) *in the order of first appearance in the text.*

References: References should be numbered to correspond with the text citations. References must be arranged as follows:

Books

Authors, Initials., Year. *Title of Book.* Edition. (only include this if not the first edition) Place: Publisher.

Example:

[1] Barker, R., Kirk, J. and Munday, R.J., 1988. *Narrative Analysis*. 3rd ed. Bloomington: Indiana University Press.

Chapters of edited books

Chapter authors' surname(s), initials., Year of book. Title of chapter. In**:** Book editor(s) initials. surnames, ed. or eds. *Title of Book*. Place of publication: Publisher. Chapter number or first and last page numbers.

Example:

[2] Samson, C., 1970. Problems of information studies in history. In: S. Stone, ed. *Humanities Information Research*. Sheffield: CRUS, pp. 44-68.

E-books

Author, Year, *Title of Book*. [e-book] Place of publication: Publisher. Available through: include e-book source/database, web address or URL.

Example:

[3] Carlsen, J. and Charters, S., eds. 2007. *Global Wine Tourism*.[e-book] Wallingford: CABI Pub. Available through: Anglia Ruskin University Library website <www.libweb.anglia.ac.uk>.

Journal articles

Author, Initials., Year. Title of article. *Full Title of Journal,* Volume number (Issue number), Page numbers.

Example:

[4] Ross, A.B., Junyapoon, S., Jones, J.M., Williams, A. and Bartle, K.D., 2005. A study of different soots using pyrolysis–GC–MS and comparison with solvent extractable material. *Journal of Analytical and Applied Pyrolysis*, 74(1-2), 494-501.

Proceedings

Author, Initials., Year. Title of article. *Full Title of Proceedings*, Place of Conference, Date, page

Example:

[5] Thanaboripat, D., Ruangrattanametee, V. and Srikitkademwat, K., 2010. Control of growth and aflatoxin production of aflatoxin producing fungi in corn by salts. *Proceeding of the 8th International Symposium on Biocontrol and Biotechnology*, Pattaya, Thailand, October 4-6, 2010, 283-289.

Patent

Inventor name, Initial(s)., Assignee., Year. *Title*. Place. Patent number (status, if an application).

Example:

[6] Leonard, Y., Super Sports Limited., 2008. *Tin Can Manufacture and Method of Sealing*. Canada. Pat. 12,789, 675.

Dissertation
Author, Year of publication. *Title of Dissertation*. Level. Official name of University.
Example:
[7] Richmond, J., 2005. *Customer Expectations in the World of Electronic Banking: a Case Study of the Bank of Britain.* Ph.D. Anglia Ruskin University.

Websites
Authorship or Source, Year. *Title of document*. [online] Available at: include web site address/URL (Uniform Resource Locator).
Example:
[8] NHS Evidence, 2003. *National Library of Guidelines*. [online] Available at: http://www.library.nhs.uk/guidelines

Acknowledgements: These should be as brief as possible.

Proofs:

Proofs will be sent to the corresponding author and *must* be returned as soon as possible. Corrections should be restricted to typesetting errors.

Copyright:

The author(s) transfer(s) the copyright of the article to Current Applied Science and Technology effective if and when the article is accepted for publication.

Page Numbering:

All pages must be sequentially numbered, preferably by using the automatic page numbering function on your computer.

Copyright Material:

It is the authors' responsibility to obtain written permission from the copyright holder (usually the book or journal publisher) to use copyright material, and to send a copy of this consent with the manuscript. This consent is not normally denied but it is an international legal requirement that it be obtained.

Note:

Please note that authors are urged to check their proofs carefully before returning, since the inclusion of late corrections cannot be guaranteed.

Author(s) are responsible for ensuring that the submitted manuscript fully meets the requirements specified in the above Instructions. Manuscripts which fail to do so will be returned unedited to the Author(s) for correction in accordance with the above requirements, before they can be submitted to the processes of Referee evaluation.

1.5 ”

TEMPLATE

Enter title here (14 PT type size, Title Case, Bold, Centered)

Author Information entered here:
Name (in full)

Affiliation
City
Country
(11 pt type size, upper and lower case, centered under the title)

How to Use This Document Template

Insert the information in your document in place of the text here. For the body of your document, use Times New Roman 10 pt. Font, upper and lower case, double-spaced. Allow an extra half space above a line containing superscripts and/or below a line containing subscripts. The whole text should be left-justified. The headings should be 12 pt size, uppercase, bold and centered.

1.5” **Abstract (12pt)** 1.5”

Maximum 250 words here. (10 pt)

.....
.....
.....
.....
.....

Keywords: (10 pt)

Maximum of 8 words

*Corresponding author: Tel.: ……..... Fax: …….
E-mail: ……

1. Introduction (12 pt)

Clearly explain the nature of the problem, previous work, purpose, and contribution of the paper (10 pt).

.....
.....
.....
.....
.....

2. Materials and Methods (12 pt)

.....
.....
.....
.....

3. Results and Discussion (12 pt)

.....
.....…

4. Conclusions (12 pt)

Clearly indicate advantages, limitations and possible applications (10 pt).

.....
.....

5. Acknowledgements (12 pt)

A brief acknowledgement section may be included here (10 pt).

.....
.....

References (12 pt)

References must be numbered in the order cited in the manuscript and indicated in the text by a number in square brackets (e.g. [1, 2]) (10 pt).

Example of References must be arranged as follows:

[1] Barker, R. Kirk, J. and Munday, R.J., 1988. *Narrative Analysis*. 3rd ed. Bloomington: Indiana University Press.

[2] Samson, C., 1970. Problems of information studies in history. In: S. Stone, ed. *Humanities Information Research*. Sheffield: CRUS, pp. 44-68.

[3] Carlsen, J. and Charters, S., 2007. *Global Wine Tourism*. [e-book] Wallingford: CABI Pub. Available through: Anglia Ruskin University Library website <www.libweb.anglia.ac.uk>.

[4] Ross, A.B., Junyapoon, S., Jones, J.M., Williams, A. and Bartle, K.D., 2005. A study of different soots using pyrolysis–GC–MS and comparison with solvent extractable material. *Journal of Analytical and Applied Pyrolysis*, 74(1-2), 494-501.

[5] Thanaboripat, D., Ruangrattanametee, V. and Srikitkademwat, K., 2010. Control of growth and aflatoxin production of aflatoxin producing fungi in corn by salts. *Proceeding of the 8th International Symposium on Biocontrol and Biotechnology*, Pattaya, Thailand, October 4-6, 2010, 283-289.

[6] Leonard, Y., Super Sports Limited., 2008. *Tin Can Manufacture and Method of Sealing*. Canada. Pat. 12,789, 675.

[7] Richmond, J., 2005. *Customer Expectations in the World of Electronic Banking: a Case Study of the Bank of Britain*. Ph.D. Anglia Ruskin University.

[8] NHS Evidence, 2003. *National Library of Guidelines*. [online] Available at: http://www.library.nhs.uk/guidelines

Note:

Tables and Graphs: Minimum of 10 pt type size, all captions should be upper and lower case, centered. Each table and figure must be on a separate page (or pages if required), ***and must not be embedded in the text.***

Illustrations and Photographs: Halftones, minimum of 10 pt type size, bold, captions should be in upper and lower case, centered. Images must be computer-designed with clearly visibility.

Contact

Editor of Current Applied Science and Technology
King Mongkut's Institute of Technology Ladkrabang
1 Soi Chalongkrung 1, Ladkrabang District
Bangkok 10520, Thailand
Tel: 662-329-8136 Fax: 662-329-8221
E-mail: cast@kmitl.ac.th
Website: https://www.tci-thaijo.org/index.php/cast/index

KING MONGKUT'S INSTITUTE OF TECHNOLOGY LADKRABANG
1 Soi Chalongkrung 1, Ladkrabang District Bangkok 10520, Thailand
Tel: 662-329-8136 Fax: 662-329-8221
E-mail: cast@kmitl.ac.th
Website: https://www.tci-thaijo.org/index.php/cast/index